Parameterizing the Random Encounter Staying Time model to generate mean and variance ungulate density and abundance estimates

By

Brendan M Carswell

A thesis submitted to the School of Graduate Studies in partial fulfilment of the requirements of Master of Science degree

Department of Biology

Memorial University of Newfoundland and Labrador

St. John's, Newfoundland and Labrador

Abstract

Understanding wildlife density and abundance is perhaps the most important and universal concept across facets of wildlife management, conversation, and research. Despite the significance of understanding species densities in ecology, methods for estimating density for large terrestrial mammals in Canada continue to have high levels of inaccuracy in addition to being a costly, exclusive practice. From the mass use of remote camera traps in wildlife life science came a series of camera trap-based density estimation models, known as viewshed density estimators, which could allow practitioners to estimate wildlife density from camera trap data. Despite the cost-effective and accessible framework, viewshed density estimators remain analytically challenging to parameterize and implement. To accurately estimate density, viewshed density estimators require a precise metric of the physical area camera traps monitor, a highly variable number that can be challenging to quantify. Here, I tested a field and analytical framework that can be used to accurately estimate the spatial footprint of camera traps with a 100% capture probability, the Effective Capture Area. Next, I use the Effective Capture Area to parameterize the Random Encounter Staying Time model of density estimation for generating density and abundance estimates for moose (*Alces alces*) and elk (*Cervus canadensis*) across camera trap grids in Riding Mountain National Park, Canada. I show that, given adequate spatial and temporal sampling periods, the Random Encounter Staying Time model produces density and abundance estimates that correlate well with historic aerial flight surveys on both fine- and coarse-spatial scales. Finally, I comment on how viewshed density estimators can improve our understanding of wildlife density and abundance estimation, as well as provide novel insights in many areas of ecological study.

Land Acknowledgements

I recognize Ktaqmkuk (the island of Newfoundland) on which I lived and studied during this thesis, as the traditional, unceded territory of the Mi'kmaq and culturally extinct Beothuk peoples. I also recognize the Innu and Innuit, and their ancestors, as the traditional peoples of Labrador. Fieldwork and data collection for the following work took place within Treaty 2 territory, the traditional lands of the Anishinabewaki, Očhéthi Šakówiŋ, Cree, Oji-Cree, and the Homeland of the Métis peoples. As a researcher of colonial descent living on stolen land, I aim to learn from my experiences and missteps from this work and build toward respectful and equitable partnerships with the diverse First Nations people on Turtle Island.

Acknowledgments

First and foremost, I would like to thank my supervisor, Eric Vander Wal for inviting me to the Wildlife Evolutionary Ecology Lab and always providing a safe, supportive, and inclusive environment. Your involvement with your students, their journeys in science, and mentorship were invaluable throughout my time in the WEEL lab. Thanks to my committee members, Tal Avgar and Garrett Street for providing instrumental feedback on my work and thesis chapters. Special shout out to Tal for his continued and frequent support despite the numerous time zones between us.

I would like to acknowledge all the members of the Wildlife Evolutionary Ecology Lab, with special thanks to Jack Hendrix, Katrien Kingdon, Alec Robitaille, Jill Kusch, Daniel Dupont, Emily Monk, and Emilie Dedeban, for your assistance and encouragement with fieldwork, analytical discussions, brainstorming, and feedback.

Thanks to all the government and industry collaborators that aided in planning and conducting fieldwork, specifically Tim Sallows, Ross Robinson, and Alyssa Brewer from Parks Canada, Lindsey Bylo and Jillian St. George with the Manitoba Wildlife Division, and Jonathon Wiens of Manitoba Hydro.

I am grateful to the Opaskayak Cree Nation for inviting me to participate in science and wildlife monitoring discussions during my time in Manitoba. Special thanks to Dianne Ballantyne for coordinating constantly changing field plans and to Nick Dumas for field support in a deep snow winter.

Finally, to my family, friends, and mentors in British Columbia, I would not be here, nor finished this master's without your unwavering support. Thank you for the continued encouragement, and willingness to travel thousands of kilometres to visit.

COVID-19 Impact Statement

Despite starting my MSc in September 2021, after the initial wave of the COVID-19 pandemic, COVID-19s impact on data collection and fieldwork were substantive to my thesis. For example, the 2021 aerial flight survey, the year I had the most substantive camera trap data, was heavily reduced to prevent unnecessary risk to Parks Canada staff. As discussed in Chapter 3, the incomplete aerial survey in 2021 was not reliable and did not merit an unbiased comparison to camera trap data. In addition, my initial field season at Riding Mountain National Park (in January 2022) had to be delayed due to the emergence of the Omicron-variant, which saw a resurgence of travel and safety restrictions for many months. My first field season began in late March 2022, and was further reduced due to safety issues from deep snow and subsequent extensive flooding in Manitoba in April 2022. As a result, field data in 2022 were heavily limited from my initial plans, where only 45 of 89 camera traps were assessed for Effective Capture Area estimation. Regardless of the impacts of COVID-19, the data presented in this thesis represent progress for understanding viewshed density estimation using camera traps and how such estimators perform relative to traditional flight surveys.

Table of Contents

Co-authorship statement

This thesis was completed for partial fulfillment for an MSc in the Biology Department at the Memorial University of Newfoundland and Labrador. I am the principal coauthor and contributor to ideas, study design, data analysis, writing, and manuscript preparation for all chapters of this thesis. Co-authors provided feedback and guidance on my decisions made throughout the thesis. I am solely responsible for Chapters 1 and 4 for this thesis, these chapters may be used or revised for other publications. Chapter 2 of this thesis was co-authored with Tal Avgar, Sean Boyle, Garrett Street, and Eric Vander Wal. Chapter 2 is currently formatted and structured for submission in *Methods in Ecology and Evolution*. Chapter 3 of this thesis was co-authored with Tal Avgar, Garrett Street, Alec Robitaille, and Eric Vander Wal, and is currently being prepared for publication. Chapter 3 will be submitted for publication upon competition of this thesis.

List of Tables

List of Figures

Figure 3.1 Aerial flight transects (black) flown by Parks Canada staff in Riding Mountain National Park in February 2022 for ungulate surveys. The central and eastern transects, representing 25% coverage, are flown 1.6 km apart. The western transects, representing 100% coverage, are flown 400 m apart. All transects are 400 m wide, i.e., assumed perfect detection on 200 m for both sides, flown at 120 m altitude, and at a speed of 120 km/hr. Including locations of camera traps (n = 81) deployed in *a priori* moose densities. Each grid contains 9 camera traps, each placed 250 m from its neighbouring cameras. The central camera in every grid is always a Reconyx Ultrafire XR6 camera trap and the surrounding cameras are always Cuddeback H-1453 camera traps.

Figure 3.2 Various 'fine-scale' polygons, 5km^2–10km^2, left to right, top to bottom, surrounding camera trap grids, showing moose observations from the 2022 aerial flight survey in Riding Mountain National Park.

Figure 3.3 Slope (± SE) and R^2 values of the linear regressions that predicted fine-scale moose density estimates, at various spatial scales (5–11km^2), from aerial flight surveys conducted in Riding Mountain National Park in February 2022. Fine-scale flight densities were predicted by mean Random Encounter Staying Time density estimates at camera trap grids (n = 9) for the 2022 study year.

Figure 3.4 The best fit and highest correlated linear regression model predicting fine-scale moose density estimates from the 2022 aerial flight survey and 2022 study year with 10km^2 polygons surrounding each camera trap grip (n = 9). Horizontal error bars represent the 95% confidence intervals generated from the theoretical REST variance equation, whereas vertical error bars represent the 95% confidence intervals from aerial flight surveys.

Figure 3.5 Mean moose densities (), per km^2, at all camera trap grids (n = 9), showing density trends of individual camera traps (n = 81) throughout the 2022 study year, deployed across *a priori* strata, high density (top row), medium density (middle row), and low density (bottom row), in Riding Mountain National Park.

Figure 3.6 Comparison of trends in elk (left) and moose (right) abundance estimates (± 95% confidence intervals) generated from camera traps using the Random Encounter Staying Time model (blue) and from line transect estimation based on aerial flight surveys (green) across six years in Riding Mountain National Park.

List of Supplementary materials

Supplement S.2.1 — Data collection on environmental covariates in Riding Mountain National Park, Case Study A

Supplement S.2.2 — Effective Capture Area sensitivity to out-of-sample prediction

Supplement S.2.3 — Determining the potential temporal footprint of a camera trap image

Supplement S.3.1 — Selection of camera trap grid candidate locations using *camtrapmonitoring*

Supplement S.3.2 — Abundance size and variance calculations for aerial flight surveys in Riding Mountain National Park

Supplement S.3.3 — Sensitivity of the Random Encounter Staying Time density estimates to spatial and temporal variability.

Supplement S.3.4 — Monitoring time of all camera traps in Riding Mountain National Park from establishment in February 2020 until the end of 2022

Supplement S.3.5 — Additional figures and analyses for elk density estimation in RMNP

Supplement S.3.6 — Partial aerial flight survey lines in Riding Mountain National Park in 2021

List of Abbreviations used

REM — Random Encounter Model

REST — Random Encounter Staying Time model

TIFC — Time in Front of Camera model

RMNP — Riding Mountain National Park

ECA — Effective Capture Area

PIR — Passive Infrared (motion sensor)

GAMM — Generalized Additive Mixed Model

ROC — Receiver Operating Characteristics

AUC — Area Under Curve

SD — Secure Digital

COVID-19 — Corona Virus Disease of 2019

Chapter 1: Theoretical framework

1.1 — Density estimation for terrestrial mammals

There is perhaps no concept more important to wildlife management than density, the number of animals per unit area, and abundance, the total number of animals in a delineated area. Understanding how wildlife density fluctuates has management implications that affect natural ecological functioning, and for human uses of wildlife (Wang et al. 2006; Vander Wal et al. 2013; van Beest et al. 2014). For example, in Canada, some wildlife harvest quotas are set using estimates of density. Additionally, many governmental and non-governmental organisations communicate about population health to the public in terms of density, i.e., a wildlife population is increasing or decreasing (e.g., see Environment and Climate Change Canada, 2021). Despite the importance and prevalence of density estimation in wildlife sciences, density estimation techniques for larger-bodied mammalian species (e.g., moose, elk, wolves) remains a difficult, costly, and often inaccurate practice (Rönnegård et al. 2008; Gable et al. 2018; Lamb et al. 2018; Nakashima et al. 2018).

Density estimation in wildlife sciences is represented as the number of animals per unit area. For terrestrial wildlife sciences, however, a clear bias of density estimation exists. It seems intuitive that we should be able to count the number of animals in a given area but density estimation remains challenging because of heterogenous habitat cover as well as clumped distributions of animals (Liberg et al. 2011; Burton et al. 2015). The accepted uncertainty due to habitat influences underappreciates error associated with density estimation, as we tend to assume certainty with any estimate. For example, aerial flight surveys to estimate ungulate density often use correction factors to account for overstory forest cover. In one study estimating moose density, forests with cover exceeding 80% had a sightability correction of 70%. This

means that during the survey if 5 moose are observed in the high-cover strata, the correction factor will estimate 4 additional moose that were never observed (Liberg et al. 2011; Burton et al. 2015). Conversely, many programs do not employ correction factors (e.g., Vander Wal et al. 2013), leaving the potential for high variability in density estimates, and a lack of repeatability across geography. Despite the numerous habitat-based uncertainties, such density estimates act as a basis for many conservation and management decisions.

Currently, the most frequently employed methods of density estimation depend on one large assumption—the ability to differentiate individuals—which has implications with ethical, logistical, and financial concerns (Rönnegård et al. 2008; Stephens and Anderson 2014; Burton et al. 2015; Gable et al. 2018). The mark-recapture method is relatively common for species with relatively small ranges (Jolly, 1965). Mark-recapture, however, can impact the survival of individuals captured and as such have ethical implications (Stephens and Anderson 2014). Additionally, the logistical constraints of continually marking and monitoring individuals make the method unrealistic for many programs. For species with larger ranges and habitat, financial and logistical constraints dominate. For example, a common way to estimate bear density is through hair DNA analyses with non-invasive barbed-wire hair snares (Woods et al. 1999; Beth Gardner et al. 2010). Yet, such apparatuses need frequent maintenance and can be used to represent density estimates at vast geographic scales. Large ungulate species (e.g., moose, elk, caribou), occupy a wide variety of habitats, and thus aerial flight surveys are the dominant method of abundance estimation. Aerial flight surveys typically employ distance sampling methods (Buckland 2004), or stratified random block surveys (Quayle et al. 2001) to count individuals in a large geography within a short period of time. The high cost and large amount of training associated with aerial surveys make them impractical for temporally frequent or

consistent estimation (Rönnegård et al. 2008). As a result, tracking density beyond infrequent, single points in time remains difficult. Further, dissimilarity in geography, habitat, and implementation of density survey can contribute to high variance in density estimates, lowering our confidence in their outcomes.

1.2 — Modern approaches to density estimation

Starting in the early 2000s, advances in statistics and technology have allowed researchers to generate likelihood-based density estimates through the use of remote camera traps (Karanth 1995; Karanth and Nichols 1998; Rowcliffe et al. 2008; Chandler and Royle 2013; Howe et al. 2017; Moeller et al. 2018; Nakashima et al. 2018). Currently, around a dozen likelihood-based models are adapted to use camera-trap data. These models fall into four general categories based on the methods they use: 1) Capture-recapture based models, 2) distance sampling-based models, 3) encounter rate-based models, and 4) space-to-event models. *Capture-recapture based models (1)* (Karanth and Nichols 1998) adapt traditional mark-recapture methods paired with marked individuals or species with distinct, identifiable markings (e.g., Choo et al. 2020). Camera-based capture-recapture models require a high level of investment to mark or identify individuals, and as such are only practical to implement for a small number of species. Adaptations to the traditional point-transect *distance sampling method (2)* (Buckland 2004) were proposed for use with camera traps (Howe et al. 2017). Much like their predecessor, camera-based distance sampling requires a measurable distance, and associated detection probability, for each species photographic capture at a camera trap. Although a useful model, the many logistical constraints of implementing distance sampling model have limited its growth while implementing camera traps. A novel viewshed density estimator, the Random Encounter Model (REM), was proposed by Rowcliffe et al. (2008). The REM method estimates density

through *encounter rates (3)*, the cumulative amount of time a species spends in front of a camera trap, given the species movement rate. The REM has been shown to produce unbiased, accurate estimates of wildlife density (Rowcliffe et al. 2008), however, requires substantive external data, i.e., telemetry, GPS, behavioural observations, to parameterize a species movement rate. The REM has seen numerous adaptations to help ameliorate its assumption of knowing a species movement rate. The *Space-to-Event model (4)* (STE; Moeller et al. 2018) built upon the REM model, however, STE replaces time as the sampling unit with space. By sampling an instantaneous point in time across spatially distinct cameras, i.e., using time-lapse photography, the STE method can provide reliable density estimates when compared with other encounter rate models.

1.3 — The Random Encounter Stay Time model to estimate density

A relatively new, popular adaptation of the Random Encounter Model, is the Random Encounter Staying Time (REST) model, proposed by Nakashima et al. (2018). The REST model removes the need to estimate animal movement speed by incorporating the length of time a species stays in a cameras viewshed. The original REST model uses videos taken from remote camera traps, trapping effort, and cameras viewshed to generate unbiased density and abundance estimates (Nakashima et al. 2018). Some researchers have further reformed Nakashima's REST model to be more broadly applicable to a wider range of camera trap programs. For example, the Time In Front of Camera (TIFC) method was adapted to use photographs instead of videos from cameras (Warbington and Boyce 2020; Becker et al. 2022; Huggard 2018).

The most recent adaptation of the REST model was proposed by Hogg (2021). Hogg (2021) reconstructed the original REST model to generate mean and theoretical variance estimates of species density and abundance. Hogg's formulation:

$$\rho = \frac{\sum T_s}{T_a * A_c} * \frac{\pi^2}{8} \qquad \textit{Equation 1}$$

Estimates species density (ρ) as a function of the cumulative time a species spends in front of a camera trap ($\sum T_s$), the total time a camera trap was active (T_a), and the spatial footprint of a camera with a 100% capture rate (A_c). Hogg's model has an additional qualifier ($\frac{\pi^2}{8}$), which arises from an assumption that the spatial footprint with perfect capture probability is circular. The theoretical variance estimator is a bit more complicated:

$$Var(\rho) = \rho^2 * (\frac{\pi^2}{8} - 1 + \frac{\pi^2}{16*r*T*S*\rho}) \qquad \textit{Equation 2}$$

Where ρ represents the species density at a camera, r represents the radius of the assumed circular viewshed, T represents the duration of the observation period, and S represents the species average displacement rate assuming ballistic movement. Hogg's (2021) REST adaptation to calculate mean and theoretical variance density estimates provides a unique opportunity to compare the robustness of viewshed density estimators to more traditional survey types.

1.4 — Camera trap viewshed

Camera trap-based density models provide freedom from many challenging assumptions implicit with traditional density methods. All camera trap models, however, require an estimate of the spatial footprint camera traps monitor. The spatial footprint a camera monitors is henceforth referred to as a cameras viewshed. Precision in estimating the viewshed area is critical when employing camera-based density estimators, especially considering no research currently provides a standardized method to estimate a cameras viewshed area. For example, assuming all other variables are constant, if we assume a cameras viewshed is 100 m2, that camera will produce density estimates an order of magnitude lower than if its actual monitoring

area was 10 m^2. Despite the importance of a cameras viewshed when using camera trap-based methods, there is no consistent or standardized approach to precisely measure camera trap viewshed.

1.5 — Riding Mountain National Park

The land currently known as Riding Mountain National Park (RMNP) is a Canadian National Park, located in southwest Manitoba, on Treaty 2 territory, the traditional lands of the Anishinabewaki, Očhéthi Šakówiŋ, Cree, Oji-Cree, and the Homeland of the Métis peoples. Despite the parks turbulent colonial history, RMNP is currently delineated as an ~3000 km^2 area located within the transition zone of the Prairie Parkland and Boreal Plains ecotones (Olson et al. 2001). Riding Mountain has been conducting aerial surveys for ungulates, i.e., moose, elk, and deer, since the 1970s (Prokopenko 2022). Though aerial survey methods have slightly changed throughout their history, they have remained consistent since the mid-2000s (Parks Canada, Unpublished data). Fixed-wing aerial surveys take place in late winter (late January–March) each winter and are split into two portions. The central and eastern portions of the park, ~2500 km^2, has 400 m wide transects flown 1.6 km apart, at an altitude of 120 m at ~ 120 km/hr. The central and eastern flight surveys represent 25% aerial coverage. The western portion of the park, ~500km^2, has the same 400 m wide transects, but flown 400m apart. The western area of the park represents 100% coverage aerial coverage (Parks Canada, Unpublished data; Vander Wal 2011). The long-standing and consistent aerial surveys at RMNP provide a detailed chronology of the changes in ungulate populations. In addition, the reliability of the aerial flight surveys in RMNP provide an excellent fine and coarse-scale benchmark to which novel density estimation techniques can be compared to and improved upon.

In this thesis, I will parameterize Hogg's (2021) REST adaptation to generate mean and theoretical variance density and abundance estimates for large ungulates in a geography located on Treaty 2 territory, the traditional lands of the Anishinabewaki, Očhéthi Šakówiŋ, Cree, Oji-Cree, and the Homeland of the Métis peoples, presently known as Riding Mountain National Park. In Chapter 2, using a novel field and analytical framework, I will generate a standardized, *a priori*, estimator for the viewshed area of camera traps with a 100% capture rate—the Effective Capture Area. In Chapter 3, I will generate mean and variance density estimates for moose (*Alces alces*, from Algonquian *moswa*) and elk (*Cervus canadensis*, from Algonquian, Cree *waapiti*) from the Hogg-REST model, and compare those estimates to historical aerial-flight surveys conducted by Parks Canada. Finally, I will provide a framework to integrate both density estimation methods to provide a more robust, accessible form of density estimation for diverse stakeholders that may be interested in wildlife management.

1.5 — Literature Cited

Becker M, Huggard DJ, Dickie M, Warbington C, Schieck J, Herdman E, Serrouya R, Boutin S. 2022. Applying and testing a novel method to estimate animal density from motion-triggered cameras. Ecosphere. 13(4). doi:10.1002/ecs2.4005.

van Beest FM, McLoughlin PD, Vander Wal E, Brook RK. 2014. Density-dependent habitat selection and partitioning between two sympatric ungulates. Oecologica. 175:1155–1165. doi:10.1007/s00442-014-2978-7.

Beth Gardner, J. Andrew Royle, Michael T. Wegan, Raymond E. Rainbolt, Paul D. Curtis. 2010. Estimating Black Bear Density Using DNA Data From Hair Snares. Journal of Wildlife Management. 74(2):318–325. doi:10.2193/2009-101.

Buckland ST. 2004. Advanced distance sampling: estimating abundance of biological populations. Anderson DR, Burnham KP, Laake JL, Borchers DL, Thomas L, editors. Oxford, UK: Oxford University Press.

Burton AC, Neilson E, Moreira D, Ladle A, Steenweg R, Fisher JT, Bayne E, Boutin S. 2015. REVIEW: Wildlife camera trapping: a review and recommendations for linking surveys to ecological processes. Stephens P, editor. J Appl Ecol. 52(3):675–685. doi:10.1111/1365-2664.12432.

Chandler RB, Royle JA. 2013. Spatially explicit models for inference about density in unmarked or partially marked populations. Ann Appl Stat. 7(2). doi:10.1214/12-AOAS610.

Choo YR, Kudavidanage EP, Amarasinghe TR, Nimalrathna T, Chua MAH, Webb EL. 2020. Best practices for reporting individual identification using camera trap photographs. Global Ecology and Conservation. 24:e01294. doi:10.1016/j.gecco.2020.e01294.

Environment and Climate Change Canada. 2021. Species at risk public registry. https://www.canada.ca/en/environment-climate-change/services/species-risk-public-registry.html.

Gable TD, Windels SK, Bump JK. 2018. Finding wolf homesites: improving the efficacy of howl surveys to study wolves. PeerJ. 6:e5629. doi:10.7717/peerj.5629.

Hogg J. 2021. The precision and accuracy of the Random Encounter Staying Time model's estimation of species population density [MSc. Thesis]. Memorial University of Newfoundland and Labrador.

Howe EJ, Buckland ST, Després-Einspenner M, Kühl HS. 2017. Distance sampling with camera traps. Matthiopoulos J, editor. Methods Ecol Evol. 8(11):1558–1565. doi:10.1111/2041-210X.12790.

Huggard DJ. 2018. Animal density from camera data. Edmonton, AB: Alberta Biodiversity Monitoring Institute.

Jolly GM. Explicit estimates from capture-recapture data with both deaths and immigration. biometrika. 52.

Karanth KU. 1995. Estimating tiger Panthera tigris populations from camera-trap data using capture—recapture models. Biological Conservation. 71(3):333–338. doi:10.1016/0006-3207(94)00057-W.

Karanth KU, Nichols JD. 1998. Estimation of tiger densities in India using photographic captures and recaptures. Ecology. 79(8):2852–2862. doi:10.1890/0012-9658

Lamb CT, Mowat G, Reid A, Smit L, Proctor M, McLellan BN, Nielsen SE, Boutin S. 2018. Effects of habitat quality and access management on the density of a recovering grizzly bear population. Marnewick K, editor. J Appl Ecol. 55(3):1406–1417. doi:10.1111/1365-2664.13056.

Liberg O, Aronson Å, Sand H, Wabakken P, Maartmann E, Svensson L, Åkesson M. 2011. Monitoring of wolves in Scandinavia. Hystrix, the Italian Journal of Mammalogy. 23(1). doi:10.4404/hystrix-23.1-4670. [accessed 2024 Jan 25]. https://doi.org/10.4404/hystrix-23.1-4670.

Moeller AK, Lukacs PM, Horne JS. 2018. Three novel methods to estimate abundance of unmarked animals using remote cameras. Ecosphere. 9(8):e02331. doi:10.1002/ecs2.2331.

Nakashima Y, Fukasawa K, Samejima H. 2018. Estimating animal density without individual recognition using information derivable exclusively from camera traps. Stephens P, editor. J Appl Ecol. 55(2):735–744. doi:10.1111/1365-2664.13059.

Olson DM, Dinerstein E, Wikramanayake ED, Burgess ND, Powell GVN, Underwood EC, D'amico JA, Itoua I, Strand HE, Morrison JC, et al. 2001. Terrestrial Ecoregions of the World: A New Map of Life on Earth. BioScience. 51(11):933. doi:10.1641/0006-3568

Prokopenko CM. 2022. Hungry wolves and dangerous prey: a tale of prey switching [PhD thesis]. [St. John's, NL]: Memorial University of Newfoundland and Labrador.

Quayle JF, MacHutchon AG, Jury' DN. 2001. Modeling moose sightability in south-central British Columbia. Alces. 37(1):43–54.

Rönnegård L, Sand H, Andrén H, Månsson J, Pehrson Å. 2008. Evaluation of four methods used to estimate population density of moose Alces alces. Wildlife Biology. 14(3):358–371. doi:10.2981/0909-6396

Rowcliffe JM, Field J, Turvey ST, Carbone C. 2008. Estimating animal density using camera traps without the need for individual recognition. Journal of Applied Ecology. 45(4):1228–1236. doi:10.1111/j.1365-2664.2008.01473.x.

Rowcliffe JM, Jansen PA, Kays R, Kranstauber B, Carbone C. 2016. Wildlife speed cameras: measuring animal travel speed and day range using camera traps. Pettorelli N, editor. Remote Sens Ecol Conserv. 2(2):84–94. doi:10.1002/rse2.17.

Stephens RB, Anderson EM. 2014. Effects of trap type on small mammal richness, diversity, and mortality: Sherman Live and Pitfall Trap Efficacy. Wildl Soc Bull. 38(3):619–627. doi:10.1002/wsb.418.

Vander Wal E. 2011. Sex, friends, and disease: Social ecology of elk (Cervus elaphus) with implications for pathogen transmission [PhD thesis]. [Saskatoon, SK]: University of Saskatchewan.

Vander Wal E, van Beest FM, Brook RK. 2013. Density-Dependent Effects on Group Size Are Sex-Specific in a Gregarious Ungulate. Fenton B, editor. PLoS ONE. 8(1):e53777. doi:10.1371/journal.pone.0053777.

Walker ABD, Ave SF, George P, Watts GS. 2006. Moose density and composition around Prince George, British Columbia.

Wang G, Hobbs NT, Boone RB, Illius AW, Gordon IJ, Gross JE, Hamlin KL. 2006. Spatial and Temporal Variability Modify Density Dependence in Populations of Large Herbivores. Ecology (Durham). 87(1):95–102. doi:10.1890/05-0355.

Warbington CH, Boyce MS. 2020. Population density of sitatunga in riverine wetland habitats. Global Ecology and Conservation. 24:e01212. doi:10.1016/j.gecco.2020.e01212.

Woods JG, Paetkau D, Lewis D, McLellan BN, Proctor M, Strobeck C. 1999. Genetic tagging of free-ranging black and brown bears. Wildlife Society Bulletin. 27(3):616–627. https://www.jstor.org/stable/3784082

Chapter 2: Dead zones, obstructions, and missed captures: a novel approach for determining the Effective Capture Area for remote camera traps

2.1 — Abstract

1. Camera traps have become cemented as an important tool of wildlife research, yet, their utility is now extending beyond researchers, as cameras can contribute to more inclusive methods of place-based wildlife management. From recent advances in analytics and technology, camera trap-based density estimates of wildlife is an emerging field of research. Most camera trap-based density methods require an estimate of the area monitored by each camera, a relatively novel parameter that may be highly variable and is rarely quantified in literature.
2. Here, we developed and tested a standardized field and analytical method allowing us to predict the probability of photographic capture as it varies within the camera viewshed. We investigated how capture probability changes due to environmental influences, i.e., vegetation structure, ambient temperature, speed of subject, time of day, in addition to internal factors from cameras themselves, i.e., sensitivity settings, number of photos taken, and camera trap brand. We then use our method to gain standardized, accurate, and predictable estimates of the area a camera monitors, the Effective Capture Area (ECA).
3. We found that ECAs in our study areas are heavily influenced by location-specific environmental factors, i.e., vegetation structure, technological delays associated with cameras themselves, i.e., refractory period, and custom internal camera settings, i.e., sensitivity, number of photographs taken. We also found that the ECAs computed using our methodology are substantially smaller than reported values in the literature.

4. Imprecision surrounding camera trap viewshed areas can create propagating bias when implementing viewshed-based density estimators. Our method and Effective Capture Area calculation may help increase the reliability of camera trap-based density estimation methods, provide a framework to help improve camera-trap occupancy modeling, and contribute to more accessible wildlife management practices.

2.2 — Introduction

In recent history, camera traps have become an established method of studying and monitoring wildlife populations (Fisher, 2023; Sollmann, 2018). Camera traps are an easy-to-operate, accessible, relatively affordable, and low-impact method of monitoring wildlife. Camera traps have become an integral part of wildlife management allowing researchers to answer location-based questions of occupancy (e.g., Tobler et al. 2015; Neilson et al. 2018), movement (e.g., Tape and Gustine 2014), and behaviour (e.g., Caravaggi et al. 2017). As a result, camera traps are heavily used among wildlife researchers in general and North American colonial governments in particular. Recently, camera traps are becoming an important tool for Indigenous nations and other interested stakeholders to monitor and manage wildlife on their own lands (Fisher et al., 2021; Kemp, 2023).

Despite their common use, ambiguities around camera trap performance lead to uncertainty and decreasing the quality of inference made from some camera trap-based science. Among their limitations (e.g., Burton et al., 2015; Foster & Harmsen, 2012; Kolowski et al., 2021; Urbanek et al., 2019), empirically estimating the viewshed area a camera trap can monitor is perhaps the least studied, yet, most critical when considering wildlife space use and occupancy. Some research, however, has used animals in captivity to estimate the distances directly perpendicular to cameras where various species will have at least one photograph taken

(Rowcliffe et al. 2011; Becker et al. 2022). Camera trap data are frequently analyzed using occupancy models or similar frameworks (Burton et al., 2015; MacKenzie et al., 2002, 2017). Such approaches attempt to account for false negatives, i.e., when a species is present in an area but not captured by a camera, by integrating both the detection probability of a species in a broad study area and the capture probability of a camera photographing a species. Occupancy models can be fit many ways; however, most commonly use *post-hoc* methods such as constructing the detection history of a species across time at each camera trap (MacKenzie et al., 2017). Occupancy models have been shown to be capable of accommodating imperfect detection, i.e., of a species within the broader study area, at camera traps; however, occupancy models are limited in creating a standardized, *apriori* method to assess capture probability, i.e., of an individual in front of a camera trap.

Numerous density and abundance estimators of wildlife species have recently emerged as a novel analysis of camera trap data (e.g., Rowcliffe et al. 2008; Moeller et al. 2018; Nakashima et al. 2020; Becker et al. 2022). Camera trap-based methods, henceforth referred to as viewshed density estimators (Moeller et al., 2023), are a family of statistical models incorporating different processes to estimate wildlife density. For example, Nakashima et al. (2018) developed the Random Encounter Staying Time (REST) model, which measures the amount of time a species spends in front of a camera trap to generate density estimates. Using camera traps to estimate wildlife density may, long term, help lower financial and logistic barriers currently in place for other traditional density estimation methods, e.g., aerial surveys. In addition, the accessibility of implementing camera traps may allow viewshed density estimators to become more popular among Indigenous nations or other groups. Some viewshed density estimators do not require the identification of individual animals and thus may constrain less (e.g., no need to mark

individuals or census a population) than their traditional counterparts, such as physical mark-recapture methods or aerial flight surveys. Each viewshed density estimator, however, comes with its own set of assumptions and require novel parameters that we lack precision in estimating.

Although viewshed density estimators free us from identifying individual animals, they require a precise estimate of the sampling area that each camera trap monitors (Becker et al., 2022; Moeller et al., 2023; Nakashima et al., 2020; Rowcliffe et al., 2008). Imprecise estimation of the viewshed area is problematic because camera traps, even a large number being used together, monitor a relatively small area—often a minute percentage of a study region. As a result, small errors in the determining the sampling area can lead to large biases in abundance estimates when extrapolating fine-scale density estimates (Moeller et al., 2023). In addition, the theoretical area camera traps monitor often does not align with the realised area. Camera trap manufacturers report an ideal area a camera can monitor given perfect conditions and assuming the camera triggers a photo for every possible activation. For example, Reconyx Hyperfire camera traps, a very popular brand in wildlife research, market a viewshed area extending up to 30 m from the camera trap and 40° angle perpendicular to the camera's lens, an area approximating 315 m^2 (Reconyx 2022; Figure 2.1A). In reality, environmental factors such as habitat structure, topography, and vegetation (Moeller et al., 2023; Moll et al., 2020; Sultaire et al., 2023), will dictate a camera's viewshed area for each unique location where cameras are placed (Apps and McNutt 2018; Urbanek et al. 2019; Figure 2.1B).

Researchers also need to account for the probability a photo will be taken given an animal is located within the camera's viewshed, henceforth referred to as capture probability (Findlay et al., 2020; Moeller et al., 2023). Capture probability is more complicated and depends

on numerous, likely interacting conditions caused by the physical environment in which cameras are placed, and the internal camera settings. Variation in capture probability is influenced by camera traps Passive Infrared (PIR) motion detectors. PIR motion detectors require recognition of movement within pre-programmed zones, that vary between camera brands and models (Urbanek et al., 2019), as well as a heat signature that contrast ambient temperature, for a photograph to be taken (Reconyx, 2022; Welbourne et al., 2016). PIR motion detector performance influences capture probability. Yet, how PIR performance contributes to camera monitoring area and thus larger ecological processes remains unknown. Variability in PIR sensor performance may contribute to reports of differential performance throughout the literature, even among similar geography (Apps & McNutt, 2018; Heiniger & Gillespie, 2018).

Internal camera functioning and settings also dictate the viewshed area and how effectively cameras take photos (Apps & McNutt, 2018; Becker et al., 2022; Lepard et al., 2019; Urbanek et al., 2019). For example, even on rapid fire modes, many camera trap user manuals report a 1–2 s refractory period from the time the PIR motion detector is triggered until that photograph can be written to the memory storage device (Del Bosco, 2021; Paula et al., 2014; Reconyx, 2022). Because a camera must reset and register another trigger for subsequent photos to be taken, this phenomenon would be sequential across the entire period an animal is in a camera's viewshed. Thus, the trigger-to-photo delay could create a 'shutter-like' effect where an animal is present in the viewshed but, because of a refractory period, missing in photos for specific locations (Figure 2.1C). Additionally, to decrease the large number of false triggers, e.g., from vegetation moving, researchers often lower camera trap sensitivity settings, influencing the space a camera trap can monitor. To aid in the identification of species from camera photos, it is common practice to set camera traps to capture multiple rapid-fire photos. When doing this,

researchers often consider a photo series (i.e., all 3, 5, 10 photos) as a single event. As it takes camera traps more time to capture more photographs, however, increasing the number of photos per trigger will reduce the total viewshed area. The effects of internal camera settings have not been empirically incorporated into camera trap literature yet will have compounding influences on how effective camera traps are at photographing wildlife.

Though camera trap data can describe broader trends in population size well (Kenney et al. 2024), viewshed based density estimators are often criticized for density estimates that inconsistently align with traditional density estimation methods (e.g., Palencia et al. 2021; Becker et al. 2022; Fisher et al. 2023; Koetke et al. 2024). Although there may be many explanations for inconsistent results from viewshed density estimators, a lack of accuracy in, or entirely absent incorporation of viewshed area is undoubtedly one reason behind these discrepancies (Moeller et al., 2023). Here, we tested a standardized field protocol to 1) determine the unique bounds of independently placed camera-trap viewsheds (Figure 2.1B), 2) account for cameras refractory period when sequential photographs are taken (Figure 2.1C), 3) enumerate a kernel-based photographic capture probability and how it changes with space in front of cameras (Figure 2.1D), and 4) summarize these capture probability kernels into an *Effective Capture Area*—the scaled area in a cameras viewshed with a 100% capture rate.

2.3 — Methods

2.3.1 — Field methods

To assess capture probability, we tested a standardized field method in two separate case studies. We applied this method to each camera trap to calculate a novel capture probability metric, unique to each camera trap in our study that in Case Study A) accounts for differences

due to habitat and other location-specific influences and in Case Study B) incorporates variation resulting from internal camera settings.

2.3.2 — Case Study A

We tested 45 camera traps actively deployed as a part of a long-term monitoring program located on Treaty 2 territory, the traditional lands of the Anishinabewaki, Očhéthi Šakówiŋ, Cree, Oji-Cree, and the Homeland of the Métis peoples (Riding Mountain National Park, Canada; RMNP). Adapting methods from other researchers (Apps & McNutt, 2018; Del Bosco, 2021; Palencia et al., 2021), we established six 20 m long transects, perpendicular to and centred at the camera's optical axis at distances of 3, 5, 10, 12, 15, and 20m (Figure 2.2) from the lens. These transects were designed to extend past cameras' viewshed to determine the spatial bounds of where the cameras could capture photos. We then performed a 'jog-test' where one researcher attempted to jog at a speed of approximately 2 m/s along each transect, six times, for a total of 36 jogs per camera. With a timer, another researcher initiated each jog-test by triggering the camera using a hand motion to take a photo and recorded the time in seconds it took to jog across the full 20 m. We conducted jog-tests on two different camera brands deployed at our research sites: Reconyx Ultrafire (n = 9; Reconyx, Holmen, USA) and Cuddeback H-1453 (n = 36; Cuddeback, Green Bay, USA). We did not vary any internal settings between trials in Case Study A—all cameras were set to a high sensitivity setting and a single photograph taken for each trigger. Instead, we measured external factors known to affect capture probability. These included: distance from camera trap (McIntyre et al., 2020), vegetation cover in front of cameras (Moeller et al., 2023; Moll et al., 2020), ambient temperature (°C) at time of survey (Urbanek et al., 2019), speed (m/s) of jog for each transect (McIntyre et al., 2020), and camera trap model (Apps and McNutt 2018). In addition, to account for a refractory period after a photographic capture (Del

Bosco, 2021; Paula et al., 2014; Reconyx, 2022), we recorded whether cameras captured a photo in the previous two seconds. To measure vegetation cover, we conducted two surveys. (1) a shrub cover survey counting multi-stemmed woody species 10m in front of each camera by using the Daubenmire method on a 4 m radius plot (Daubenmire, 1959); and, (2) horizontal cover via a cover pole, placed 10m in front of cameras to quantify vegetation height.

2.3.3 — Case Study B

We conducted a series of jog-tests in an open, non-vegetated, flat field in a local park located on traditional unceded territories of the Beothuk and Mi'kma'ki peoples (St. John's, Canada). The trial used a controlled habitat to isolate the effect of internal camera settings on capture probability. In total, we surveyed 27 Reconyx Hyperfire 2 (Reconyx, Holem, USA) camera traps across 3 trials: two during daylight (~1400h) and one after sunset (~2300h). These trials were conducted to measure the influences of the internal camera sensitivity settings (Heiniger & Gillespie, 2018), the number of photos taken per motion trigger and refractory period following a photograph capture (Paula et al., 2014). In addition, we wanted to measure the deterioration of camera trap performance during the nighttime. We held camera settings constant across trials using specific combinations of settings (see Table 1 for all combinations). Due to the lack of visual obstructions during the daytime trials in the open field, we observed a higher-than-expected capture probability on the 20 m transect. Thus, for the two daytime trials we jogged an additional two transects at 30 and 40 m parallel to cameras to fully enumerate the decay of capture probability with distance (Figure 2.2).

2.3.4 — Analytical methods

To calculate a capture rate, we determined the time elapsed (s) between the transect start times and the time when each photograph was taken. Next, we calculated the speed of each transect jog

as the time taken to cross each transect divided by transect distance (m/s). We calculated spatial locations where all photographs were taken, i.e., used locations, by multiplying the time elapsed at each photograph by jog velocity to calculate the distance traveled along the transect. For trials where more than one photo were taken per trigger, we filtered photo series down to the first instance when a photograph of the jogger was taken. By using the same jog velocities, and transect start and end time, we calculated all spatial locations where photographs could have occurred, i.e., available locations. We excluded locations where photographs did occur from the available data thus, creating a 1-m grid-system along each transect where each cell had a binary outcome, whether a photographic capture occurred or not.

2.3.5 — Statistical models

We fit the binary capture data using Generalized Additive Mixed Models (GAMMs) using the mgcv package in Program R (Wood 2017) for each case study, separately. We used GAMMs to allow for a non-linear viewshed, that changes with space in front of cameras, by implementing a Gaussian Process spline on the parallel and perpendicular locations from cameras (Wood, 2017). For Case Study A, we created a single, saturated model including covariates measured in the field, i.e., parallel and perpendicular distances from camera trap, percent shrub, and vegetation cover in front of camera, ambient temperature (°C), velocity (m/s) of each jog, camera trap model (categorical), and whether a photograph had occurred in the previous 2 seconds (binary). Additionally, we implemented unique camera trap ID as a random factor smoother (Wood, 2017, 2023). For cameras assessed in Case Study B, in addition to the smoothed parallel and perpendicular locations (McIntyre et al., 2020), we included categorical covariates for each of the variables of interest: camera sensitivity setting, number of photos taken per motion trigger, time of day, and whether a capture had been taken in the previous two seconds (Table 2).

We used both GAMM models, along with covariate data from each trial, and the *predict_gamm()* function (Wood 2023) to predict the probability of photographic capture occurring across a 1x1-m extrapolated spatial grid both between transect lines and beyond the cameras' field of view, 10 m in both directions of the focal axis 40 m from the lens (e.g., 2.1D). We further applied these models to also predict capture probability at any cameras where data were collected (e.g., vegetation cover, ambient temperature) but that were not included in the trial tests.

Our primary goal was to determine the area that camera traps monitor with 100% capture probability: the Effective Capture Area (ECA). To achieve this, we multiplied the average probability of photographic capture in each of 800 predicted grid cells by their area ($1m^2$). Our approach assumes equivalency between predicted probabilities of photographic capture and the percent area monitored in each cell (discussed more below). Thus, the resulting values represent the equivalent area within each cell that a photograph would be captured with certainty. For example, a capture probability of 0.33 in a 1 m^2 cell is equivalent to having 0.33 m^2 of area with a perfect capture probability. We then took the sum of predicted values across all cells, representing the adjusted space in front of cameras with a 100% capture probability (Figure 2.1E), which we defined as the ECA. In addition, we determined standard error and confidence bounds for all ECA calculations. Because the ECA was determined through prediction, we wanted to ensure sufficient predictive accuracy of our analysis for our Case Study A field trial. Because a camera's monitoring area is unknown, we employed *k*-folds cross validation on the probability of photographic capture for spatial locations in front of each camera (Geisser, 1975). Using unique camera ID as a blocking variable, we withheld entire cameras to assess the predictive accuracy of each 1x1-m cell across camera traps and thus the validity of our method at

cameras where jog-tests were not conducted (Fielding & Bell, 1997). We generated Receiver Operating Characteristics (ROC) Area Under Curve (AUC) scores for each of these validations.

To determine how strongly the numeric covariates in Case Study A influence a cameras ECA, we calculated a *post-hoc* effect size through prediction. We ran separate predictions for each numeric covariate of interest—percent shrub cover, percent horizontal cover, velocity of jog, and ambient temperature—and generated ECA values across the observed range of each covariate while holding all other variables at their mean values. For example, horizontal cover ranged from 42–99%, thus we ran an ECA prediction for each unit (percent) value in that range. Next, we calculated the mean of all unit-change differences in ECA predictions. The resulting values represent the mean influence of a 1-unit change by a covariate on a camera's ECA. For Case Study B, we ran similar predictions, but for each level in the categories of interest, i.e., sensitivity setting and number of photos per trigger, while holding all other variables at constant values.

2.4 — Results

2.4.1 — Case Study A

We determined the predicted probability of a successful photographic capture occurring within a camera viewshed at a 1x1-m resolution (Figure 2.3A). For all cameras where we collected local site data, we calculated their unique capture probability distributions and scaled them to an ECA. For example, Figure 3A represents a Reconyx Ultrafire camera within our Riding Mountain National Park field site, with an average 62 % shrub cover, 79% horizontal cover, and an ambient air temperature of 1.5°C during survey time. Assuming a subject moving at a velocity of 2 m/s in the cameras viewshed area, we scaled these probabilities to an ECA of 15 m^2 and a standard error ranging from 8–27 m^2 (Figure 2.3A). Ambient temperature at time of jog-test

surveys ranged from -2–10°C, velocity of each jog from 0.76–2.86 m/s, percent shrub cover from 0–176 %, and percent horizontal cover from 42–98 %.

Covariates in the model showed varying levels of significance (Table 2). The parallel and perpendicular locations from camera traps, fit in a Gaussian process spline, was highly significant ($F = 42.655$, $p < 0.001$). In addition, the binary refractory period variable showed a significant negative relationship with photographic capture ($\beta = -0.955$, $p < 0.001$). Other covariates showed varying effects on ECAs (see Table 2). Percent unit changes in shrub ($\bar{x} = 0.211 m^2$) and horizontal cover ($\bar{x} = 0.213\ m^2$) had a relatively small influence on ECA. Absolute differences between the largest and smallest ECA prediction, however, were larger. The difference between the largest and smallest ECA was 86 m^2 for shrub cover and 50 m^2 for horizontal cover (Figure 2.6). A unit change in temperature (°C) had a larger influence on ECA, with a mean of $2.546 m^2$, and a maximum of $79 m^2$ difference between the maximum and minimum ECA predictions (Figure 2.6). Finally, unit changes in velocity (m/s) of each jog had the largest influence of ECA prediction, with a mean of $34.630 m^2$ and a maximum of $69 m^2$ between the largest and smallest predictions (Figure 2.6). The predictive accuracy of the model, assessed at each 1x1 m cell between camera traps, was good (AUC=0.76; Boyce et al. 2002).

2.4.2 — Case Study B

Our controlled, open field trials suggested that predetermined sensitivity settings have a large, significant influence on the probability of photographic capture and thus the ECA (Table 2). For example, our model estimated a maximum difference of approximately 250 m^2 in ECAs between the lowest and highest sensitivity settings on the Reconyx Hyperfire 2 cameras (Figure 2.4). The number of photos taken per trigger had a significant negative influence on ECA, where 3 and 5 photographs per capture produced significantly lower ECAs than 1 photo but were not different

from each other (Table 2, Figure 2.4). Jog-tests conducted in the daytime produced significantly higher ECAs ($\bar{x}$ = 151 m^2, SE =122–191 m^2) than the post-sunset jog-tests ($\bar{x}$ = 73 m^2, SE = 51–101 m^2, Table 2, Figure 2.5). The smoothed terms of the Case Study B model, i.e., parallel and perpendicular locations fit in a Gaussian process spline (F = 39.969, p <0.001), and refractory period variable (β = 1.669, p <0.001) were both highly significant.

2.5 — Discussion

Our study provides a tested field and analytical framework for determining the Effective Capture Area (ECA) of camera traps, an accurate viewshed area with a 100% capture probability, that incorporates capture probability and how it is influenced by local environmental variables and internal camera settings. We determined the ECA through a spatially predictive kernel-based photographic capture probability analysis, providing new insight into how capture probability varies within a camera's viewshed. Our metric to determine ECA, relied on the assumption of equivalency between predicted probability of photographic capture and percent area monitored in viewshed space. Though this assumption of equivalency may have varying validity depending on the study, we think here our assumption is robust as we rely heavily on the average effect of covariates. Additionally, our study design, which assessed locations multiple times in quick succession, has been shown to reduce bias in similar space-for-time equivalencies (Kendall and White, 2009). Our analysis, however, suggested that capture probabilities and the associated ECA are sensitive metrics and can vary substantially depending on both environmental influences and user-defined settings. Understanding and accurately estimating the ECA is crucial when implementing viewshed density estimators and may also contribute how researchers interpret camera-based occupancy analyses.

2.5.1 — Case Study A

In Case Study A, our goal was to develop an accurate metric to estimate the physical space camera traps monitor, specifically for use with viewshed density estimators. Though not statistically significant, our environmental covariates, i.e., shrub cover, horizontal cover, temperature, and jog velocity, still contributed considerable variability in ECA. For example, when holding other covariates at mean values, average per-unit changes in vegetation structure, shrub cover and horizontal cover can influence ECA by ~0.2 m^2. Although changes are small over single percentage changes, if we consider cameras with 50% differences in either shrub or horizontal cover, ECA could be influenced by over 10 m^2. Vegetation influences are likely even greater in affecting ECA, considering shrub and horizontal cover are additive, resulting in a compounded effect on ECA.

Though our jog-tests were conducted at relatively consistent velocities, we detected a large difference in ECA between unit (m/s) changes in jog velocity, with a mean of ~35 m^2. Further, our predictions show that slower jog speeds lead to higher ECAs. Our jog velocity results stand in contrast to previous findings (e.g., Del Bosco, 2021) who found that faster jog velocities generally lead to higher capture rates at camera traps. This discrepancy may be explained by the habitat in which jog-tests were conducted. Specifically, our tests took place in primary and secondary conifer and mixed forests whereas Del Bosco's (2021) work occurred in more open, sagebrush-mountain habitat. We suggest researchers consider both habitat composition as well as effective movement speed of the species of interest when implementing the jog-test method.

We detected a relatively small influence of unit changes of temperature on ECA, with a mean of ~2 m^2 per °C. This small influence is intuitive given the short duration when we

conducted jog-tests. For example, we conducted our Case Study A jog-tests on the edges of winter (April and November 2023). The time of year allowed us to safely access remote field sites, in addition to providing conditions consistent with when traditional density estimation surveys take place (e.g., aerial flight surveys in late winter) for future applications of this work. As a result, many of our covariates show little range. Ambient air temperatures at time of survey only ranged from -2–10°C, and total shrub was measured after leaf senescence in the fall, limiting observed variability. Although we would not expect camera traps to decrease performance until -20°C or below (Reconyx, 2022), it is worth noting that other research has observed camera traps performing best around 0°C, where higher false-negatives occur in positive temperature ranges (Jacobs & Ausband, 2018), and negative temperature ranges and associated weather can contribute to decreased performance (Maile et al., 2023). Conducting jog-tests during other seasons and within a greater range of forest types and habitat will likely contribute to detecting statistical differences in environmental covariates and help determine if a cameras ECA varies more substantially across space and time (e.g., as in McIntyre et al., 2020; Moeller et al., 2023; Moll et al., 2020; Sultaire et al., 2023; Urbanek et al., 2019).

ECA values generated from our Case Study A model are substantially smaller than other published literature. For example, an average Reconyx Ultrafire camera in our study was estimated to monitor an area of 16m^2 (ranging from 12–22m^2) with a perfect capture probability. Our average Reconyx ECA, in the Case Study A field trial, was less than 10% of the total possible area the camera trap advertises (Reconyx, 2022) and still smaller than other published monitoring areas (Becker et al., 2022; Garland et al., 2020). This indicated that implementing these detection areas on viewshed density estimators could produce density estimates that differ by an order of magnitude. Although cameras' capture probability area cannot be unilaterally

applied across different studies in varying geography and with different external influences, our work highlights the importance of conducting a standardized test on all cameras of a study when attempting to estimate monitoring areas.

Cross-validation of the probability of photographic capture occurring in each 1x1-m cell assessed during jog-tests highlighted that our ECA modeling framework has useful predictive accuracy. In addition, environmental covariates explained substantial variation in our model, as determined through average unit-changes. This result, along with our cross-validation results, suggest that, in our geography, we can predict ECA well at cameras where we did not conduct jog-tests, but did collect vegetation data.

2.5.2 — Case Study B

Overall, sensitivity settings on Reconyx Hyperfire II cameras greatly influenced the predicted ECA. Differences between lower sensitivity settings were smaller but became more pronounced as the sensitivity settings became higher. Model results on sensitivity settings show how drastically a camera traps monitoring zone can change with sensitivity settings, e.g., from ~75m^2 to ~350m^2 in open conditions, reinforcing the importance of consistency and assessing cameras in each location they are placed. Our results highlight the balance researchers need to consider when altering sensitivity settings to decrease false negative photographic captures, while risking tremendous loss of area in photographable space.

Predicted ECAs for trials set to take 3 or 5 photos per trigger were significantly smaller than trials with 1 photo per trigger, but not different from each other. As we take more photographs per event, the camera trap will be less able to capture future photographs. This is simply because, even on rapid fire modes, it takes longer for to capture and write 3 or 5 photographs than a single photograph. When considering a refractory period as well (discussed below) setting cameras to take more photos will greatly reduce the available time a camera has to take a photo and thus, the ECA. Though additional photos per trigger can be very useful in the identification of species, additional photos have an overall negative influence on a cameras viewshed area. Intuitively, trials conducted in the daytime had significantly higher detection, and thus ECA, compared to post-sunset trials. This is likely because the visible range of the camera trap will be reduced during nighttime, in addition to a reduced contrast from the subject to the background. Nighttime ECAs will be particularly important on camera trap studies for species that are predominately nocturnal, as viewshed area may be lower than anticipated.

2.5.3 — Camera refractory period

Our two case studies observed opposite effects of the refractory period variable. In Case Study A, we observed a significant negative relationship between capture probability within a 1x1-m cell and whether a photo was captured in the previous two seconds. This result met our null expectations that, due to a refractory delay, our cameras deployed in the field were less able to capture photos immediately after a previous photo had been taken. Our Case Study B model, however, exhibited the opposite trend and the refractory period variable was significantly positively correlated with capture probability, i.e., photos were more likely to be taken immediately following a previous capture. Contrasting results between the two Case Study models were likely due to the way we structured the Case Study B trials, where many trials took more than one photo per trigger. For example, in trials where cameras took 3 or 5 images per trigger, by artifact of camera trap shutter speed, the time it takes to capture 3 or 5 images is longer than 1 image. Thus, the refractory period of a camera would be longer if the camera trap is set to capture more images per trigger, e.g., potentially 3–6 seconds after the first photo in the series is captured.

The elongated refractory period caused by trials with more than 1 photograph taken per trigger is also likely responsible for the divergence in capture probability observed in our graphical representation of ECA in Case Study B (Figure 2.5). During trials where cameras were set to take multiple photos, if captures were registered at the start and end of transects, where a refractory period occurred near the midpoint of the trial, the pattern we observe of decreased capture probability directly perpendicular to cameras past ~14m could be explained (Figure 2.5). The gap in photograph captures would not be observed at closer distances to cameras because of

camera lens angle—there is physically less space within a camera's viewshed, explaining the gap in detection probability for trials with multiple photos per activation (Figure 2.5).

2.5.4 — Limitations and future directions

The functioning and performance of camera traps remains a heavily understudied facet of the field that certainly influences occupancy and density-based camera analyses and thus interpretation of camera trap-based research. In our work, how PIR sensors perform across temperature and seasonal gradients is particularly important. PIR detectors in camera traps function by sensing a difference in temperature of a subject from ambient temperature, in addition to movement, to capture a photograph (Reconyx, 2022; Welbourne et al., 2016). The interacting effects of ambient temperature and seasonality will influence the amount of heat wildlife subjects will emit. For example, in winter, ungulates have thick winter coats that allow them to retain heat and survive harsh conditions and as such, less heat may be escaping the coat (Parker and Robbins 2018). A lack of heat emission has been previously observed in thermal imaging studies, where thermal cameras have a difficult time picking up certain species during certain temperature ranges (Kuhn & Meyer, 2009; Zabel et al., 2023). As a result, capture probability may be even lower during mid-winter months for some wildlife species.

Camera traps are influenced, to some degree, by the size of the subject they are capturing (DeWitt & Cocksedge, 2023). For example, Urbanek et al. (2019) observed that raw number of photographs at camera traps were similar for species groups that were generally the same size. The pattern in Urbanek et al. (2019) data suggests a potential trigger threshold where above certain body sizes, the number of photographs taken (and thus ECA) may increase. We think that our approach will work well for some species, particularly ungulates, based on height, but would not work well for others, such as species generally smaller than humans.

Our GAMM model was developed to incorporate important predictor variables specifically at our field site in Riding Mountain National Park (MB, Canada). We hypothesized the largest influencing factor to cameras would be vegetation, specifically shrub cover. Although vegetation cover in our study had a relatively lower influence on ECA (Table 2, Figure 2.6), the importance of different predictor variables, will likely depend on the geography and habitat conditions of the study. For example, topography (Sultaire et al., 2023) and weather (Madsen et al., 2020) have been found to influence camera trap capture probabilities in some geographies. Thus, if implementing our method, researchers should consider all potential important predictor variables that may influence capture probability at their study sites.

2.5.5 — Conclusion

We use a standardized, *apriori* field and analytical protocol to predict the variable probability of photographic capture at camera traps while incorporating internal and environmental influences on camera performance. We use our predictions of capture probability to estimate the Effective Capture Area (ECA), a novel estimator that represents the scaled area in front of cameras with a 100% capture probability. Our results highlight how variable camera trap performance can be and provide a framework for researchers and other camera trap users to account for variable viewshed areas and capture probabilities for some taxa of wildlife. ECA may contribute to increasing the reliability and precision of camera-based occupancy modeling as well as viewshed density estimators and thus forward the growing branch of camera trap research.

2.6 — Literature cited

Apps, P., & McNutt, J. W. (2018). Are camera traps fit for purpose? A rigorous, reproducible and realistic test of camera trap performance. *African Journal of Ecology*, *56*(4), 710–720. https://doi.org/10.1111/aje.12573

Becker, M., Huggard, D. J., Dickie, M., Warbington, C., Schieck, J., Herdman, E., Serrouya, R., & Boutin, S. (2022). Applying and testing a novel method to estimate animal density from motion-triggered cameras. *Ecosphere*, *13*(4). https://doi.org/10.1002/ecs2.4005

Boyce, M. S., Vernier, P. R., Nielsen, S. E., & Schmiegelow, F. K. A. (2002). Evaluating resource selection functions. *Ecological Modeling*, *157*, 281–300. https://doi.org/10.1016/S0304-3800(02)00200-4

Burton, A. C., Neilson, E., Moreira, D., Ladle, A., Steenweg, R., Fisher, J. T., Bayne, E., & Boutin, S. (2015). Wildlife camera trapping: A review and recommendations for linking surveys to ecological processes. *Journal of Applied Ecology*, *52*(3), 675–685. https://doi.org/10.1111/1365-2664.12432

Caravaggi, A., Banks, P. B., Burton, A. C., Finlay, C. M. V., Haswell, P. M., Hayward, M. W., Rowcliffe, M. J., & Wood, M. D. (2017). A review of camera trapping for conservation behaviour research. *Remote Sensing in Ecology and Conservation*, *3*(3), 109–122. https://doi.org/10.1002/rse2.48

Daubenmire, R. (1959). A canopy-coverage method of vegetational analysis. *Northwest Science*, *33*, 43–64.

Del Bosco, T. (2021). *An eulerian perspective on spring migration in mule deer* [MSc. Thesis]. Utah State University.

DeWitt, P. D., & Cocksedge, A. G. (2023). A simple framework for maximizing camera trap detections using experimental trials. *Environmental Monitoring and Assessment*, *195*(11), 1381. https://doi.org/10.1007/s10661-023-11945-9

Fielding, A. H., & Bell, J. F. (1997). A review of methods for the assessment of prediction errors in conservation presence/absence models. *Environmental Conservation*, *24*(1), 38–49. https://doi.org/10.1017/S0376892997000088

Findlay, M. A., Briers, R. A., & White, P. J. C. (2020). Component processes of detection probability in camera-trap studies: Understanding the occurrence of false-negatives. *Mammal Research*, *65*(2), 167–180. https://doi.org/10.1007/s13364-020-00478-y

Fisher, J. T. (2023). Camera trapping in ecology: A new section for wildlife research. *Ecology and Evolution*, *13*(3), e9925. https://doi.org/10.1002/ece3.9925

Fisher, J. T., Dickie, M., Burgar, J. M., Burton, A. C., & Serrouya, R. (2023). Density estimates of unmarked mammals: comparing two models and assumptions across multiple species and years. *Canadian Journal of Zoology*, *102(3)*, 286–297. cjz-2023-0055. doi:10.1139/cjz-2023-0055.

Fisher, J. T., Grey, F., Anderson, N., Sawan, J., Anderson, N., Chai, S.-L., Nolan, L., Underwood, A., Amerongen Maddison, J., Fuller, H. W., & Frey, S. (2021). Indigenous-led camera-trap research on traditional territories informs conservation decisions for resource extraction. *FACETS*, *6*, 1266–1284. https://doi.org/10.1139/facets-2020-0087

Foster, R. J., & Harmsen, B. J. (2012). A critique of density estimation from camera-trap data. *The Journal of Wildlife Management*, *76*(2), 224–236. https://doi.org/10.1002/jwmg.275

Garland, L., Neilson, E., Avgar, T., Bayne, E., & Boutin, S. (2020). Random Encounter and Staying Time Model Testing with Human Volunteers. *The Journal of Wildlife Management*, *84*(6), 1179–1184. https://doi.org/10.1002/jwmg.21879

Geisser, S. (1975). The predictive sample reuse method with applications. *Journal of American Statistical Association*, *70*, 320–328. https://doi.org/10.1080/01621459.1975.10479865

Heiniger, J., & Gillespie, G. (2018). High variation in camera trap-model sensitivity for surveying mammal species in northern Australia. *Wildlife Research*, *45*(7), 578. https://doi.org/10.1071/WR18078

Jacobs, C. E., & Ausband, D. E. (2018). An evaluation of camera trap performance – What are we missing and does deployment height matter? *Remote Sensing in Ecology and Conservation*, *4*(4), 352–360. https://doi.org/10.1002/rse2.81

Kemp, C. (2023). *Optimizing Community-Based Wildlife Monitoring: Prioritizing Indigenous Knowledge and Values* [MSc. thesis]. University of Guelph.

Kendall, W. L., & White, G. C. (2009). A cautionary note on substituting spatial subunits for repeated temporal sampling in studies of site occupancy. *Journal of Applied Ecology, 46*, 1182–1188. https://doi.org/10.1111/j.1365-2664.2009.01732.x

Koetke, L. J., Hodder, D. P., & Johnson, C. J. (2024). Using camera traps and N-mixture models to estimate population abundance: Model selection really matters. *Methods in Ecology and Evolution, 2024;00:1–16.* https://doi.org/10.1111/2041-210X.14320

Kolowski, J. M., Oley, J., & McShea, W. J. (2021). High-density camera trap grid reveals lack of consistency in detection and capture rates across space and time. *Ecosphere*, *12*(2). https://doi.org/10.1002/ecs2.3350

Kenney AJ, Boutin S, Jung TS, Murray DL, Johnson N, Krebs CJ. 2024. Motion-sensitive cameras track population abundance changes in a boreal mammal community in

southeastern Yukon, Canada. Journal of Wildlfie Management. 88:e22564. https://doi.org/10.1002/jwmg.22564

Kuhn, R., & Meyer, W. (2009). Infrared thermography of the body surface in the Eurasian otter Lutra lutra and the giant otter Pteronura brasiliensis. *Aquatic Biology*, *6*, 143–152. https://doi.org/10.3354/ab00176

Lepard, C. C., Moll, R. J., Cepek, J. D., Lorch, P. D., Dennis, P. M., Robison, T., & Montgomery, R. A. (2019). The influence of the delay-period setting on camera-trap data storage, wildlife detections and occupancy models. *Wildlife Research*, *46*(1), 37. https://doi.org/10.1071/WR17181

MacKenzie, D. I., Nichols, J. D., Lachman, G. B., Droege, S., Andrew Royle, J., & Langtimm, C. A. (2002). Estimating site occupancy rates when detection probabilities are less than one. *Ecology*, *83*(8), 2248–2255. https://doi.org/10.1890/0012-9658(2002)083[2248:ESORWD]2.0.CO;2

MacKenzie, D. I., Nichols, J. D., Royle, J. A., Pollock, K. H., Bailey, L. L., & Hines, J. E. (2017). Occupancy estimation and modelling: Inferring patterns and dynamics of species occurrence. Elsevier.

Madsen, A. E., Corral, L., & Fontaine, J. J. (2020). Weather and exposure period affect coyote detection at camera traps. *Wildlife Society Bulletin*, *44*(2), 342–350. https://doi.org/10.1002/wsb.1080

Maile, R. E., Duggan, M. T., & Mousseau, T. A. (2023). The successes and pitfalls: Deep-learning effectiveness in a Chernobyl field camera trap application. *Ecology and Evolution*, *13*(9), e10454. https://doi.org/10.1002/ece3.10454

McIntyre, T., Majelantle, T. L., Slip, D. J., & Harcourt, R. G. (2020). Quantifying imperfect camera-trap detection probabilities: Implications for density modeling. *Wildlife Research*, *47*(2), 177. https://doi.org/10.1071/WR19040

Moeller, A. K., Lukacs, P. M., & Horne, J. S. (2018). Three novel methods to estimate abundance of unmarked animals using remote cameras. *Ecosphere*, *9*(8), e02331. https://doi.org/10.1002/ecs2.2331

Moeller, A. K., Waller, S. J., DeCesare, N. J., Chitwood, M. C., & Lukacs, P. M. (2023). Best practices to account for capture probability and viewable area in camera-based abundance estimation. *Remote Sensing in Ecology and Conservation*, *9*(1), 152–164. https://doi.org/10.1002/rse2.300

Moll, R. J., Ortiz-Calo, W., Cepek, J. D., Lorch, P. D., Dennis, P. M., Robison, T., & Montgomery, R. A. (2020). The effect of camera-trap viewshed obstruction on wildlife detection: Implications for inference. *Wildlife Research*, *47*(2), 158. https://doi.org/10.1071/WR19004

Nakashima, Y., Fukasawa, K., & Samejima, H. (2018). Estimating animal density without individual recognition using information derivable exclusively from camera traps. *Journal of Applied Ecology*, *55*(2), 735–744. https://doi.org/10.1111/1365-2664.13059

Nakashima, Y., Hongo, S., & Akomo-Okoue, E. F. (2020). Landscape-scale estimation of forest ungulate density and biomass using camera traps: Applying the REST model. *Biological Conservation*, *241*, 108381. https://doi.org/10.1016/j.biocon.2019.108381

Neilson, E. W., Avgar, T., Burton, A. C., Broadley, K., & Boutin, S. (2018). Animal movement affects interpretation of occupancy models from camera-trap surveys of unmarked animals. *Ecosphere*, *9*(1). https://doi.org/10.1002/ecs2.2092

Palencia, P., Rowcliffe, J. M., Vicente, J., & Acevedo, P. (2021). Assessing the camera trap methodologies used to estimate density of unmarked populations. *Journal of Applied Ecology*, *58*(8), 1583–1592. https://doi.org/10.1111/1365-2664.13913

Parker, K. L., & Robbins, C. T. (2018). Thermoregulation in ungulates. In *Bioenergetics of wild herbivores* (pp. 161–182). CRC press.

Paula, J. J. S., Bispo, R. M. B., Leite, A. H., Pereira, P. G. S., Costa, H. M. R. G., Fonseca, C. M. M. S., Mascarenhas, M. R. T., & Bernardino, J. L. V. (2014). Camera-trapping as a methodology to assess the persistence of wildlife carcasses resulting from collisions with human-made structures. *Wildlife Research*, *41*(8), 717. https://doi.org/10.1071/WR14063

Reconyx. (2022). *Reconyx Hyperfire 2 high performance camera instruction manual*. https://www.reconyx.com/img/file/HyperFire_2_User_Guide_2018_07_05_v5.pdf

Rowcliffe, J. M., Field, J., Turvey, S. T., & Carbone, C. (2008). Estimating animal density using camera traps without the need for individual recognition. *Journal of Applied Ecology*, *45*(4), 1228–1236. https://doi.org/10.1111/j.1365-2664.2008.01473.x

Rowcliffe, J. M., Carbone, C., Jansen, P.A., Kays, R., & Kranstauber, B. (2011). Quantifying the sensitivity of camera traps: an adapted distance sampling approach. *Methods in Ecology and Evolution*, 2, 464–476. doi: 10.1111/j.2041-210X.2011.00094.x

Sollmann, R. (2018). A gentle introduction to camera-trap data analysis. *African Journal of Ecology*, *56*(4), 740–749. https://doi.org/10.1111/aje.12557

Sultaire, S. M., Millspaugh, J. J., Jackson, P. J., & Montgomery, R. A. (2023). The influence of fine-scale topography on detection of a mammal assemblage at camera traps in a mountainous landscape. *Wildlife Biology*, *2023*(2). https://doi.org/10.1002/wlb3.01026

Tape, K. D., & Gustine, D. D. (2014). Capturing Migration Phenology of Terrestrial Wildlife Using Camera Traps. *BioScience*, *64*(2), 117–124. https://doi.org/10.1093/biosci/bit018

Tobler, M. W., Zúñiga Hartley, A., Carrillo-Percastegui, S. E., & Powell, G. V. N. (2015). Spatiotemporal hierarchical modeling of species richness and occupancy using camera trap data. *Journal of Applied Ecology*, *52*(2), 413–421. https://doi.org/10.1111/1365-2664.12399

Urbanek, R. E., Ferreira, H. J., Olfenbuttel, C., Dukes, C. G., & Albers, G. (2019). See what you've been missing: An assessment of Reconyx® PC900 Hyperfire cameras. *Wildlife Society Bulletin*, *43*(4), 630–638. https://doi.org/10.1002/wsb.1015

Welbourne, D. J., Claridge, A. W., Paull, D. J., & Lambert, A. (2016). How do passive infrared triggered camera traps operate and why does it matter? Breaking down common misconceptions. *Remote Sensing in Ecology and Conservation*, *2*(2), 77–83. https://doi.org/10.1002/rse2.20

Wood, S. (2017). *Generalized Additive Mixed Models: An introduction with R*. CRC press.

Wood, S. (2023). mgcv: Mixed GAM computation vehicle with automatic smoothness estimation. *R Package: Version 1.9-0*. https://cran.r-project.org/web/packages/mgcv/index.html

Zabel, F., Findlay, M. A., & White, P. J. C. (2023). Assessment of the accuracy of counting large ungulate species (red deer *Cervus elaphus*) with UAV-mounted thermal infrared cameras during night flights. *Wildlife Biology*, *2023*(3), e01071. https://doi.org/10.1002/wlb3.01071

Table 2.1 The combinations of camera sensitivity settings, number of photos taken for each passive infrared motion trigger, and time of day we implemented on to Reconyx Hyperfire 2 (n = 26) camera traps during Case Study B, in a controlled, open field setting, in St. John's Canada.

Trial type	Number of cameras	Sensitivity setting	Number of photos per trigger	Time of day
Sensitivity	3	Low	1	Day
	3	Medium	1	Day
	3	Very high	1	Day
Number of photos	3	High	1	Day
	3	High	3	Day
	3	High	5	Day
Night	9	High	1	Night

Table 2.2 Binary Generalized Additive Mixed Models (GAMMs) used in determining the Effective Capture Areas of (a) camera traps (n = 46) in Riding Mountain National Park, Canada and (b) camera traps (n = 27) in a non-vegetated local park near St. John's, Canada. Showing different predictor variables used in each model, with their respective explanations, coefficient values, and probability values. Both models contain the parallel and perpendicular locations in front of each camera trap with splines implemented, in addition to unique camera identification implemented as a random intercept.

Riding Mountain National Park field data (Case Study A) model:				Controlled setting data Case Study B) model:			
Covariate	Explanation	Coefficient (χ^2 for smoothed terms)	p-value	Covariate	Explanation	Coefficient (χ^2 for smoothed terms)	p-value
s(parallel distance, perpendicular distance)	Gaussian process spline of the parallel (locations in front) and perpendicular (locations to the side) of camera traps	**829.978**	**<0.001**	**s(parallel distance, perpendicular distance)**	Gaussian process spline on parallel (in front) and perpendicular locations (to the side) of camera traps	**1009.3**	**<0.001**
te(shrub cover, horizontal cover)	Tensor product spline of percent shrub cover (determined by Daubenmire plots) and horizontal cover (determined from cover pole)	1.435	0.707	Low camera sensitivity	Categorical variable for the sensitivity setting chosen on each camera trap for a specific trial	Set as intercept	
				Medium camera sensitivity		**1.076**	**<0.001**
				High camera sensitivity		**1.837**	**<0.001**
				Very high camera sensitivity		**3.479**	**<0.001**
Photo taken in previous 2 seconds	Binary variable of whether the camera took a photo in the previous two seconds	**-1.064**	**<0.001**	1 photo per trigger	Categorical variable for the number of photos taken per trigger setting chosen on each camera	Set as intercept	
				3 photos per trigger		**-1.266**	**<0.001**
				5 photos per trigger		**-1.186**	**<0.001**

					trap for a specific trial		
Jog velocity	Velocity of each transect jog during the field surveys	0.211	0.126	Nighttime trial	Whether or not trials occurred during daylight or night hours	Set as intercept	
				Day-time trial		**1.072**	**<0.001**
Ambient temperature	Ambient temperature (°C) measured from camera traps at time of survey	0.082	0.428	**Photo taken in previous 2 seconds**	Binary variable of whether the camera took a photo in the previous two seconds	**0.173**	**0.047**
Camera model	Categorical variable for the brand of camera trap (Reconyx or cuddeback) used in the field trials	-0.370	0.527				
s**(unique camera ID)**	Random factor smooth implemented on each unique camera trap	**358.793**	**<0.001**	**s(unique camera ID)**	Random factor smooth implemented on each unique camera trap	**24.7**	**<0.001**

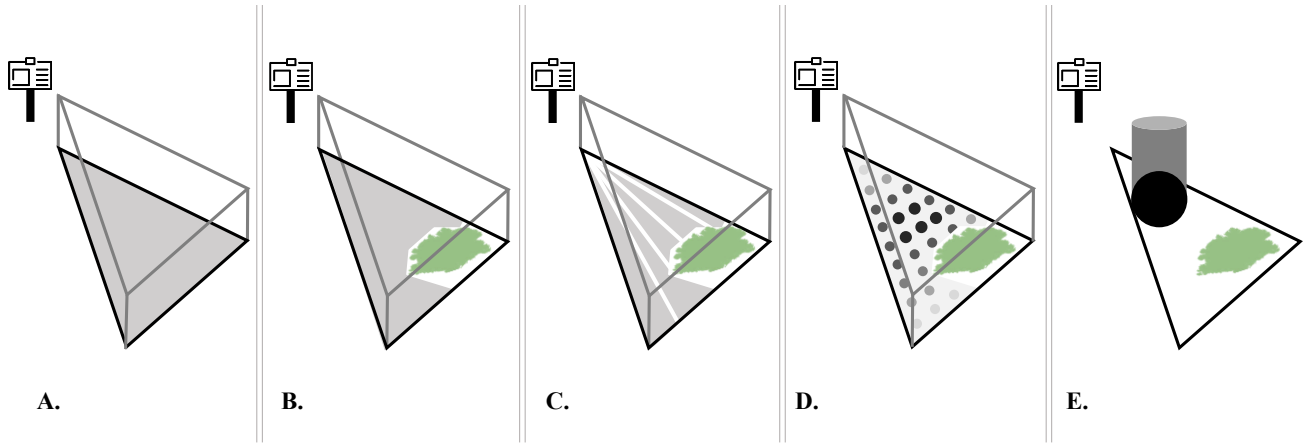

Figure 2.1 Viewshed areas for camera traps (grey shading) **A.** theoretical viewshed based on Reconyx Hyperfire 2 specification, e.g., 40° angle and 30 m distance, **B.** theoretical viewshed that might account for vegetation obstruction **C.** a theoretical viewshed that addresses refractory period in a camera trap, e.g., a camera could be triggered in the entire viewshed, but lacking photos for certain locations **D.** differential capture probabilities in a viewshed, where darker dots indicate a higher probability of photographic capture occurring and **E.** differential capture probabilities scaled down into our *Effective Capture Area*—an estimated area in front of a camera with 100% capture probability.

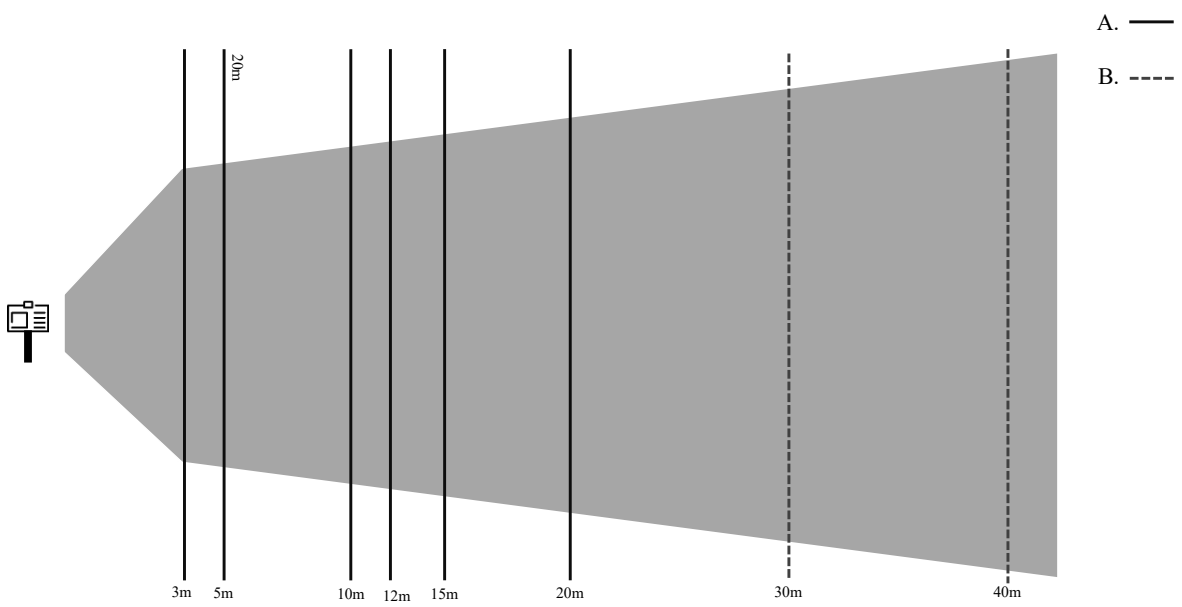

Figure 2.2 Transects and distances assessed on 'jog-tests' during **A.** field trials in Riding Mountain National Park, Canada (n = 45 cameras) at 3, 5, 10, 12, 15, and 20 m perpendicular to each camera trap and **B.** additional transects assessed at our daytime controlled setting trials in St. John's, Canada (n = 26 cameras) at 3, 5, 10, 12, 15, 20, 30, and 40 m perpendicular to camera traps. All transects were assessed 6 times at an approximate velocity of 2 m/s.

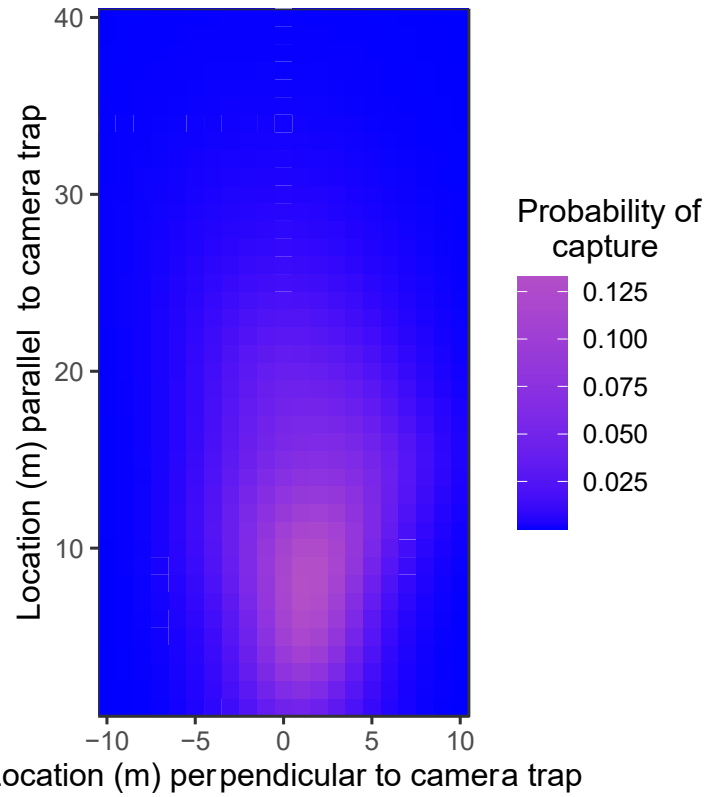

Figure 2.3 Predicted probabilities of photographic capture, determined by Generalized Additive Mixed Models, on a 1x1 m grid for an average Reconyx Ultrafire camera in Case Study A, with 62 % shrub cover, a subject moving at a 2 m/s velocity, and an ambient air temperature of 1.5°C. The predicted Effective Capture Area (± 1 standard error) for this camera was determined to be 15 m^2 (8–27m^2). The camera traps is located at position [0,0] on the grid.

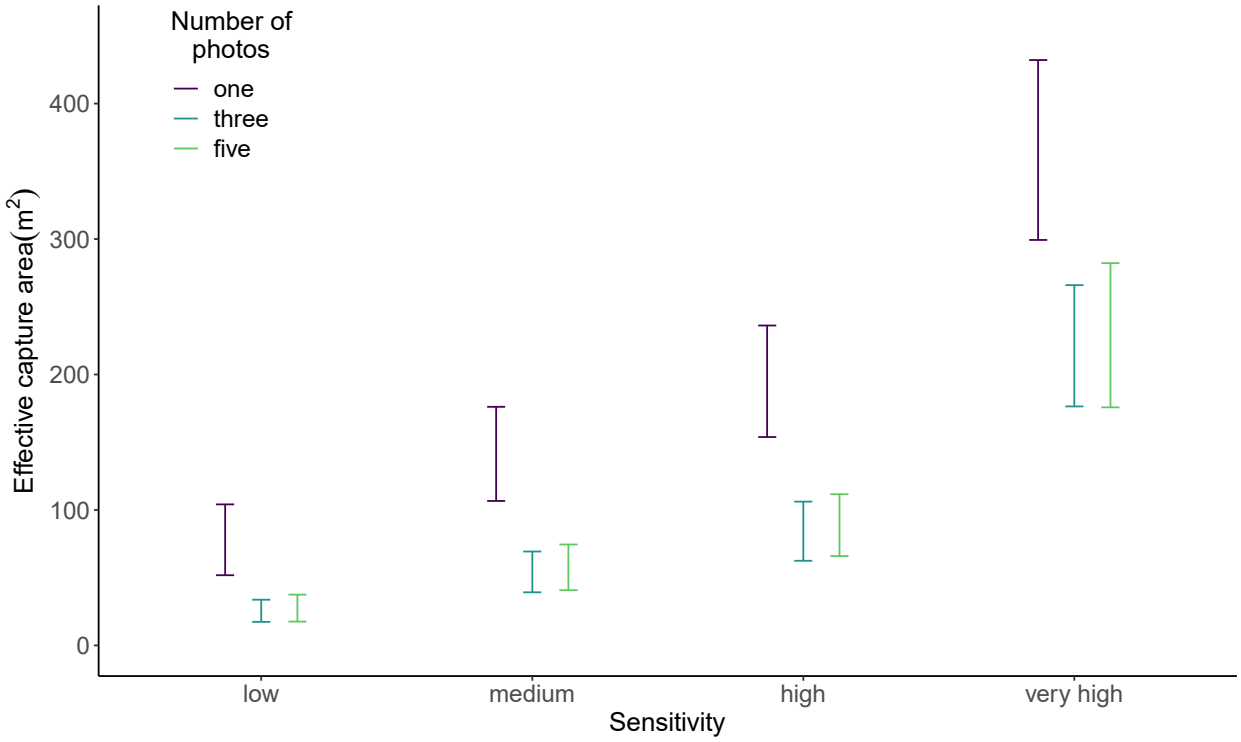

Figure 2.4 Effects of different sensitivity settings (low, medium, high, very high) and number of photos taken per each Passive Infrared Motion trigger (one, three, five) on the predicted Effective Capture Areas ($m^2 \pm$ standard error) of Reconyx Hyperfire 2 camera traps ($n = 26$) predicted from Generalized Additive Mixed Models during our controlled setting trials for Case Study B.

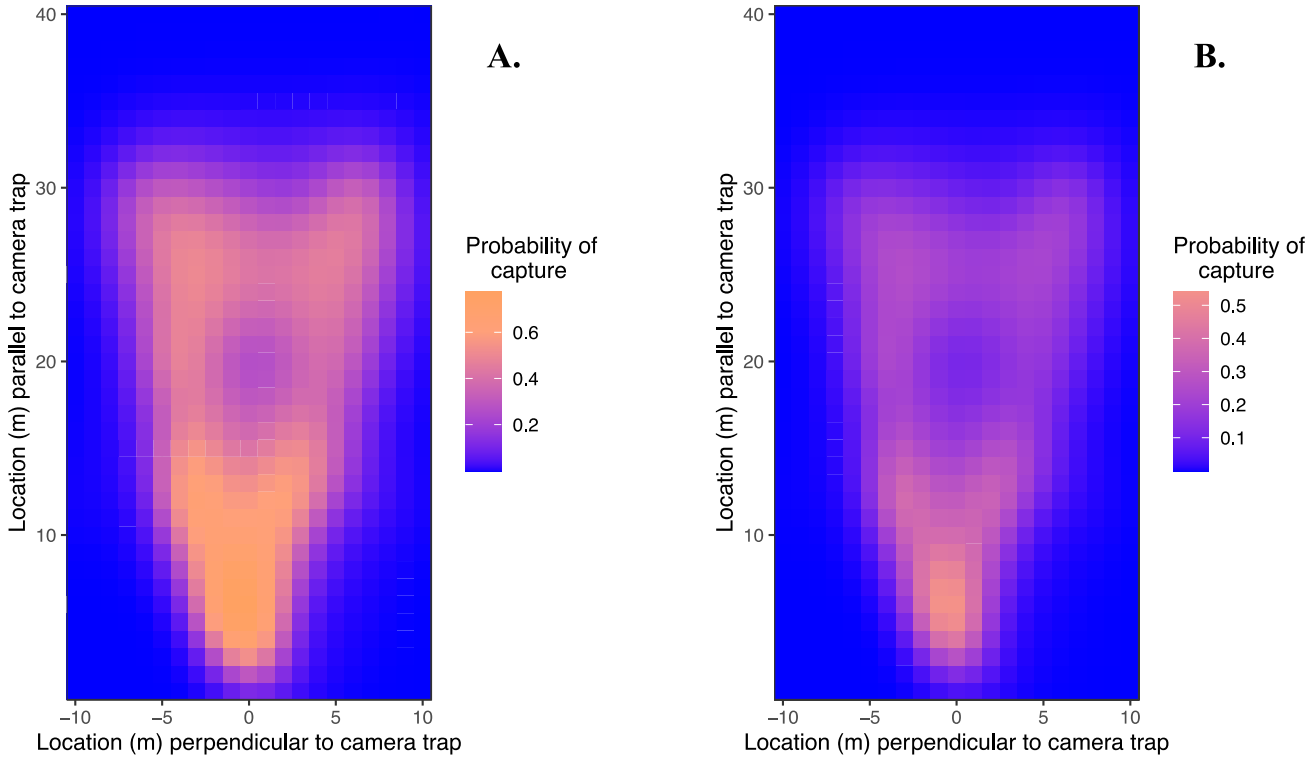

Figure 2.5 Predicted probabilities of photographic capture, predicted with Generalized Additive Mixed Models, on a 1x1 m grid for Reconyx Hyperfire 2 cameras, assuming a "medium" sensitivity setting, and a single photo taken for each Passive Infrared motion detector trigger during **A**. daytime trials and **B.** nighttime trials. Cameras are located at position [0,0] on each figure. The Adjusted Detection Areas (± standard error) were determined to be 151 m^2 (122–191 m^2) for daytime (**A**) and 73 m^2 (53–101 m^2) for nighttime (**B**).

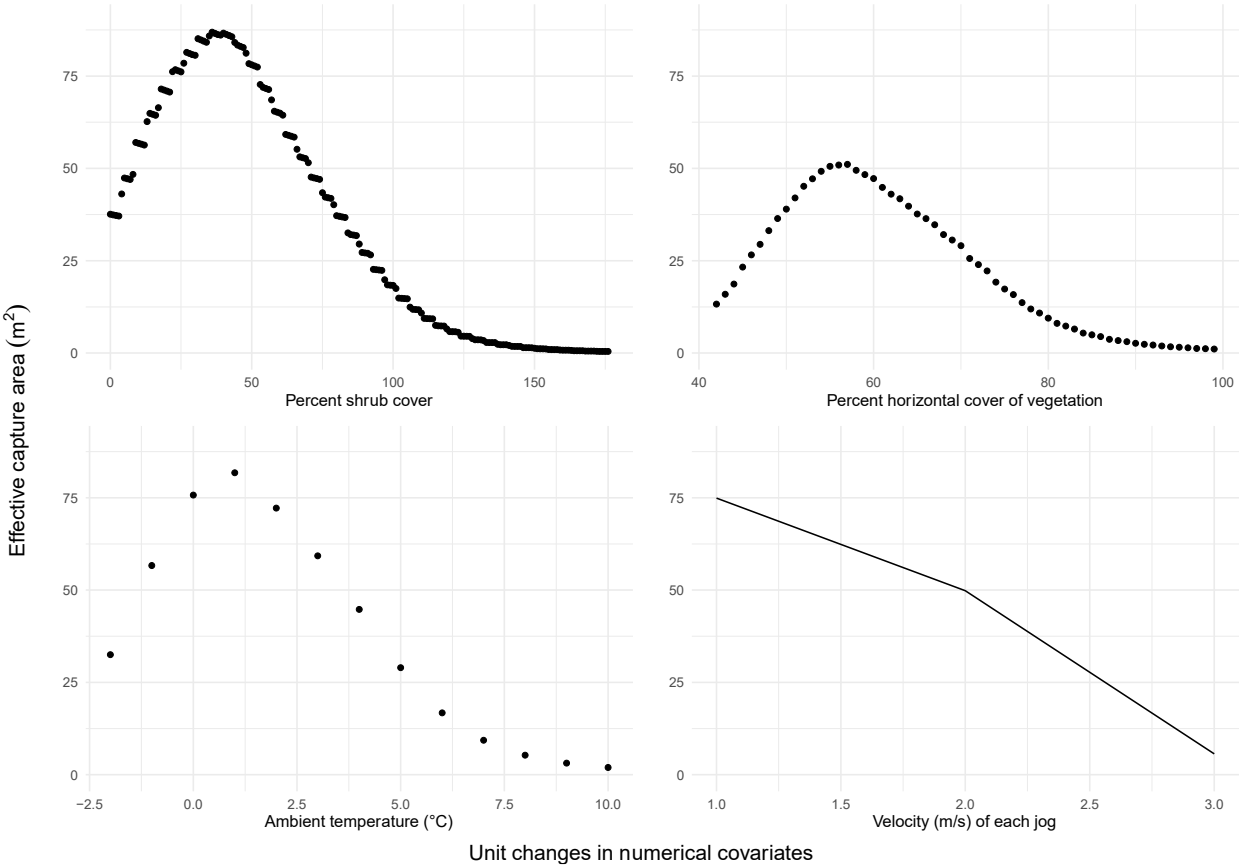

Figure 2.6 The predicted influence of unit changes of numerical covariates across their measured range in Case Study A, i.e., percent shrub cover, percent horizontal cover of vegetation, ambient air temperate (°C) at time of survey, and velocity (m/s) of each jog, on the Effective Capture Area at a given camera trap. For each numerical covariate of interest, all other covariates are held at their mean value for all predictions.

2.7 — Supplementary materials Chapter 2

Supplement S.2.1 Data collection on environmental covariates in Riding Mountain National Park, Case Study A

During our jog-tests in the field, we collected data on several environmental covariates in front of cameras. For the purposes of the Effective Capture Area in Case Study A, we wanted a comprehensive measure of vegetation in front of camera traps. We created a central point for all camera traps assessed 10 m directly in front of the camera lens. To account for vegetation height, we collected an average horizontal cover at each camera trap. We placed a cover pole at the central marker, and took four readings (A.1, A.2, A.3, A.4), each 10 m away from the pole in each cardinal direction (Robel et al. 1970). We also established a 3.99 m radius plot at the central marker and conducted a Daubenmire plot, where we measured the species and respective cover of all woody-stemmed species in the plot (Daubenmire 1959). These surveys combined were designed to account for both the vegetation height (horizontal cover) and vegetation thickness (shrub cover) at each camera trap.

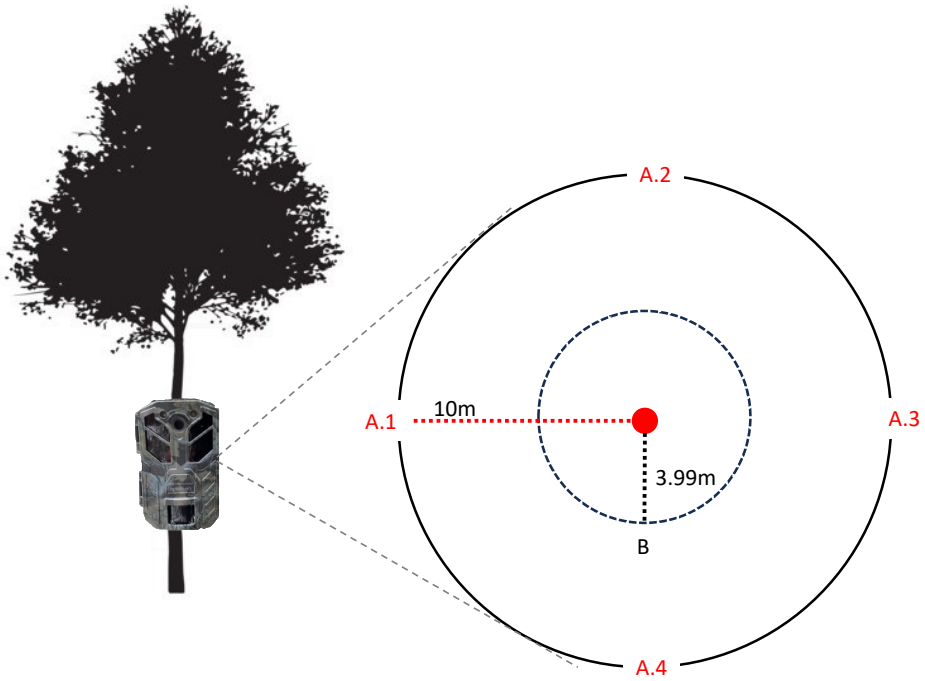

Figure S.2.1.1 How vegetation covariates were collected at camera traps (n = 54) within Riding Mountain National Park, for our Case Study A analysis. Showing (A), locations where horizontal cover measurements were taken with a cover pole, and (B), location where 3.99 m vegetation surveys were conducted. Note: the red, central point, was located 10 m directly in front of camera traps.

Daubenmire, R. 1959. A canopy-coverage method of vegetational analysis. Northwest Science. 33, 43-64.

Robel, RJ., JN. Briggs, Dayton, AD., and Hulbert, LC. 1970. Relationships between visual obstruction measurements and weight of grassland vegetation. *Journal of Range Management*, *23*(4), 295–297. https://doi.org/10.2307/3896225

Supplement S.2.2 Determining the potential temporal footprint of a camera trap image

As a result of technological delays, even on the fastest firing settings, remote camera traps may not be able to capture photographs at every possible second they are active (Reconyx, 2022). This technological delay phenonenom, referred to here as a refractory peroid, is a result of the cumulative time it takes for a camera trap to 1) register a motion with its PIR motion detector, 2) capture a photograph, 3) write a photograph to its Secure Digital (SD) card, and 4) reset before registering a subsequent motion. Previous works (e.g., Paula et al., 2014) have noted delays in camera trap sensors contributing to a loss of data, and one work (i.e., Del Bosco, 2021) suggested this refractory peroid may be ~2 s in time. Enumerating a camera refractory peroid will influence the temporal footprint of a cameras photograph, i.e., how much time a single photograph represnets. In addition, a refractory peroid may influence what is considered 'available' in our jog-test analysis.

To determine an images temportal footprint, we investigated the range of times between subsequent photographs for each (n = 36) jog during our jog-tests at all cameras for both Case Study A and B (Table S.2.2.1). The mean and maximum values of this metric are inherently flawed, as they represent the infleunce of both a refractory peroid or a missed photographic capture due to other infuences (e.g., vegetation cover). The mininum value, however, will represent the fastest possible time, in seconds, that a camera is able to capture subsequent photographs. For our Case Study B jog-tests, where some cameras were set to capture multiuple rapid-fire photos, we calculated the time between the first photo in the photoseries. This decision reflects the commonality of researchers setting cameras to take multiple, rapid-fire photos for species identification purposes, yet only considering a single photo in the series.

Table S.2.2.1 and Figure S.2.2.2 shows that in both Case Study A and B, the mininum possible time for subsequent photographs in our jog-tests is 1 s. In addition, the mean time between subsequent photos is 2.33 s, and 1.53 s in Case Study A and B respectively. This proposes that photographic captures could be possible every second of the jog-test, however, the mean time between subsequent images sugggest that technolgical delays put a photographs temporal footprint at ~2 s. This result forms the basis of our decision to only exclude locations where photographs were taken from the available set in the jog-test analysis, but model the infleunce of a 2 second refractory peroid as a covariate in the GAMM model (see Chapter 2 methods).

Table S.2.2.1 Determining the range (mininum, maximnum, and mean) of time between subsequent photographic captures for our jog-tests in Case Study A and B. The mininum and mean time between subsequent photographs suggests camera traps refractory peroid, and aids in delineating the temporal footprint of a single photograph.

	Case Study A	Case Study B
Mean time between subsequent images (seconds)	2.33	1.53
Maximum time between subsequent images (seconds)	8	7
Mininum time between subsequent images (seconds)	1	1

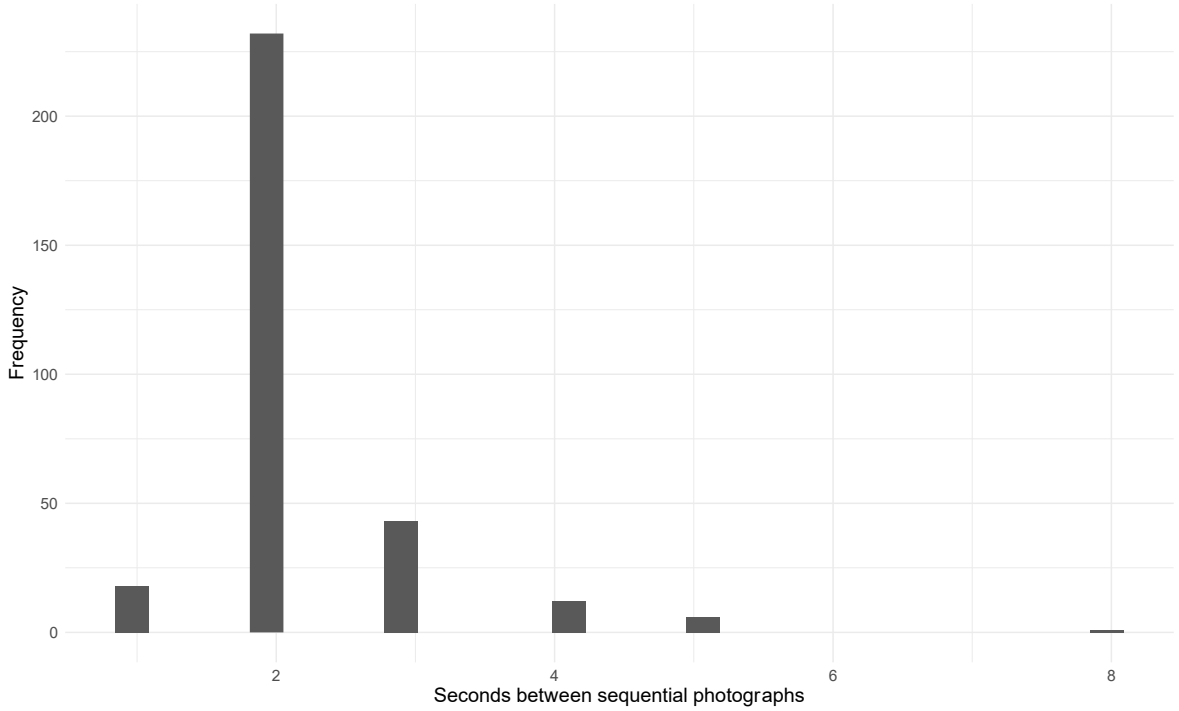

Figure S.2.2.2 Distribution of the calculated difference in time between sequential photographs taken during individual transect jogs (n = 36), for each camera trap (n = 45) in Case Study A, i.e., the Riding Mountain National Park field trial.

Del Bosco, T. (2021). *An eulerian perspective on spring migration in mule deer* [MSc. thesis]. Utah State University.

Paula, J. J. S., Bispo, R. M. B., Leite, A. H., Pereira, P. G. S., Costa, H. M. R. G., Fonseca, C. M. M. S., Mascarenhas, M. R. T., & Bernardino, J. L. V. (2014). Camera-trapping as a methodology to assess the persistence of wildlife carcasses resulting from collisions with human-made structures. *Wildlife Research*, *41*(8), 717. https://doi.org/10.1071/WR14063

Reconyx. (2022). *Reconyx Hyperfire 2 high performance camera instruction manual*. https://www.reconyx.com/img/file/HyperFire_2_User_Guide_2018_07_05_v5.pdf

Supplement S.2.3 Effective Capture Area sensitivity to out-of-sample prediction

During our Case Study B, controlled setting, field trails, due to the extremely open nature of the setting, we witnessed higher-than-expected capture rates at the 20 m transect. Because of this, we did not appropriately capture the decay of capture probability with distance away from the camera trap. Thus, when extrapolating our model to 40 m, our initial Effective Capture Area (ECA) predictions were much higher than a realistic situation would predict (Figure S.2.2.1). These unrealistically large predictions are because our method utilized generalized additive models, which, are generally poor with out-of-sample predictions due to their highly non-linear relationships (Figure S.2.2.2). Thus, the distance that practitioners predict to when implanting our ECA method may be a highly sensitive parameter. We recommend that either a) jog-tests fully encapsulate the decay of capture probability with distance at sites where they are conducted or b) predictions extend no further than the furthest distance where jog-tests occurred. Otherwise, situations like in Figure S.2.2.1 may arise, where ECA estimates become unrealistically large.

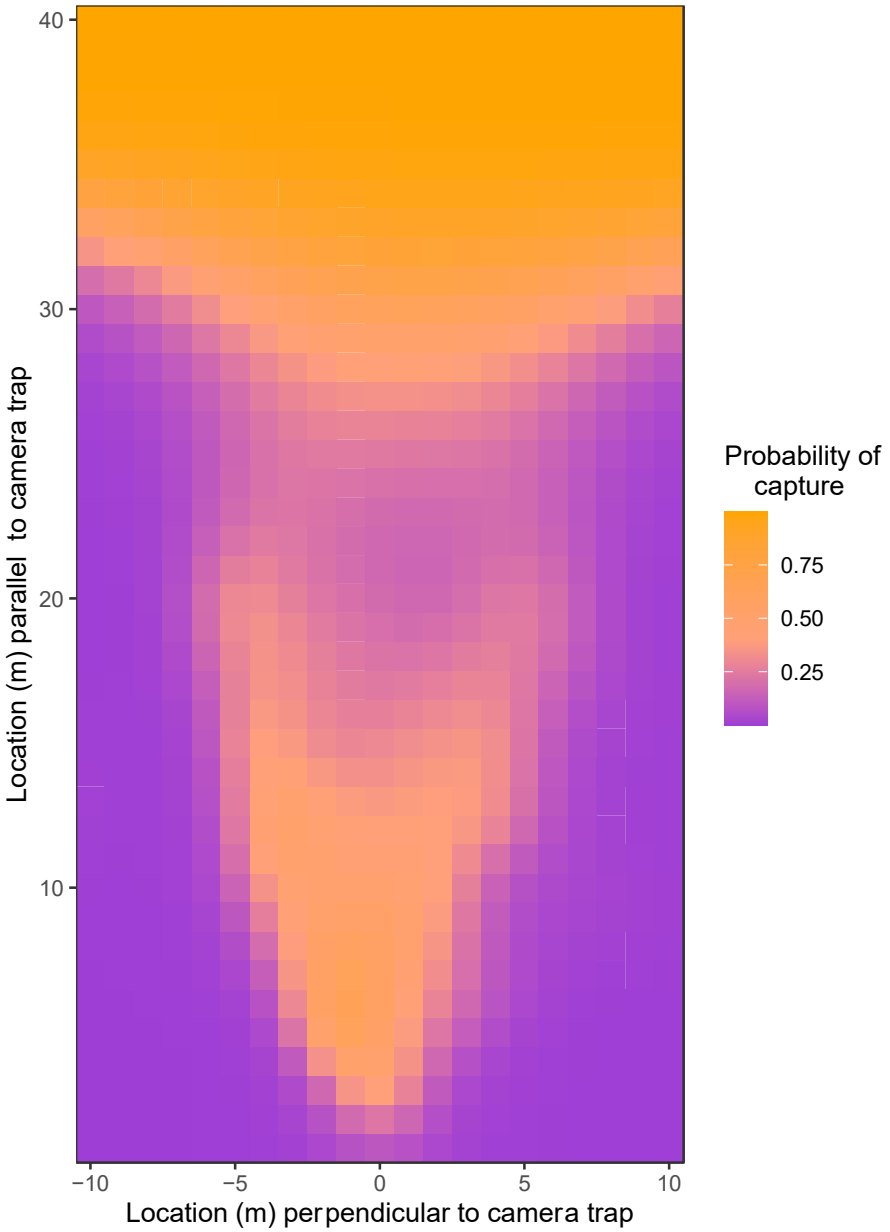

Figure S.2.3.1 Predicted probabilities of photographic capture determined from Generalized Additive Mixed Models from Case Study B when we only assessed up to 20 m parallel to camera traps. Due to the structure of the model, probability of photographic capture is predicted nearing 100% at distances not assessed, i.e., 30+m parallel to the camera.

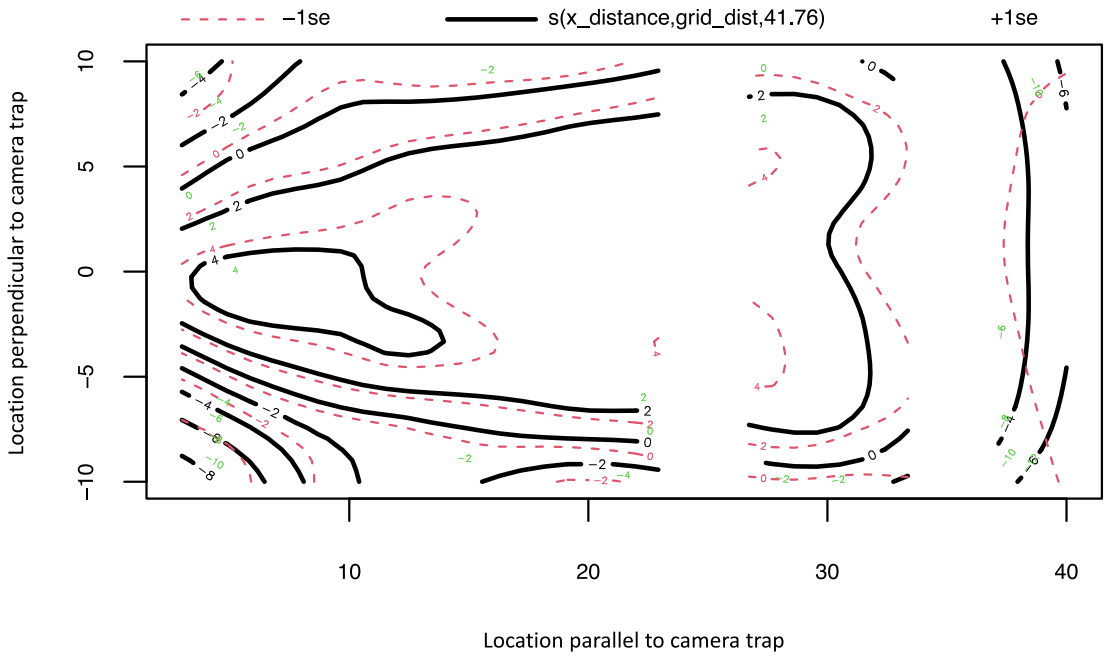

Figure S.2.3.2 The degree of the non-linear relationship between locations parallel and perpendicular to camera traps and how it changes with space, fit in a gaussian process spline, and modelled using generalize additive mixed models for our Case Study B analysis.

Chapter 3: At what scales—if any—does the relationship between camera trap-based and aerial survey estimates of density hold?

3.1 — Introduction

Generating precise and reliable density and abundance estimates are of high interest to researchers, wildlife managers, and governments alike. Understanding density can aid researchers in a myriad of ecological questions such as species distributions (Becker et al. 2021; Ramirez et al. 2021), social interactions (Vander Wal et al. 2013; Webber and Vander Wal 2020), competition (Corlatti et al. 2019), and predation dynamics (Marrotte et al. 2022; Prokopenko 2022). Wildlife managers and various levels of government aim to understand how wildlife densities change with time to implement and adapt different conservation practices. Regardless, high uncertainty plagues many forms of density estimation, decreasing our confidence with any method, particularly when researchers attempt to implement a novel method.

Researchers and wildlife managers typically use estimates of species abundance to describe general trends in wildlife populations, i.e., an increasing, decreasing, or stable population, as uncertainty and inconsistency are very well documented for any method (Buckland 2004; Morellet et al. 2007; Moll et al. 2022; Fisher et al. 2023). Despite the limitations of any abundance estimator, much research uses large-scale abundance estimates to answer fine-scale questions of density-dependent processes for a given species. For example, many studies use winter aerial flight surveys for ungulates, which represent distributions and total abundance at a single point in time, to comment on habitat-specific density-dependent population and community dynamics (e.g., Latham et al. 2013; Vander Wal et al. 2013; van Beest et al. 2014). As such, having confidence in fine-scale densities is just as crucial as

population level abundancies for our understanding and conclusions drawn from numerous ecological studies.

As methods and analytics advanced, many density estimate techniques favoured visual observations over physically marking or handling individuals. With the increase in use of remote camera traps for wildlife research came the development of camera trap-based methods of density estimate, henceforth referred to as viewshed density estimators (Moeller et al. 2023). At their core viewshed density estimators are the same as their traditional counterparts, a metric of animal occurrence intensity divided by a spatial unit of sampling effort. Despite their relatively simple framework, parameterizing viewshed density estimators is not an easy endeavour. For example, camera traps can be set to photographs, videos, or time-lapse settings, all of which will influence how animal use is measured (e.g., Royle 2004; Nakashima et al. 2018; Warbington and Boyce 2020; Moeller and Lukacs 2022). In addition, sampling effort, i.e., area monitored by cameras, can be highly variable and influenced by cameras used, broad-scale geography, and fine-scale habitat (Moll et al. 2020; Moeller et al. 2023). As a result, viewshed density estimators have seen infrequent application in many monitoring programs. However, because viewshed density estimators monitor fixed space over prolonged temporal intervals, their novel insights can be complementary to traditional, density estimation methods that span broader geographies over a short temporal period.

The few works that have implemented viewshed density estimators have seen mixed results when compared to traditionally employed methods. In simulation studies, and some field trials, viewshed density estimators have been shown to produce accurate and unbiased density estimates (Nakashima et al. 2018; Nakashima et al. 2020). In addition, in highly controlled settings with human volunteers, one viewshed estimator produced reliable density estimates

throughout a variety of experimental conditions (Garland et al. 2020). Viewshed density estimators in natural settings, however, have seen less application and consistency. For example, one large-scale study found viewshed abundance estimates were, on average, 1.3–2.5 times higher than traditional aerial surveys for moose density depending on the modeling framework implemented (Becker et al. 2022). When comparing two different viewshed density methods, one study found that certain methods produce consistently biased results with a low degree of precision (Fisher et al. 2023). As many viewshed density estimators are relatively novel, the inconsistencies in their parameterization may be a large reason behind discrepancies in their answers.

Here, I explore the spatial and temporal sensitivities of a unique adaptation of the Random Encounter Staying Time (REST) viewshed density model (Hogg 2021). I overview how I parameterized the REST model, including a novel metric of the spatial footprint a camera trap monitors, to estimate densities of moose (*Alces alces*) and elk (*Cervus canadensis*) across multiple years, in a highly managed area, i.e., Riding Mountain National Park (RMNP), Manitoba, Canada. I then compare REST-generated density estimates to traditional aerial flight surveys across spatial scales. First (***Objective 1***), I investigate the similarity of fine-scale camera and flight density estimates, at location surrounding camera traps. Second (***Objective 2***), I compare total abundance estimates from camera traps to long-term, historic abundance data derived from aerial flight surveys. Finally, I comment on how viewshed density estimators may be used complementary with traditional aerial flight surveys to increase our understanding of species densities and increase the reliability of long-term population monitoring.

3.2 — Methods

3.2.1 — Study Area

The land known as Riding Mountain National Park (RMNP), is an approximately 3000 km^2 Canadian National Park, located in Treaty 2 territory, on the traditional lands of Anishinabewaki, Očhéthi Šakówiŋ, Cree, Oji-Cree, and the Homeland of the Métis peoples. RMNP is situated in the transition zone of two ecotones, the Prairie Parklands and Boreal Plains (Olson et al. 2001). As a result, mixed deciduous-conifer forests and conifer dominate forests are connected by a matrix of grasslands and wetlands. RMNP is home to five large ungulate species: moose (*Alces alces*), elk (*Cervus canadensis*), white tailed deer (*Odocoileus virginianus*), mule deer (*Odocoileus hemionus*), and plains bison (*Bison bison*).

3.2.2 — Aerial flight surveys

Every year since the 1970s, Parks Canada has conducted consistent, standardized aerial flight surveys in RMNP to obtain abundance estimates for moose, elk, and white-tailed deer (Rounds 1981; Vander Wal et al. 2013; van Beest et al. 2014, Parks Canada, Unpublished data). Most of the park (~2000 km^2) is surveyed at 25% coverage, where 400 m wide transects (n = 50) are flown every 1.6 km, at 120 m altitude, and at a speed of 120 km/hr. The remainder of the park (~1000 km^2) is surveyed at 100% coverage, with transects (n = 50–69 depending on the year) flown 400 m apart (Figure 3.1). Flight surveys are flown in late winter every year (late January to March) over the course of a few days to a week, depending on weather conditions.

Density and abundance estimates from aerial surveys are derived from two complementary methods. First, the 100% coverage area is treated as a census of all visible animals, where all counted individuals are assumed to represent the total number within the ~1000 km^2. Second, the 25% coverage area uses a simple line transect method to estimate

density (Burnham et al. 1980; Vander Wal et al. 2013). Despite the analytical improvements on the line transect method, Parks Canada's consistent use of line transect estimation on the 25% coverage area provides a dependable and comparable abundance record across 5 decades. RMNP derives theoretical variance for all abundance estimates conducted in the 25% coverage area (Trottier 1987; Tarleton 1992; Vander Wal et al. 2013). Variance estimates are based on the variation between the number of animals on each transect and the variation between the sampling area on each transect (see Supplement S.3.2 for variance formulation).

3.2.3 — Camera trap layout

In February 2020, camera traps (n = 81) were deployed in RMNP in grid layouts by researchers at the Memorial University of Newfoundland and Labrador and Parks Canada staff. Candidate grid locations were determined using the *camtrapmonitoring* R package (Robitaille 2024). Deployments followed a stratified-random grid design, where nine grids of nine cameras each were randomly chosen based on *a priori* moose densities. Using old aerial survey data when moose were purportedly at a high density in RMNP, three strata of moose density, each containing three camera trap grids, were created from 400 m cells along flight transects, 1) low density if no moose were observed, 2) medium density if one moose was observed, and 3) high density if 2 or more moose were observed. Once candidate locations were chosen, camera trap grids were established in a 3x3 grid design, with 250 m between neighbouring cameras (Figure 3.1). The central camera in each grid (n = 1) was always a Reconyx Ultrafire XR6 (Reconyx, Holmen, USA), and the surrounding cameras (n = 8) were always Cuddeback H-1453 (Cuddeback, Green Bay, USA). Cameras were fixed on trees, stumps, or snags, at a height of approximately 1.5 m from the ground. Cameras were positioned facing directly north or south, depending on location, to minimize glare from the sun. Camera traps were maintained

approximately every 4 months, or as access conditions allowed, to change batteries and SD cards. See Supplement S.3.1 for additional details on camera location selection criteria.

3.2.4 — Random Encounter Staying Time model

In this thesis, I use an adapted form of the Random Encounter Staying Time (REST) model (Nakashima et al. 2018), proposed by Hogg (2021). The adaptation allows for the estimation of mean and variance animal densities at individual cameras, within camera grids, and across larger spatial scales, i.e., all RMNP. Below, I describe how I parameterized the REST model from Equation 3.1 to generate density and abundance estimates for moose and elk in RMNP.

$$\rho = \frac{\sum T_s}{T_a * A_c} * \frac{\pi^2}{8} \qquad \textit{Equation 3.1}$$

3.2.5 — T_s: Time species was captured by photos

Our program used camera traps set to capture photographs. To calculate cumulative time that species were in front of cameras, I summed the cumulative number of photos at each camera trap for each species and multiplied by 2 s, the assumed temporal footprint of a photograph in Chapter 2 (see Supplement S.2.2). Because I did not need to differentiate individuals with the Hogg-REST adaptation, I did not consider the time between subsequent photographs, or gaps within a certain time threshold (e.g., as in the Time in Font of Camera adaptation; Warbington and Boyce 2020; Becker et al. 2022, which implement a 120 s cutoff between subsequent photos to differentiate indepdent events). Photographs containing two or more individuals were duplicated to reflect the total number of distinct individuals in the photo. I did not ignore the presence of juvenile or young animals in photos with adults, as it is impossible to determine if the adult or juvenile triggered the camera trap, thus, all estimates contain the presence of juvenile animals.

3.2.6 — A_c: Viewshed area with 100% capture probability

To estimate viewshed area with a perfect capture probability, I used the Effective Capture Area (ECA) modeling approach in Chapter 2. Out of 81 camera traps, I conducted jog-tests at 37, and vegetation surveys at 59 cameras. I constructed an ECA model using the jog-test data from 37 cameras following the same framework and covariates as Case Study A in Chapter 2 (see Table 2.2, Case Study A). For the 59 cameras traps where I collected vegetation data, I predicted ECAs using the local site covariate data. Because I did not have jog-test or vegetation data for every camera trap, I excluded the random effect, i.e., unique camera ID, from ECA predictions. In addition, I excluded the binary covariate for camera refractory period from predictions due to difficulty in parameterizing the variable. Finally, for camera traps where no jog-tests or vegetation data were collected, I generated a single ECA value applying the mean values of all covariates in the model, while excluding camera ID and refractory period from the prediction.

3.2.7 — T_a: Time camera traps were active

Aerial flight surveys in RMNP take place in late winter each year, usually mid-February to mid-March. To generate unbiased comparisons, I first tested the sensitivity of REST density estimates at varying temporal intervals around aerial flight survey dates (see Supplement S.3.3). I used this sensitivity analysis to determine the minimum time interval around flight surveys that produced stable density estimates, ~16 weeks on both sides of the flight survey. I calculated the total time that each camera trap was active during the 32-week interval. When camera traps were operational the entire period between maintenance checks, I calculated the time difference between the last photograph of researchers leaving, and the first photograph of researchers returning to each camera site. Calculating the time between researcher visits estimates the total time a camera was active while excluding the time when camera trap maintenance were being

conducted. If camera traps failed prior to researchers returning for maintenance, I assumed that the camera trap died one minute after the last recorded photograph.

3.2.8 — Fine- and coarse-scale comparisons

To assess both the fine and coarse scale validity of REST estimates, I compared park-level abundance, and within camera grid density estimates from camera traps and aerial flight surveys. For fine-scale REST estimates (***Objective 1***), I calculated mean species density at each of the nine camera grids for the 32-week monitoring period surrounding flight surveys. To generate park-level abundance estimates from the REST model (***Objective 2***) I averaged the mean densities from the 32-week monitoring period at all nine camera grids (above) to represent mean species density across the entire park, and multiplied park-level mean density by RMNPs area, 3089 km^2. I calculated theoretical REST variance for total abundance and fine-scale density estimates by taking the sum of ECAs and camera operation time across grouped cameras, i.e., grouped across camera grids, or the entire park (Equation 3.2).

$$Var(\bar{\rho}) = \bar{\rho}^2 * (\frac{\pi^2}{8} - 1 + \frac{\pi^2}{16*(\sum_{i=1}^{n} r_i * T_i)*s*\bar{\rho}}) \qquad \textit{Equation 3.2}$$

For flight survey abundance estimates, I used a simple line transect estimator (Seber 1973; Burnham et al. 1980) for the 25% coverage area and added this number to the total count from the 100% survey area (***Objective 2***). I calculated the theoretical variance for the 25% survey area (See Supplement S.3.2), but because the 100% coverage area represents a small census, the calculated variance represents the total population variation. Because aerial surveys represent a single point in time, species locations during the time of survey are likely not reflective of distributions throughout the winter season or the entire year. Thus, I used the aerial survey data to generate fine-scale densities from different spatial resolutions surrounding camera trap grid locations (***Objective 1***). I produced multiple square polygons from 5–11 km^2 (Figure 3.2) around

all camera trap grids. I calculated fine-scale density and variance for flight surveys using the same line transect estimator (Seber 1973; Burnham et al. 1980), as a ratio from the area surveyed by transects in each polygon size. Using linear regression models with the y-intercept set to 0, I predicted fine-scale flight survey densities from each polygon size by fine-scale camera trap densities as a predictor. I used the regression model with the best fit, i.e., the highest R^2, from which to base my subsequent inferences.

In this chapter, I generated and compared fine-scale density (***Objective 1***) and park wide abundance (***Objective 2***) estimates for moose and elk in RMNP in 2022. Although a flight survey did occur in the park in 2021, due to safety issues from the COVID-19 pandemic, the 2021 survey covered a small fraction of previous years, i.e., only 18 survey lines at 25% coverage. As such, the 2021 survey has a higher risk of being inaccurate and cannot produce unbiased comparisons. In addition, because camera traps were only established in February 2020, REST density and abundance estimates for 2020 were generated using 6 months of data post camera setup. See supplement S.3.4 for details on when camera traps were operational and aerial flight survey dates from 2020–2022. Thus, because of two years of unfavourable data, I only estimated park-level abundance for moose and elk in 2020 and 2021 to broadly comment on population trends through time.

3.3 — Results

3.3.1 — Fine-scale comparisons (Objective 1)

Fine-scale density estimates for moose in 2022, between flights and cameras, had the highest correlation ($R^2 = 0.89$) at a spatial scale of 10 km^2 surrounding camera grid locations (Figure 3.3). The slope ($m = 1.15 \pm 0.1331$ SE) of the linear regression of mean camera trap grid densities and fine-scale flight survey densities, suggests that, at the fine-scale, camera traps

typically estimate more moose than aerial flight surveys (Figure 3.4). At a scale of ~10 km^2, however, Figure 3.4 suggests that at relatively higher moose densities, camera traps generally estimate more individuals, whereas, at relatively lower moose densities, flight surveys tend to estimate more individuals. In addition, the fine-scale density estimates at each camera grid largely agreed with the *a priori* moose density strata generated from old flight surveys (Figure 3.5).

3.3.2 — Park abundance comparisons (Objective 2)

Moose abundance estimates from the REST model were lower than flight survey estimates in 2022, though their confidence intervals almost fully overlapped, 1430 ± 144 moose for camera traps and 1747 ± 437 moose for flight surveys (Figure 3.6). The camera trap abundance estimate of moose, however, were significantly lower for camera traps (1514 ± 152) than flight surveys (2545 ± 355) in 2020 (Figure 3.6). Moose abundance estimates generated with the REST model are consistently lower than flight survey estimates for 2020 and 2021, with overlap in 2022 (Figure 3.6). Although lower, and non-significant for the camera trap-based density estimates, the camera trap estimates seem to capture the same trends observed with flight surveys, i.e., a decreasing moose population into 2022. REST generated density and abundance estimates showed little sensitivity to spatial variation, however, were highly sensitive to the varying temporal windows (See Supplement S.3.3). Park-level elk abundance estimates were comparable in 2022 between viewshed and aerial survey estimators, 972 ± 98 elk for camera traps and 773 ± 409 elk for flight surveys. In 2020, park-level abundance estimates for elk were smaller but again comparable between camera traps (964 ± 97, 95% CI) and flight surveys (1302 ± 834, 95% CI). See Supplement S.3.5 for additional information and analyses on elk densities in RMNP.

3.4 — Discussion

3.4.1 — Fine-scale comparisons (Objective 1)

My fine-scale analysis suggested that at the camera grid level, moose density estimates are well correlated with flight survey data at a scale of ~10 km^2. The linear regression of fine-scale flight survey data and mean camera grid moose densities provides interesting insight to some assumptions of both survey methods. For example, the REST model seems to estimate more moose in areas with higher relative density, i.e., on the west end of RMNP where 100% survey lines are flown. Conversely, flight surveys seem to estimate more moose in areas with relatively lower density, i.e., the east end of RMNP where only 25% surveys are flown. These relative comparisons at the fine-scale suggest that the line transect method used by Parks Canada may be overestimating animal density when 25% survey lines are flown, particularly when animal density is lower.

The fine-scale comparisons also suggest the line transect method may underestimate density, compared to camera traps, in areas of relatively higher abundance. Underestimating density from the line transect method could be because it becomes more difficult for surveyors to accurately count animals as their numbers increase (Southwell and Weaver 1993). For example, it may be more difficult to count multiple groups of animals simultaneously during flight surveys. Additionally, heterogeneous habitat cover across RMNP, i.e., the western and eastern proportions of RMNP are relatively more open than the central portion, as they contain more open deciduous forests, and grasslands (Olson et al. 2001), add uncertainty as individuals can be missed during counts. Moose in RMNP tend to primarily occupy mixed conifer-hardwood forests (van Beest et al. 2014), which could contribute to sightability issues from aerial surveys

that are not incorporated for in the line transect method (Burnham et al. 1980; Vander Wal et al. 2011; Peters et al. 2014).

Despite potential location specific biases, my results show that mean REST moose densities at the camera grid level largely agree with *a priori* moose strata—which were generated from old aerial survey data when moose were at a high density. In addition, moose density estimates from flight surveys and the REST model are highly correlated at multiple spatial scales surrounding camera grids. Together, these results provides a validation for many works that use aerial flight surveys for ecological questions of density dependence (e.g., van Beest et al. 2014; Prokopenko 2022; Zabihi-Seissan et al. 2022).

3.4.2 — Coarse-scale comparisons (Objective 2)

Estimates for moose abundancies in RMNP, between the REST method and aerial flight surveys, were comparable and highly overlapping in 2022 but not 2020. The significantly lower REST abundance estimates in 2020 were likely due to the limited sampling time in the 2020 winter. For example, flight surveys in 2020 occurred from 3–9 February, yet camera traps were first established on 21 February 2020. As such, I likely did not have sufficient camera trap observations to produce reliable REST abundance estimates. Considering my temporal validations (Supplement S.3.3) suggested 16 weeks of data before and after flight surveys occurred are needed to generate stable REST estimates, the 2020 comparison may not have enough camera trap data to be reliable. Although confidence intervals of estimate types did overlap for elk in 2020, the REST method did estimate fewer animals. Because of the limited camera trap operation time for winter 2020, these results should be interpreted cautiously.

The 2022 study period had more consistent camera trap data, both before and after flight surveys occurred in late February. In addition, both moose and elk comparisons in 2020 were

highly comparable and with overlapping confidence intervals. Moose abundance estimates were ~300 individuals lower and elk estimates ~200 individuals higher for camera traps over flight surveys. The 2022 comparisons highlights that given an adequate camera sampling period, the REST equation used here can provide comparable abundance and density estimates to traditional survey types. The most consistent and reliable camera trap data were collected in the 2021 study year. Unfortunately, the 2021 aerial flight survey was heavily reduced (only 18 survey lines all at 25% coverage; See Supplement S.3.6), and as such cannot be used to make a valid comparison. Although moose abundance estimates were always higher for aerial flight surveys, the fine-scale regression results for 2022 suggest that, overall, aerial flight surveys overestimate moose in the park by a factor of 1.15.

3.4.3 — Viewshed density estimators

REST-adapted density estimates, implemented on field data, have rarely shown consistency in literature. For example, many studies have shown that REST estimates are considerably higher to both traditional methods and other viewshed density estimators (Becker et al. 2022; Fisher et al. 2023). Here, I found that REST density estimates were comparable to flight surveys, given an adequate monitoring period, or significantly lower in years with reduced camera monitoring time and partial flight surveys. The deviation in my results from other published works could be from two differences in parameterization of the REST model. First, I used the novel Effective Capture Area (ECA) to estimate the perfect monitoring zone of camera traps. As described in Chapter 2, the ECA is determined from a standardized survey that derives monitoring zone estimates at each unique camera trap. Second, I only considered single photographs, and their assumed temporal footprint, to determine the time species spent in front of camera traps, whereas other studies include all time in between subsequent photographs. The

combination of the previous differences in REST parameterization could contribute to producing more reliable REST density and abundance estimates.

3.4.4 — Limitations

Despite having two years, 2020 and 2021, of unfavourable comparisons between REST and flight survey density estimates, both survey types still exhibit similar trends. Aerial flight surveys exhibit a decline in moose abundance of nearly 1000 individuals over 7 years. Because of the partial flight survey in 2021 and potential overestimate of moose in low density areas, however, we do not know exactly when the decline, observed by aerial fight surveys, started. Although camera trap estimates start with low moose estimates due to limited sampling period, they still exhibit the same declining trend into 2022. Elk estimates between both survey types again follow the same trends of a slight decline in elk numbers (Supplement S.3.5), but the inaccuracy of the 2021 partial flight survey is even more pronounced. Maintaining aerial flight surveys consistently on a yearly basis is an unattainable for most wildlife monitoring programs.

Changes in flight survey design have occurred numerous times over their history in RMNP, making absolute comparisons between different implementations difficult (Prokopenko 2022). In addition, most provincial and federal governments in Canada conduct flight surveys infrequently, once every 5–10 years, in wildlife management areas throughout their jurisdiction (e.g., Manitoba Fish and Wildlife 2020; 2022). Though flight surveys are generally meant to represent changes in populations through time, it is clear all metrics of abundance and density hold sensitivities and biases. Having a camera-trap based monitoring program, in addition to infrequent aerial surveys, can help provide accurate abundance estimates, with a sufficient monitoring period, and contribute to describing population trends in years when aerial surveys do not happen or are unreliable.

3.4.5 — Conclusion

At the fine-scale (***Objective 1***), REST moose density estimates are highly correlated with aerial flight moose estimates at numerous spatial scales from 6–11km^2. Overall, at the 10km^2 scale, when compared to REST estimates, flight surveys may overestimate animals by a factor of 1.15, especially in locations with lower relative moose density. Given a sufficient temporal monitoring period for remote camera traps and an extensive spatial extent of aerial flight surveys, my results show that in Riding Mountain National Park, abundance estimates from the camera trap-based Random Encounter Staying Time model and aerial flight-based methods largely agree (***Objective 2***). Implementing a camera trap monitoring program and estimating species density with the REST model, can help increase the reliability of inferences drawn from aerial flight surveys in addition to providing better information on a population with infrequent or unreliable flight surveys.

3.5 — Literature Cited

Becker JA, Hutchinson MC, Potter AB, Park S, Guyton JA, Abernathy K, Americo VF, Da Conceição A, Kartzinel TR, Kuziel L, et al. 2021. Ecological and behavioral mechanisms of density-dependent habitat expansion in a recovering African ungulate population. Ecological Monographs. 91(4):e01476. doi:10.1002/ecm.1476.

Becker M, Huggard DJ, Dickie M, Warbington C, Schieck J, Herdman E, Serrouya R, Boutin S. 2022. Applying and testing a novel method to estimate animal density from motion-triggered cameras. Ecosphere. 13(4). doi:10.1002/ecs2.4005. [accessed 2023 Jul 25]. https://onlinelibrary.wiley.com/doi/10.1002/ecs2.4005.

van Beest FM, McLoughlin PD, Vander Wal E, Brook RK. 2014. Density-dependent habitat selection and partitioning between two sympatric ungulates. Oecologica. 175:1155–1165. doi:10.1007/s00442-014-2978-7.

Buckland ST. 2004. Advanced distance sampling: estimating abundance of biological populations. Anderson DR, Burnham KP, Laake JL, Borchers DL, Thomas L, editors. Oxford, UK: Oxford University Press.

Burnham KP, Anderson DR, Laake JL. 1980. Estimation of density from line transect sampling of biological populations. Wildlife Monographs. 72:3–302.

Corlatti L, Bonardi A, Bragalanti N, Pedrotti L. 2019. Long-term dynamics of Alpine ungulates suggest interspecific competition. Journal of Zoology. 309(4):241–249. doi:10.1111/jzo.12716.

Fisher JT, Dickie M, Burgar JM, Burton AC, Serrouya R. 2023. Density estimates of unmarked mammals: comparing two models and assumptions across multiple species and years. Canadian Journal of Zoology. cjz-2023-0055. doi:10.1139/cjz-2023-0055.

Garland L, Neilson E, Avgar T, Bayne E, Boutin S. 2020. Random Encounter and Staying Time Model testing with human volunteers. The Journal of Wildlife Management. 84(6):1179–1184. doi:10.1002/jwmg.21879.

Hogg J. 2021. The precision and accuracy of the Random Encounter Staying Time model's estimation of species population density [MSc. thesis]. [St. John's, NL]: Memorial University of Newfoundland and Labrador.

Latham ADM, Latham MC, Knopff KH, Hebbewhite M, Boutin S. 2013. Wolves, white-tailed deer and beaver: implications of seasonal prey switching for woodland caribou declines. Ecography. 36:1276–1290. doi:10.1111/j.1600-0587.2013.00035.x

Manitoba Fish and Wildlife division. 2020 big game surveys. 2020. Winnipeg, MB: Manitoba Fish and Wildlife division

Manitoba Fish and Wildlife division. 2022 big game surveys. 2022. Winnipeg, MB: Manitoba Fish and Wildlife division

Marrotte RR, Patterson BR, Northrup JM. 2022. Harvest and density-dependent predation drive long-term population decline in a northern ungulate. Ecological Applications. 32(6):e2629. doi:10.1002/eap.2629.

Moeller AK, Lukacs PM. 2022. spaceNtime: an R package for estimating abundance of unmarked animals using camera-trap photographs. Mammalian Biology. 102(3):581–590. doi:10.1007/s42991-021-00181-8.

Moeller AK, Waller SJ, DeCesare NJ, Chitwood MC, Lukacs PM. 2023. Best practices to account for capture probability and viewable area in camera-based abundance estimation. Remote Sensing in Ecology and Conservation. 9(1):152–164. doi:10.1002/rse2.300.

Moll RJ, Ortiz-Calo W, Cepek JD, Lorch PD, Dennis PM, Robison T, Montgomery RA. 2020. The effect of camera-trap viewshed obstruction on wildlife detection: implications for inference. Wildlife Research. 47(2):158. doi:10.1071/WR19004.

Moll RJ, Poisson MKP, Heit DR, Jones H, Kantar L. 2022. A review of methods to estimate and monitor moose density and abundance. Alces. 58:31–49

Morellet N, Gaillard J, Hewison AJM, Ballon P, Boscardin Y, Duncan P, Klein F, Maillard D. 2007. Indicators of ecological change: new tools for managing populations of large herbivores. Journal of Applied Ecology. 44(3):634–643. doi:10.1111/j.1365-2664.2007.01307.

Nakashima Y, Fukasawa K, Samejima H. 2018. Estimating animal density without individual recognition using information derivable exclusively from camera traps. Journal of Applied Ecology. 55(2):735–744. doi:10.1111/1365-2664.13059.

Nakashima Y, Hongo S, Akomo-Okoue EF. 2020. Landscape-scale estimation of forest ungulate density and biomass using camera traps: Applying the REST model. Biological Conservation. 241:108381. doi:10.1016/j.biocon.2019.108381.

Olson DM, Dinerstein E, Wikramanayake ED, Burgess ND, Powell GVN, Underwood EC, D'amico JA, Itoua I, Strand HE, Morrison JC, et al. 2001. Terrestrial Ecoregions of the World: A New Map of Life on Earth. BioScience. 51(11):933. doi:10.1641/0006-3568

Peters W, Hebblewhite M, Smith KG, Webb SM, Webb N, Russell M, Stambaugh C, Anderson RB. 2014. Contrasting aerial moose population estimation methods and evaluating sightability in west-central Alberta, Canada. Wildlife Society Bulletin. 38(3):639–649. doi:10.1002/wsb.433.

Prokopenko CM. 2022. Hungry wolves and dangerous prey: a tale of prey switching [PhD thesis]. [St. John's, NL]: Memorial University of Newfoundland and Labrador.

Ramirez JI, Zwerts JA, Van Kuijk M, Iacobelli P, Li X, Herdoiza N, Jansen PA. 2021. Density dependence of daily activity in three ungulate species. Ecology and Evolution. 11(12):7390–7398. doi:10.1002/ece3.7570.

Robitaille A. 2024. camtrapmonitoring: an R package for camera trap monitoring and estimating wildlife density. R package: version 0.12.1. doi:https://robitalec.r-universe.dev/camtrapmonitoring.

Rounds RC. 1981. First Approximation of Habitat Selectivity of Ungulates on Extensive Winter Ranges. The Journal of Wildlife Management. 45(1):187. doi:10.2307/3807886.

Royle JA. 2004. *N* -Mixture Models for Estimating Population Size from Spatially Replicated Counts. Biometrics. 60(1):108–115. doi:10.1111/j.0006-341X.2004.00142.

Seber G. 1973. The estimation of animal abundance and related parameters. New York, USA: Halfner Press.

Southwell C, Weaver K. 1993. Evaluation of analytical procedures for density estimation from line-transect data: data grouping, data truncation and the unit of analysis. Wildlife Research. 20:433–443.

Tarleton P. 1992. Cervid monitoring and status report, Riding Mountain National Park, 1990–1991. Parks Canada Unpublished report.

Trottier GC. 1987. Riding Mountain large mammal systems study — Final report. Winnipeg, MB: Parks Canada.

Vander Wal E, Van Beest FM, Brook RK. 2013. Density-Dependent effects on group size are sex-specific in a gregarious ungulate. PLoS ONE. 8(1):e53777. doi:10.1371/journal.pone.0053777.

Vander Wal E, McLoughlin PD, Brook RK. 2011. Spatial and temporal factors influencing sightability of elk. The Journal of Wildlife Management. 75(6):1521–1526. doi:10.1002/jwmg.208.

Warbington CH, Boyce MS. 2020. Population density of sitatunga in riverine wetland habitats. Global Ecology and Conservation. 24:e01212. doi:10.1016/j.gecco.2020.e01212.

Webber QMR, Vander Wal E. 2020. Heterogeneity in social network connections is density-dependent: implications for disease dynamics in a gregarious ungulate. Behavioral Ecology and Sociobiology. 74(6):77. doi:10.1007/s00265-020-02860-x.

Zabihi-Seissan S, Prokopenko CM, Vander Wal E. 2022. Wolf spatial behavior promotes encounters and kills of abundant prey. Oecologia. 200(1–2):11–22. doi:10.1007/s00442-022-05218-4.

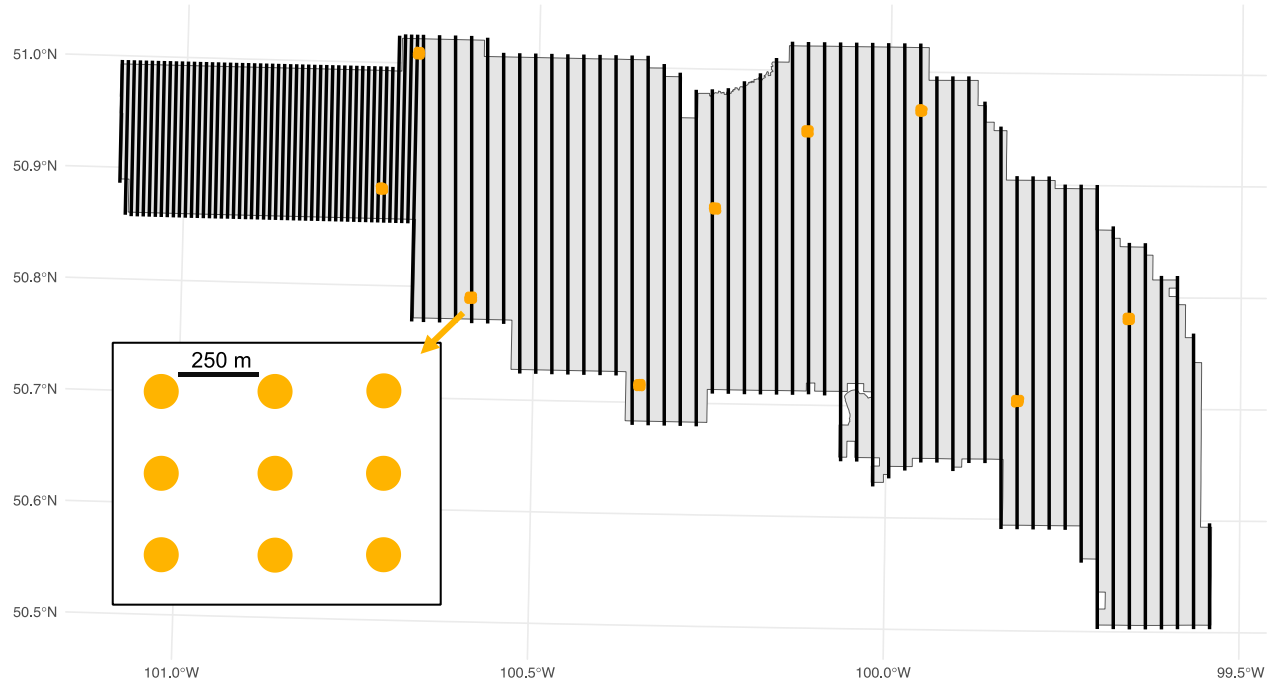

Figure 3.1 Aerial flight transects (black) flown by Parks Canada staff in Riding Mountain National Park in February 2022 for ungulate surveys. The central and eastern transects, representing 25% coverage, are flown 1.6 km apart. The western transects, representing 100% coverage, are flown 400 m apart. All transects are 400 m wide, i.e., assumed perfect detection on 200 m for both sides, flown at 120 m altitude, and at a speed of 120 km/hr. Including locations of camera traps (n = 81) deployed in *a priori* moose densities. Each grid contains 9 camera traps, each placed 250 m from its neighbouring cameras. The central camera in every grid is always a Reconyx Ultrafire XR6 camera trap and the surrounding cameras are always Cuddeback H-1453 camera traps.

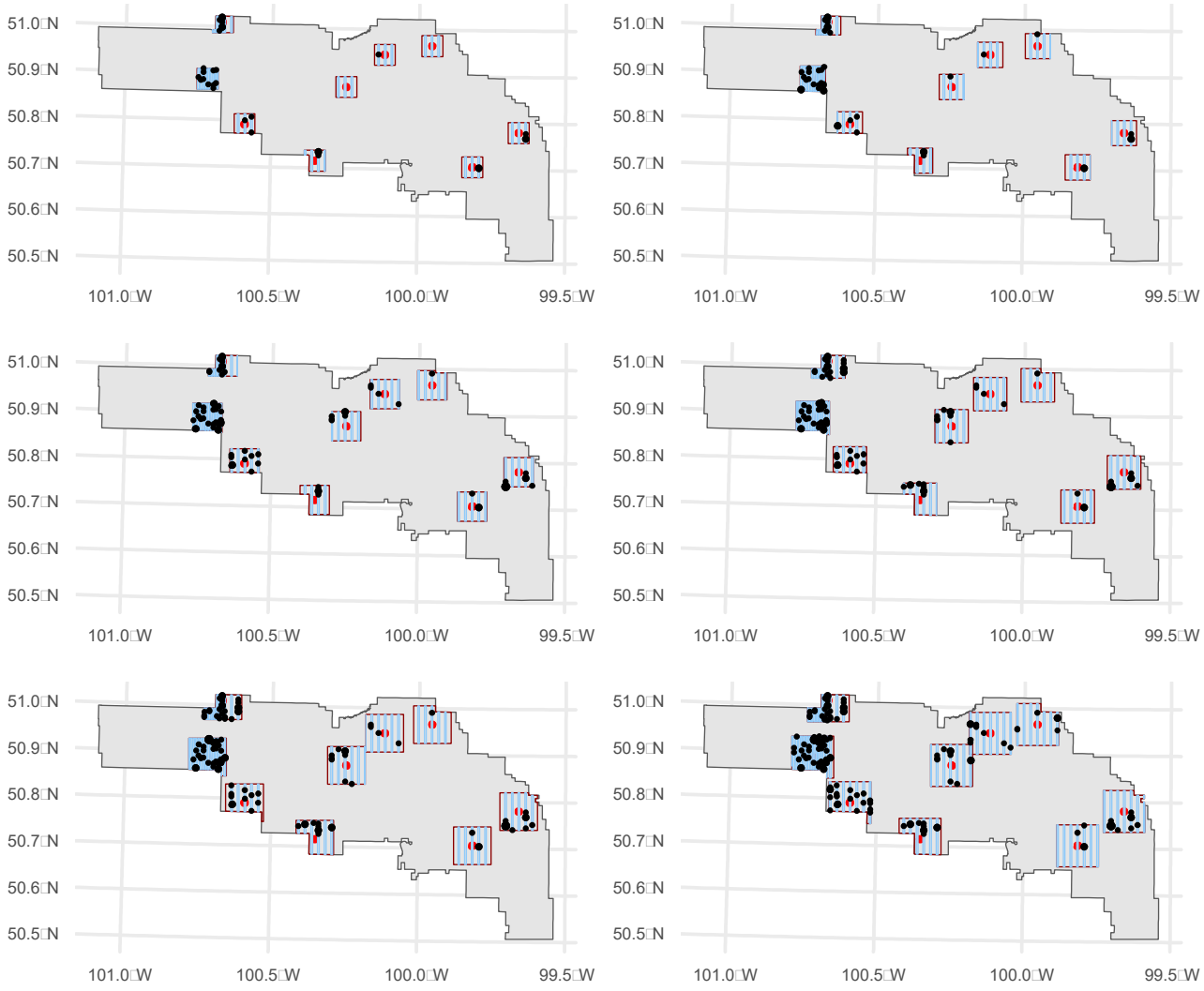

Figure 3.2 Various 'fine-scale' polygons, 5km^2–10km^2, left to right, top to bottom, surrounding camera trap grids (red dots) and showing moose observations (black dots) from the 2022 aerial flight survey (blue lines) in Riding Mountain National Park.

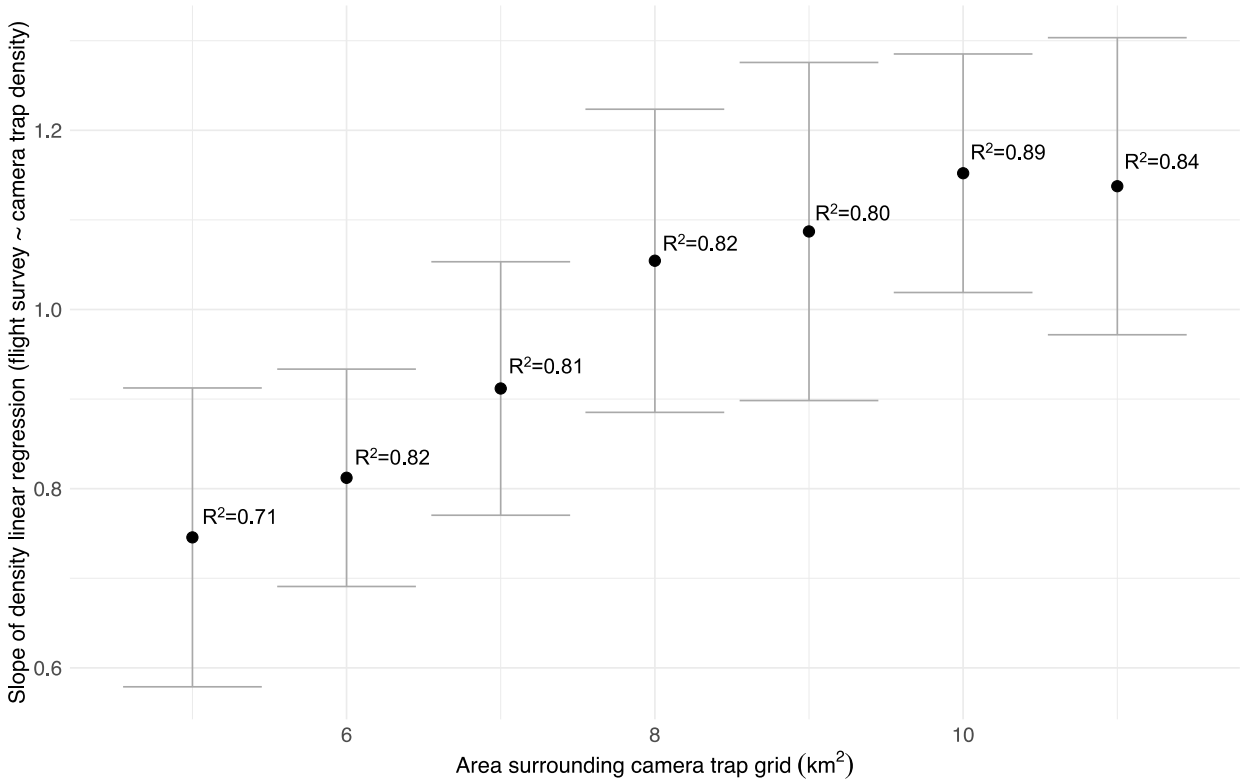

Figure 3.3 Slope (± SE) and R^2 values of the linear regressions that predicted fine-scale moose density estimates, at various spatial scales (5–11km^2), from aerial flight surveys conducted in Riding Mountain National Park in February 2022. Fine-scale flight densities were predicted by mean Random Encounter Staying Time density estimates at camera trap grids (n = 9) for the 2022 study year.

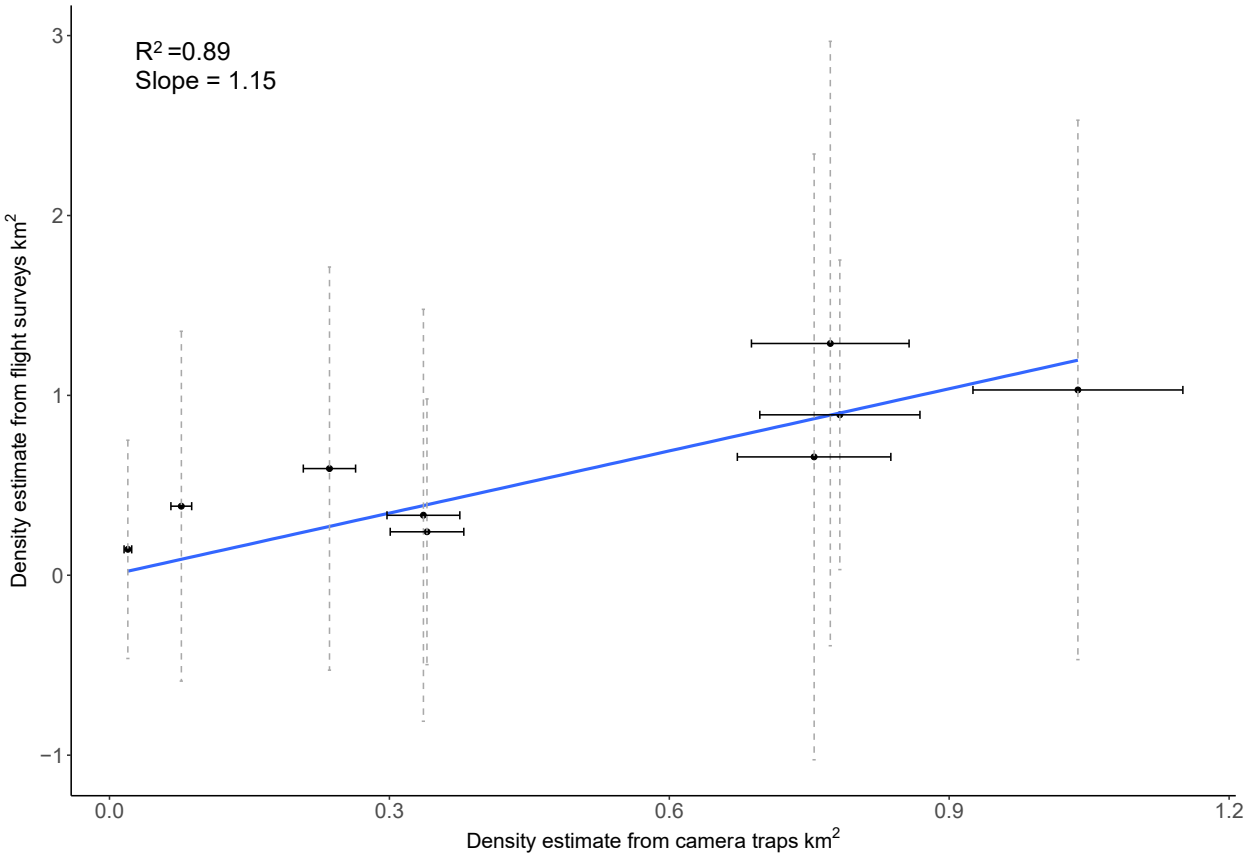

Figure 3.4 The best fit and highest correlated linear regression model predicting fine-scale moose density estimates from the 2022 aerial flight survey and 2022 study year with 10km^2 polygons surrounding each camera trap grip (n = 9). Horizontal error bars represent the 95% confidence intervals generated from the theoretical REST variance equation, whereas vertical error bars represent the 95% confidence intervals from aerial flight surveys. The slope of the linear regression was 1.15 (± 0.1331 SE), and with an R^2 of 0.89.

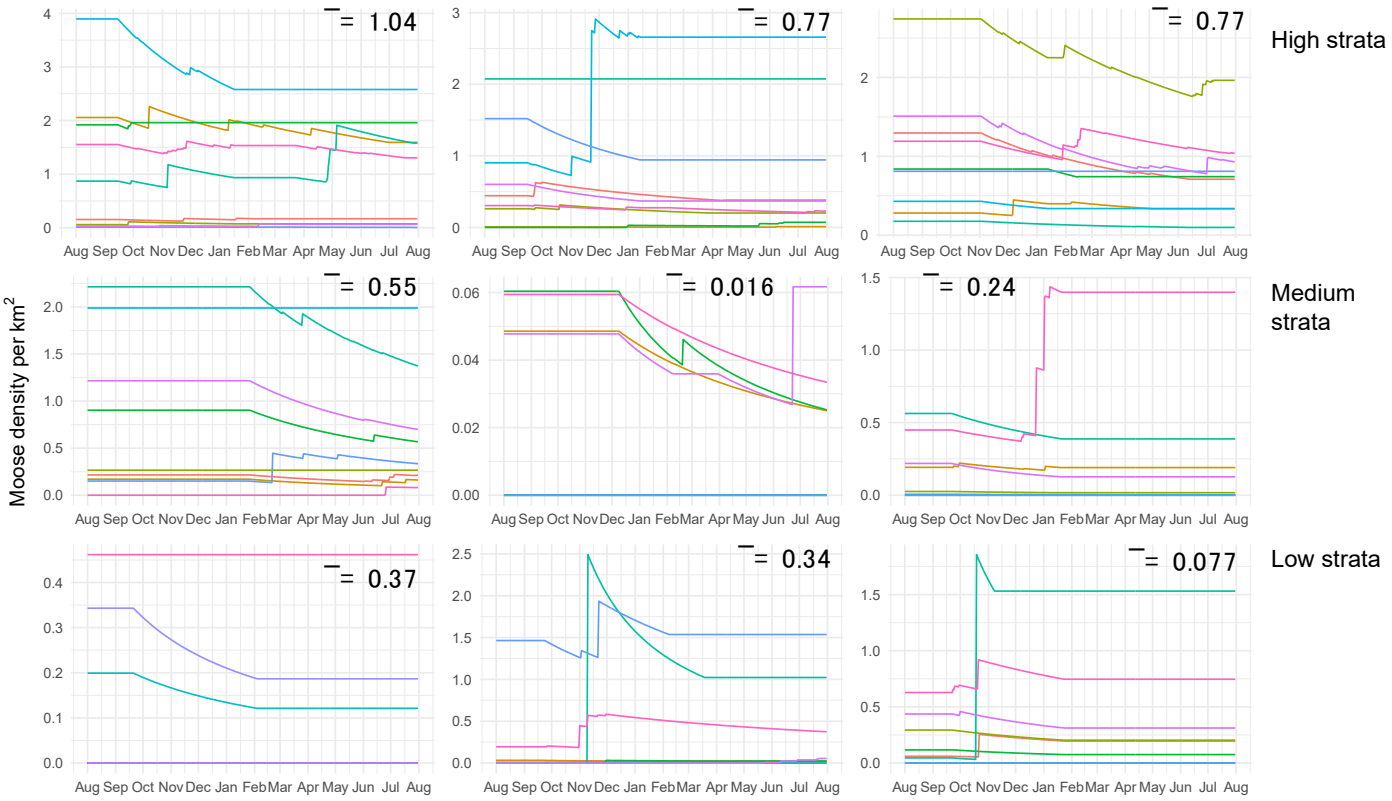

Figure 3.5 Mean moose densities (), per km^2, at all camera trap grids (n = 9), showing density trends of individual camera traps (n = 81) throughout the 2022 study year, deployed across *a priori* strata, high density (top row), medium density (middle row), and low density (bottom row), in Riding Mountain National Park.

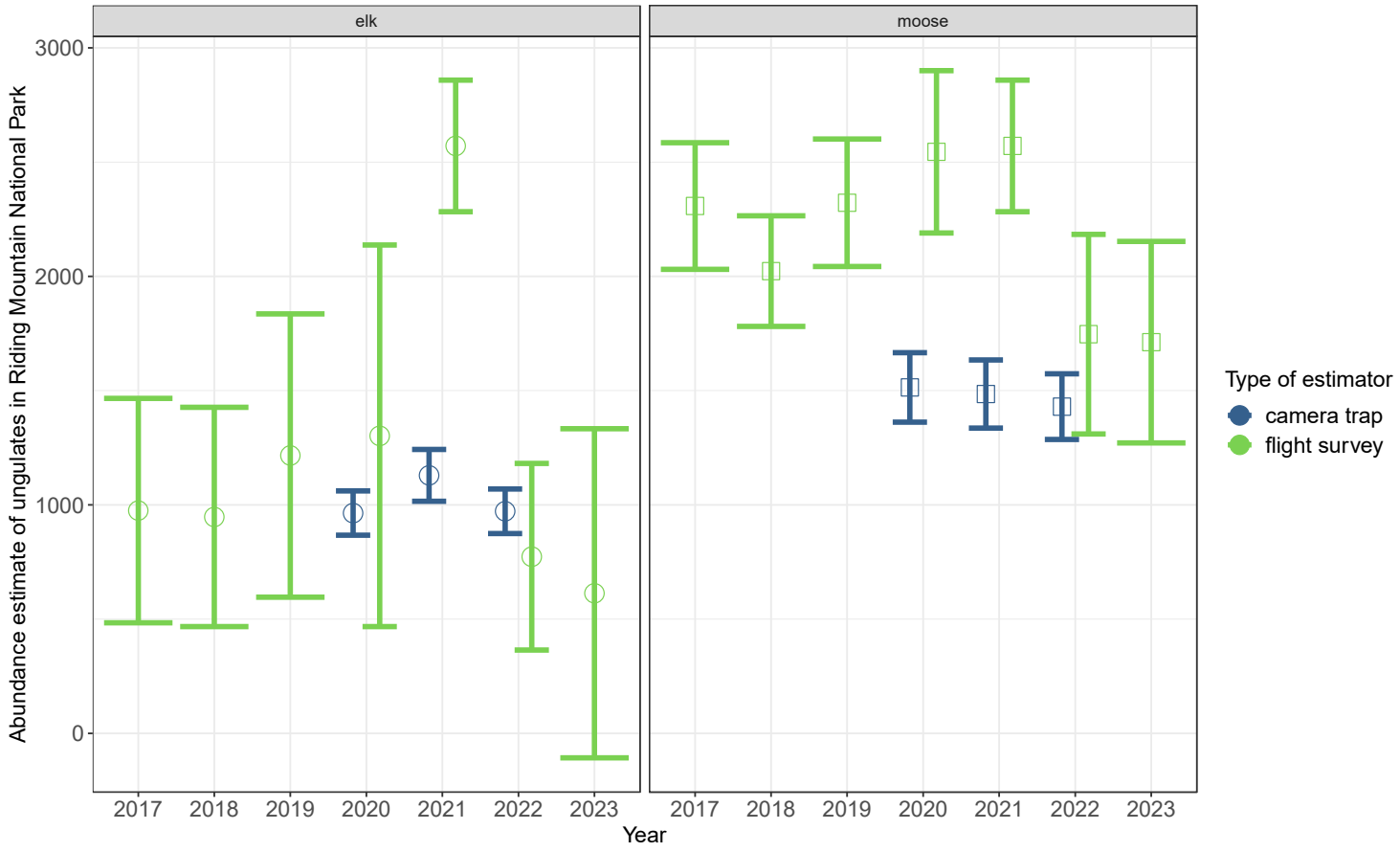

Figure 3.6 Comparison of trends in elk (left) and moose (right) abundance estimates (± 95% confidence intervals) generated from camera traps using the Random Encounter Staying Time model (blue) and from line transect estimation based off aerial flight surveys (green) across six years in Riding Mountain National Park.

3.6 — Supplementary materials Chapter 3

Supplement S.3.1 — Selection of camera trap grid candidate locations using camtrapmonitoring

Code Written by Alec Robitaille, adapted by Brendan Carswell

Convert flight transects to moose density
Flight transects have full coverage in the West and reduced coverage in the East
Cells in raster have 400m resolution

Density classes:
"1" - 0 moose
"2" - 1 moose
"3" - >1 moose

```
# Packages

library(data.table)
library(sf)

## Linking to GEOS 3.10.2, GDAL 3.4.2, PROJ 8.2.1; sf_use_s2() is TRUE

library(raster)

## Loading required package: sp
# Load density and flight transects

flight <- st_read('./survey_lines/Flightlines.shp')

## Geometry type: LINESTRING
## Dimension:     XY
## Bounding box:  xmin: 352900.3 ymin: 5594682 xmax: 461600 ymax: 5654031
## Projected CRS: NAD83 / UTM zone 14N

dens <- fread('./Ungulate_survey_2016.csv')

# Rasterize flight transects with specific resolution (400)

res <- 400
buf <- st_buffer(flight, res)

ras <- raster(buf, resolution = c(res, res))

fcells <- cellFromPolygon(ras, as_Spatial(buf))
```

```
# Preserve true zeroes

ras[unlist(fcells)] <- 1
# Fill point counts into cells
moose <- dens[Species == 'm']
mcells <- cellFromXY(ras, moose[, .(X, Y)])

# Reclass counts

moose[Count == 1, countClass := 2]
moose[Count > 1, countClass := 3]

ras[mcells] <- moose[, countClass]
plot(ras)
```

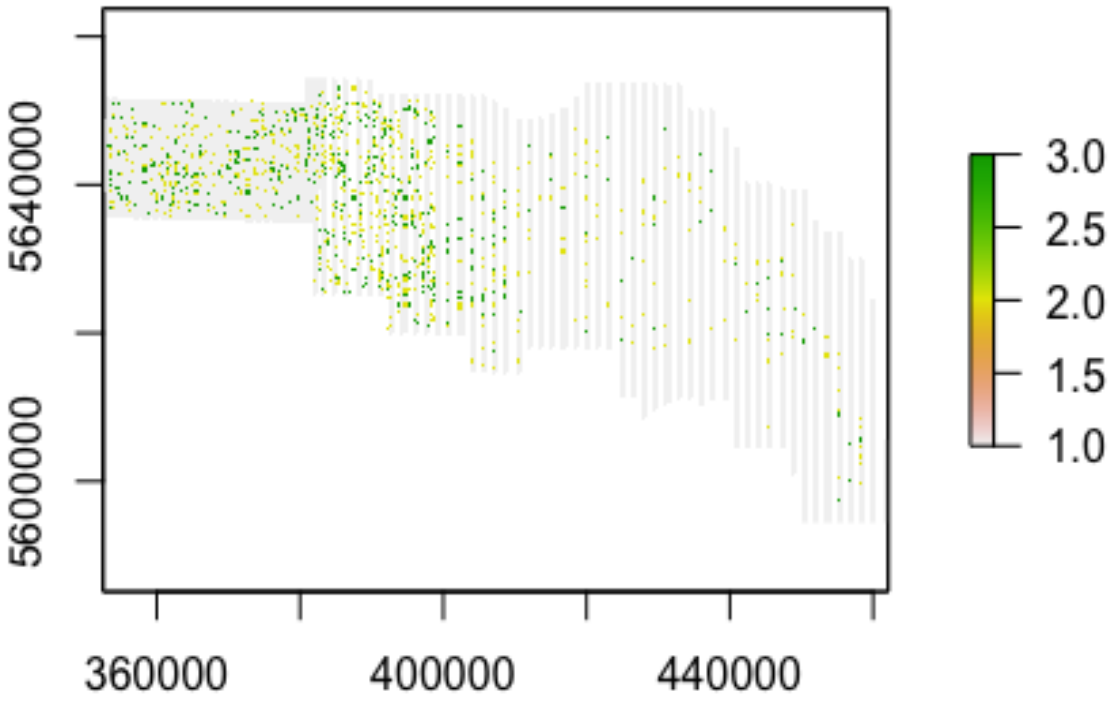


```
#writeRaster(ras, 'data/derived-data/rmnp-density-rst.tif')
```

Supplement S.3.2 — Abundance size and variance calculations for aerial flight surveys in Riding Mountain National Park

Density estimate

Variation between area sampled on transects

Variation between number of animals counted on transects

Covariance between area sampled and number of animals counted on transects

Theoretical variance estimate

Where:

R = Density estimate
y_i = Number of counted individuals on transect i
z_i = Area of transect i
S_z^2 = variance between sampling unit area
n = number of transects sampled
N = Total number of sample units in population (269 transects)
Z = Total area surveyed
Y = total number of animals counted
R = Ratio of animals counted to area searched

Additional Literature

Tarleton P. 1992. Cervid monitoring and status report, Riding Mountain National Park, 1990–1991. Parks Canada Unpublished report.

Trottier GC. 1987. Riding Mountain large mammal systems study — Final report. Winnipeg, MB: Parks Canada.

Vander Wal E, Van Beest FM, Brook RK. 2013. Density-Dependent Effects on Group Size Are Sex-Specific in a Gregarious Ungulate. Fenton B, editor. PLoS ONE. 8(1):e53777. doi:10.1371/journal.pone.0053777.

Richards LKM. 1997. Elk/Moose Population Dynamics in Riding Mountain National Park [MSc thesis]. [Winnipeg Manitoba, Canada]: University of Manitoba.

Supplement S.3.3 — Sensitivity of the Random Encounter Staying Time density estimates to spatial and temporal variability.

To assess the sensitivity of moose density estimates produced by the Random Encounter Staying Time model to different spatial and temporal scales, I conducted a series of validations using bootstrapping as well as theoretical variance calculations. To investigate the similarity of moose density estimates across time, I generated mean moose density estimates for all of Riding Mountain National Park in each Julian calendar month from September 2021 to July 2022. I randomly sampled with 1000 bootstrap iterations from all camera traps across RMNP (n = 81). I used probability sampling to preferentially select cameras with a higher effort, i.e., cameras that were operational for more time and with higher Effective Capture Areas. In Figure S.3.3.1, I show the mean and variance of 1000 bootstrapped iterations at each calendar month. Next, using the actual data from the same Julian months, I calculated the mean and variance density estimates for all RMNP using the Hogg (2021) equations (Figure S.3.3.2). My investigations into temporal sensitivity show that, in my study, park-level density estimates are highly sensitive to the Julian month that I use data from. Due to generation and recruitment intervals of moose (i.e., years), density cannot realistically fluctuate to the extent viewed in my temporal validations. Thus, the high variability seen are likely an influence of species movement rate, a limitation of the spatial distribution of camera traps, or an inadequate monitoring period at many cameras.

Given the high temporal variability observed in density, I wanted to use a temporal period in my park-level abundance estimates that were a) long enough to produce stable density estimates and b) short enough to not encompass actual biological changes in density. To enumerate this temporal window, I calculated park-level density, and 95% confidence intervals using Hogg (2021) equations, at increasing biweekly intervals surrounding the aerial flight survey (Figure S.3.3.3). For example, staring with one week before and one week after the 2022

flight survey occurred, I increased the temporal interval by adding one week before and after the survey date, ending at 6 months, or 28 weeks. This analysis suggests that my park-level density estimates stabilize at a temporal window of ~ 16 weeks before and after aerial flight surveys occurred. This result was the basis of my decision to use a 32-week interval around aerial survey dates to compare density and abundance estimates. Next, I wanted to investigate the spatial sensitivity of REST density estimates, i.e, which camera traps are used in density estimation. I generated 500 bootstrap estimates on the 2022 park-level density estimate, randomly removing half (n = 40) of all camera traps from each iteration. I then compared the bootstrapped spatial sensitivity to the theoretical 95% confidence intervals generated by the Hogg-REST variance equation (Figure S.3.3.4).

Hogg J. 2021. The precision and accuracy of the Random Encounter Staying Time model's estimation of species population density [MSc. thesis]. [St. John's, NL]: Memorial University of Newfoundland and Labrador.

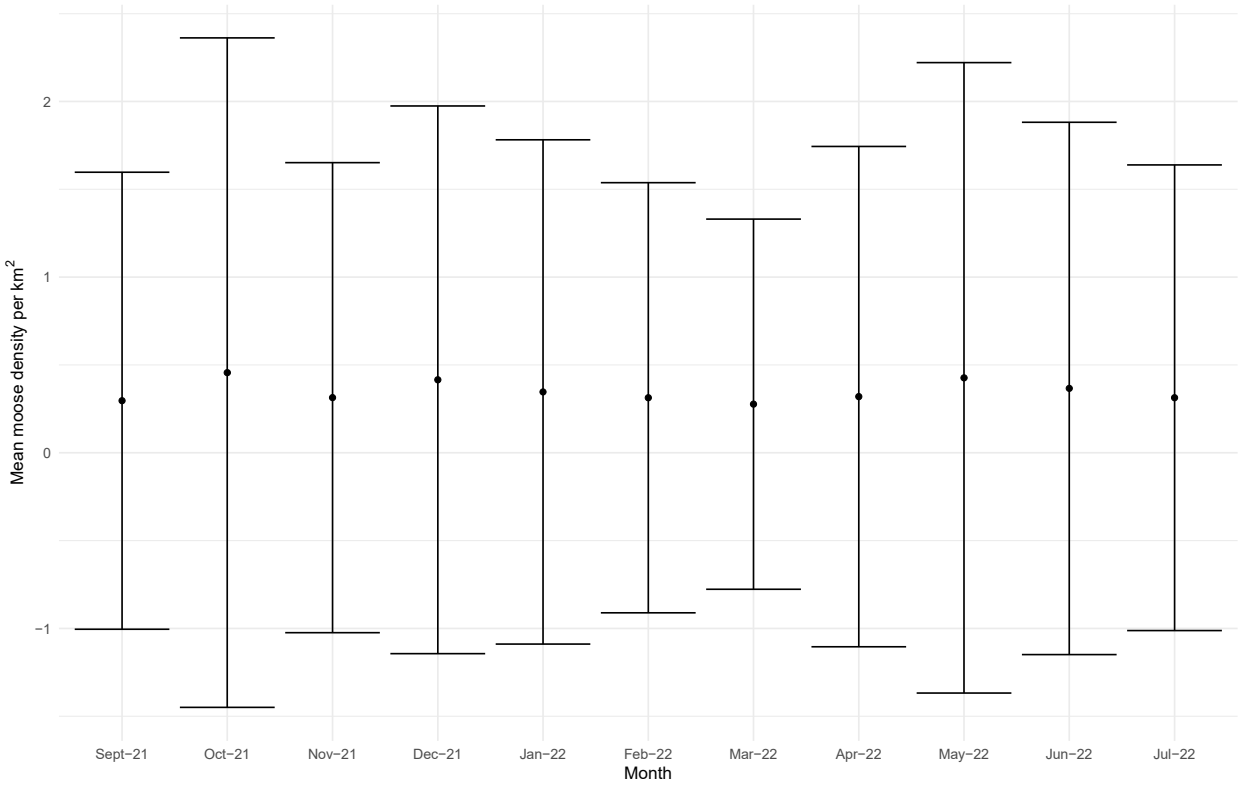

Figure S.3.3.1 Mean and variance moose density estimates, per km^2, generated from 1000 bootstrapped iterations sampled by weighted effort, from all camera traps (n = 81) in Riding Mountain National Park across different Julian months in late 2021 and early 2022.

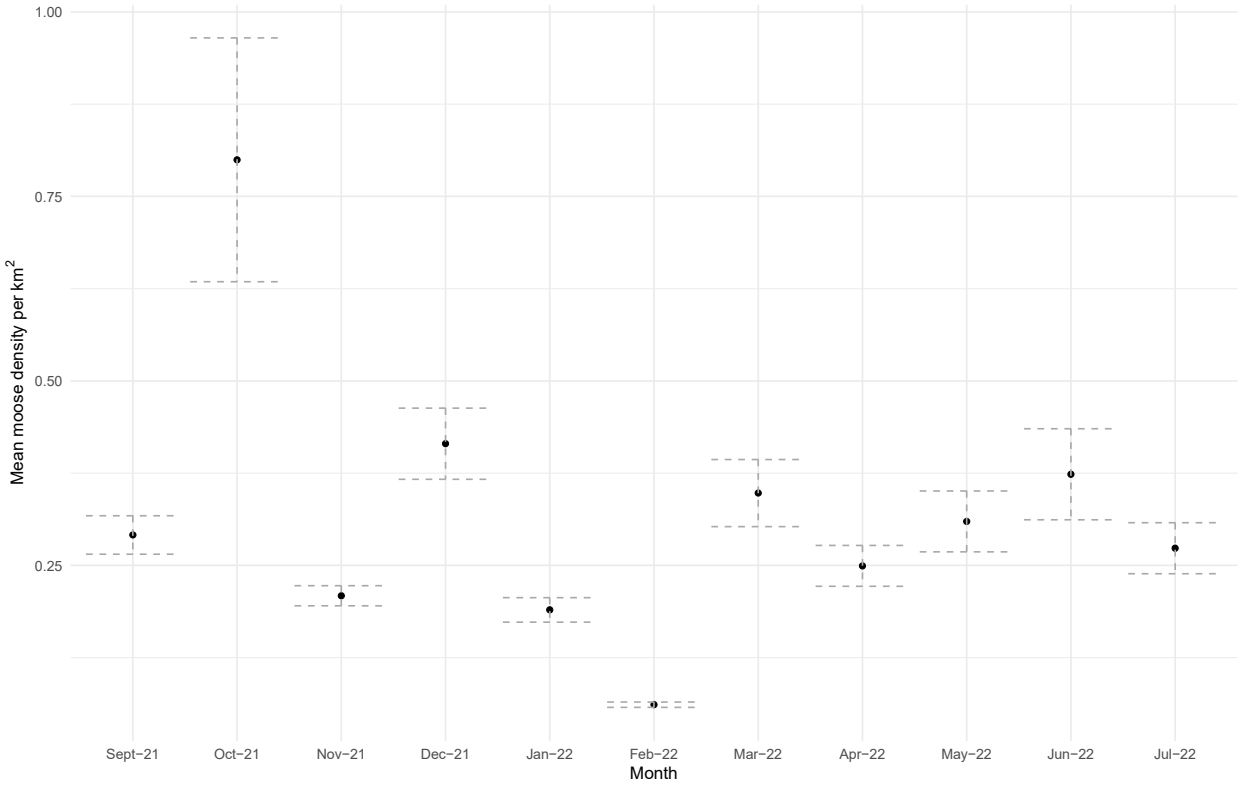

Figure S.3.3.2 Mean and theoretical 95% confidence intervals of moose density, per km^2, estimated from the Hogg-Random Encounter Staying Time Model, from all camera traps (*n* = 81) in Riding Mountain National Park across different Julian months in late 2021 and early 2022.

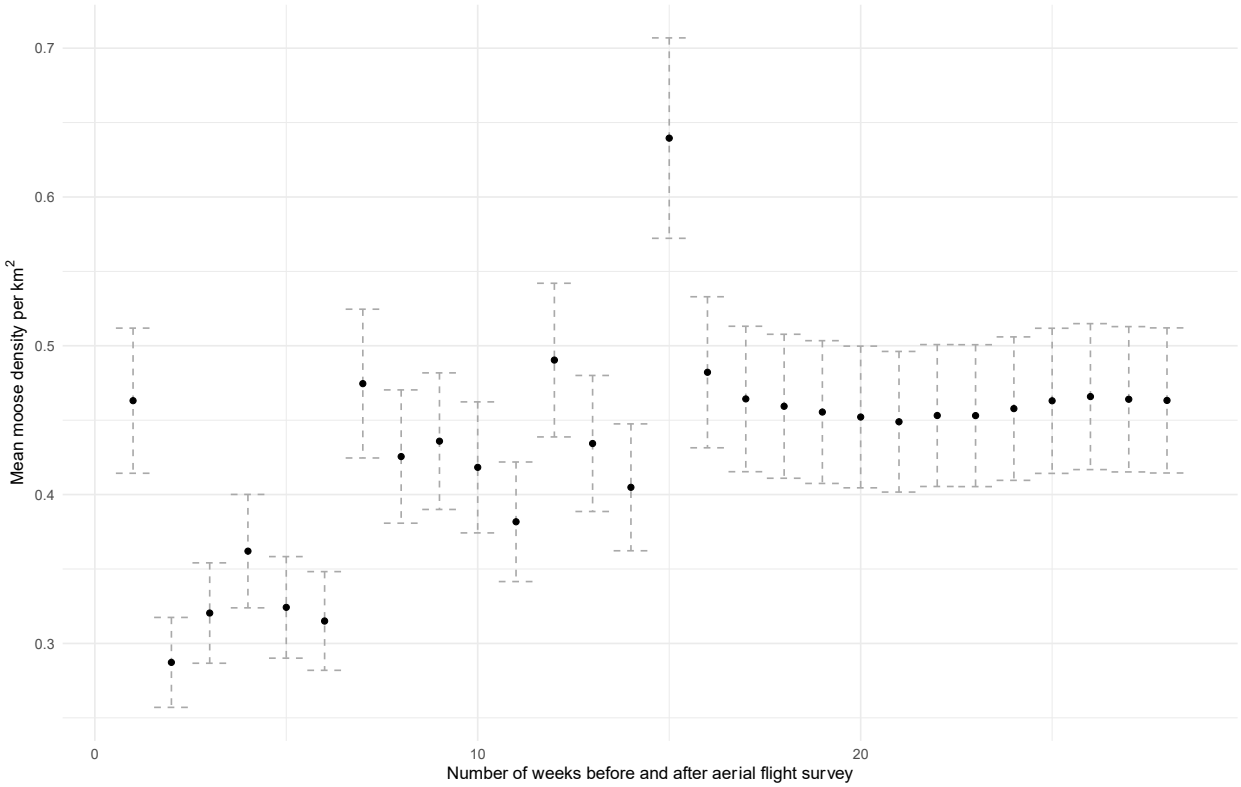

Figure S.3.3.3 Mean and theoretical 95% confidence intervals of moose density, per km^2, estimated from the Hogg-Random Encounter Staying Time Model, from all camera traps (n = 81) in Riding Mountain National Park at increasing biweekly time intervals surrounding aerial flight surveys in February 2022.

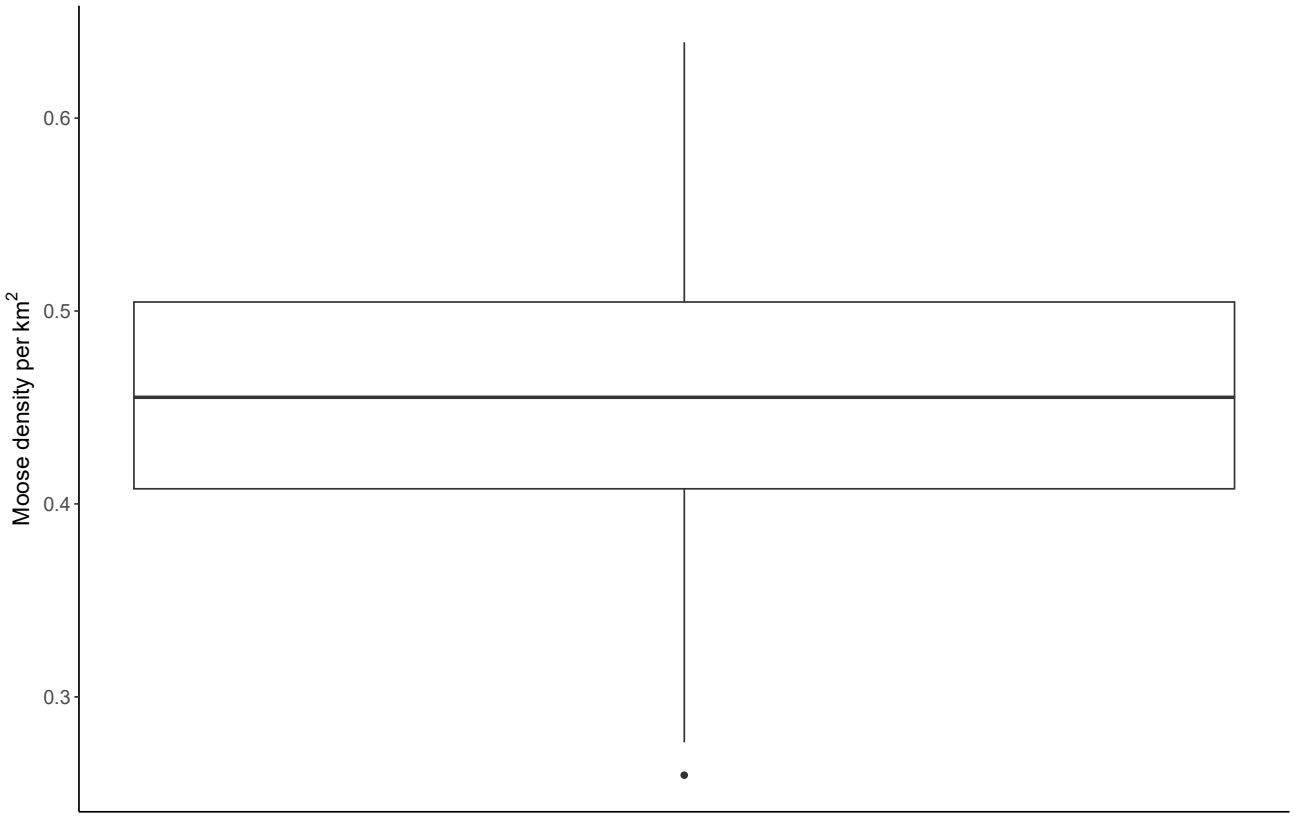

Figure S.3.3.4 Boxplot of observed spatial variability of park-level moose density estimates, per km^2, compared to the theoretical mean and 95% confidence intervals from the Hogg-REST mean and variance equation from all camera traps (n = 81) in the 2022 study year.

Supplement S.3.4 — Monitoring time of all camera traps in Riding Mountain National Park from establishment in February 2020 until the end of 2022.

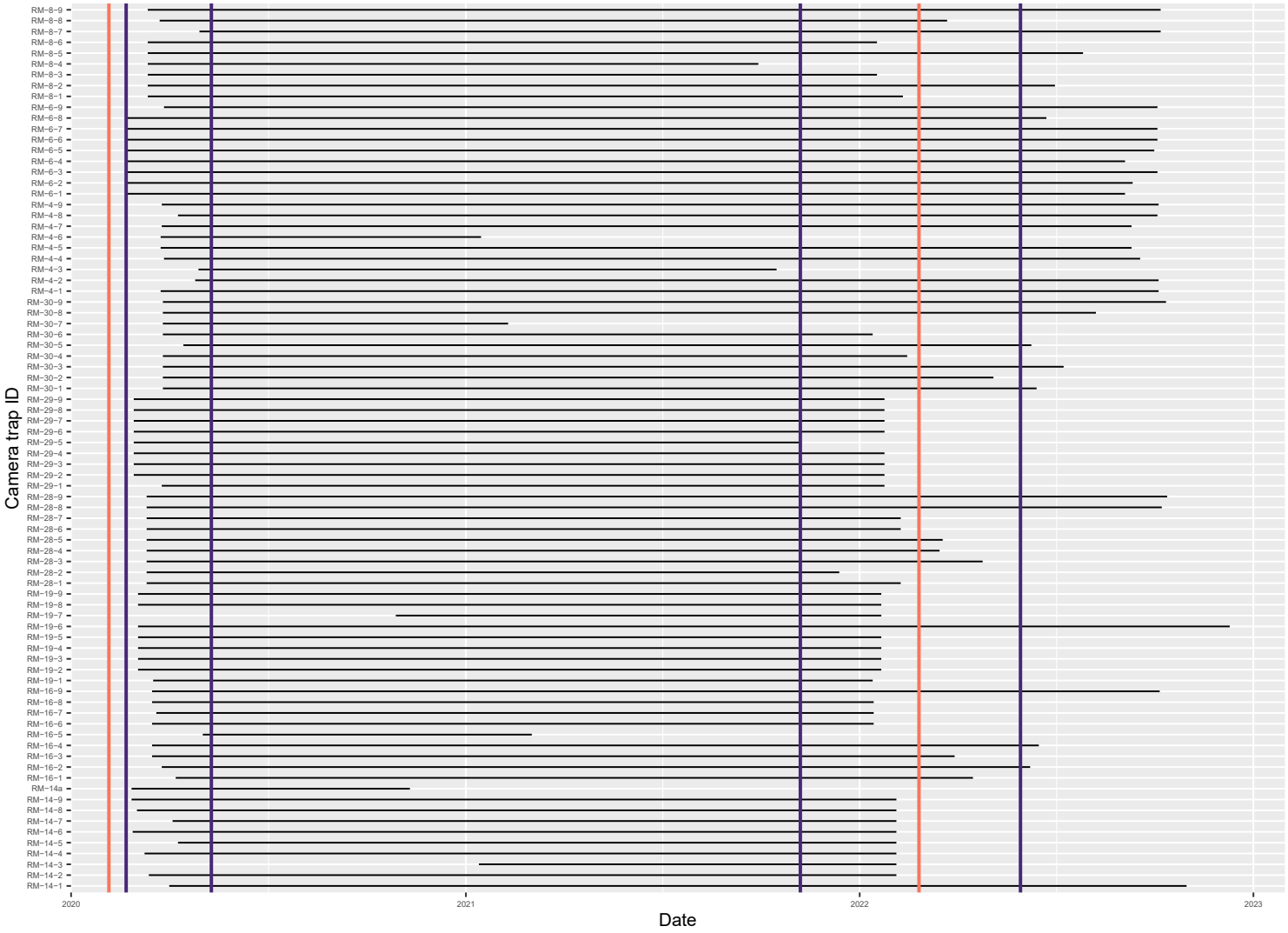

Figure S.3.4.1 The total operation time of each camera trap (n = 81) deployed across Riding Mountain National Park from February 2020 until November 2022, highlighting the temporal periods used in the 2020 and 2022 study years to density estimates with the Random Encounter Staying Time model (purple), and dates when aerial flight surveys occurred (orange).

Supplement S.3.5 — Additional figures and analyses for elk density estimation in RMNP

Similarly to the moose density estimate validations in Supplement S.3.3, I conducted a series of spatial and temporal validations using bootstrapping as well as theoretical variance calculations for elk density estimates. For the similarity of elk density estimates through time, I generated mean and 95% confidence intervals around density (Hogg 2021) throughout Riding Mountain National Park in each Julian calendar month from September 2021 to July 2022. Much like the moose density estimates, monthly elk densities are highly variable to the Julian month used (Figure S.3.5.1).

Next, to see the temporal window when elk densities stabilized, I calculated park-level density, and 95% confidence intervals using Hogg (2021) equations, at the same increasing biweekly intervals surrounding the aerial flight survey (Figure S.3.5.2). For elk, the analysis suggests that park-level density estimates stabilize slightly sooner than moose density estimates, at a temporal window of ~ 14 weeks before and after aerial flight surveys occurred.

For spatial sensitivity of elk density estimates, I generated 500 bootstrap estimates on the 2022 park-level density estimate, randomly removing half (n = 40) of all camera traps from each iteration. I then compared the bootstrapped spatial sensitivity to the theoretical 95% confidence intervals generated by the Hogg-REST variance equation (Figure S.3.5.3). Much like the moose density estimates, elk estimates showed little sensitivity to spatial variation.

Our camera trap grid locations were initially deployed following *a priori* moose densities (determined from previous aerial survey data). Despite this, I wanted to investigate whether fine-scale densities from camera trap grids and aerial surveys correlated for elk as well as moose. Following the same approach as moose, outlines in Chapter 3 methods, I investigated on which spatial scale camera grid and flight survey fine-scale densities best correlated, and how linear

that correlation was. Similar to moose, elk densities best correlated at a spatial scale of 10 km^2. Unlike moose however, the slopes of correlations were much lower than one (Figure S.3.5.5). When regressed, elk densities were very poorly correlated (R^2= -0.05), and with a low slope (*m*=0.29; Figure S.3.5.6). Although elk abundancies match at the coarse spatial scale, across RMNP, they do elk densities are very poorly correlated at the fine-scale. This poor correlation between fine-scale camera and flight densities is likely because our camera traps were never deployed explicitly to monitor elk, and do not represent a stratified distribution of elk at the time of the aerial survey.

Hogg J. 2021. The precision and accuracy of the Random Encounter Staying Time model's estimation of species population density [MSc. thesis]. [St. John's, NL]: Memorial University of Newfoundland and Labrador.

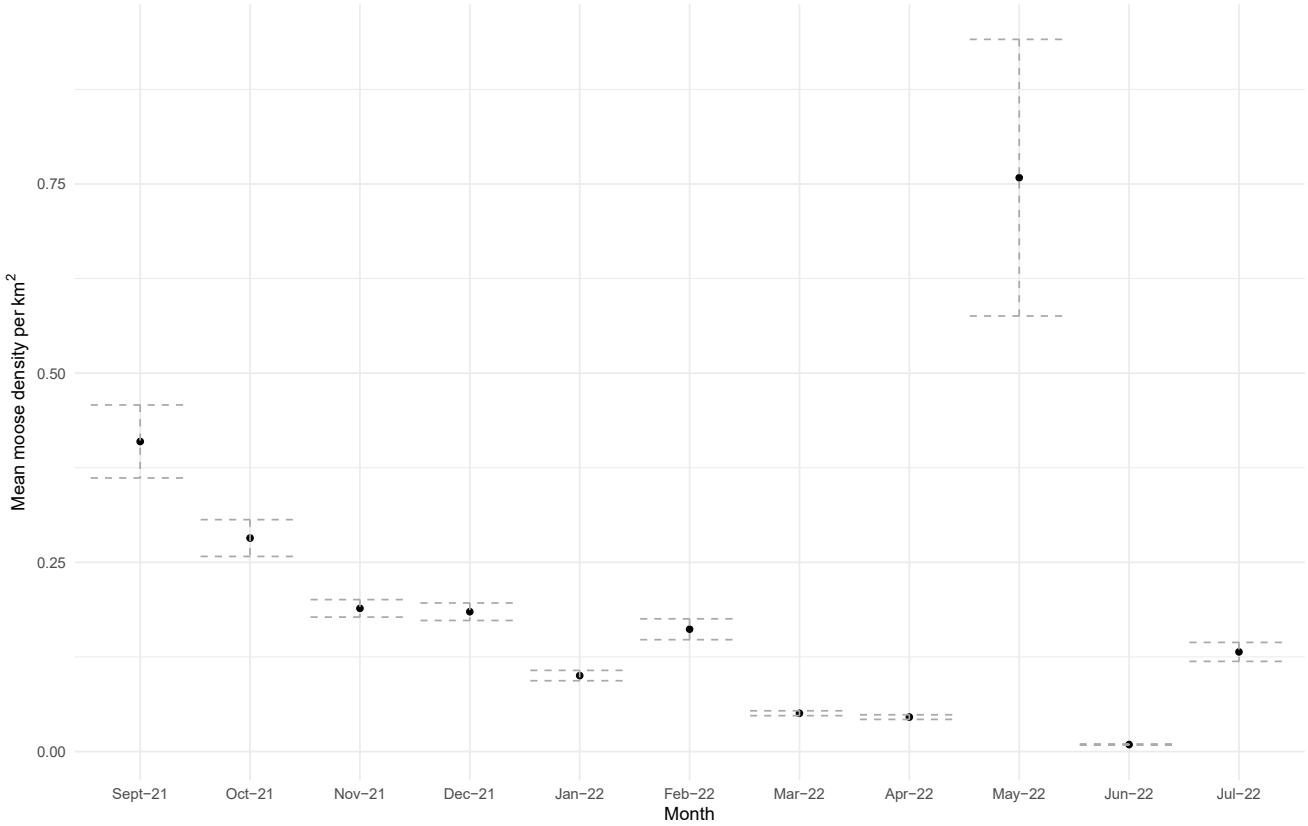

Figure S.3.5.1 Mean and theoretical 95% confidence intervals of elk density, per km^2, estimated from the Hogg-Random Encounter Staying Time Model, from all camera traps (n = 81) in Riding Mountain National Park across different Julian months in late 2021 and early 2022.

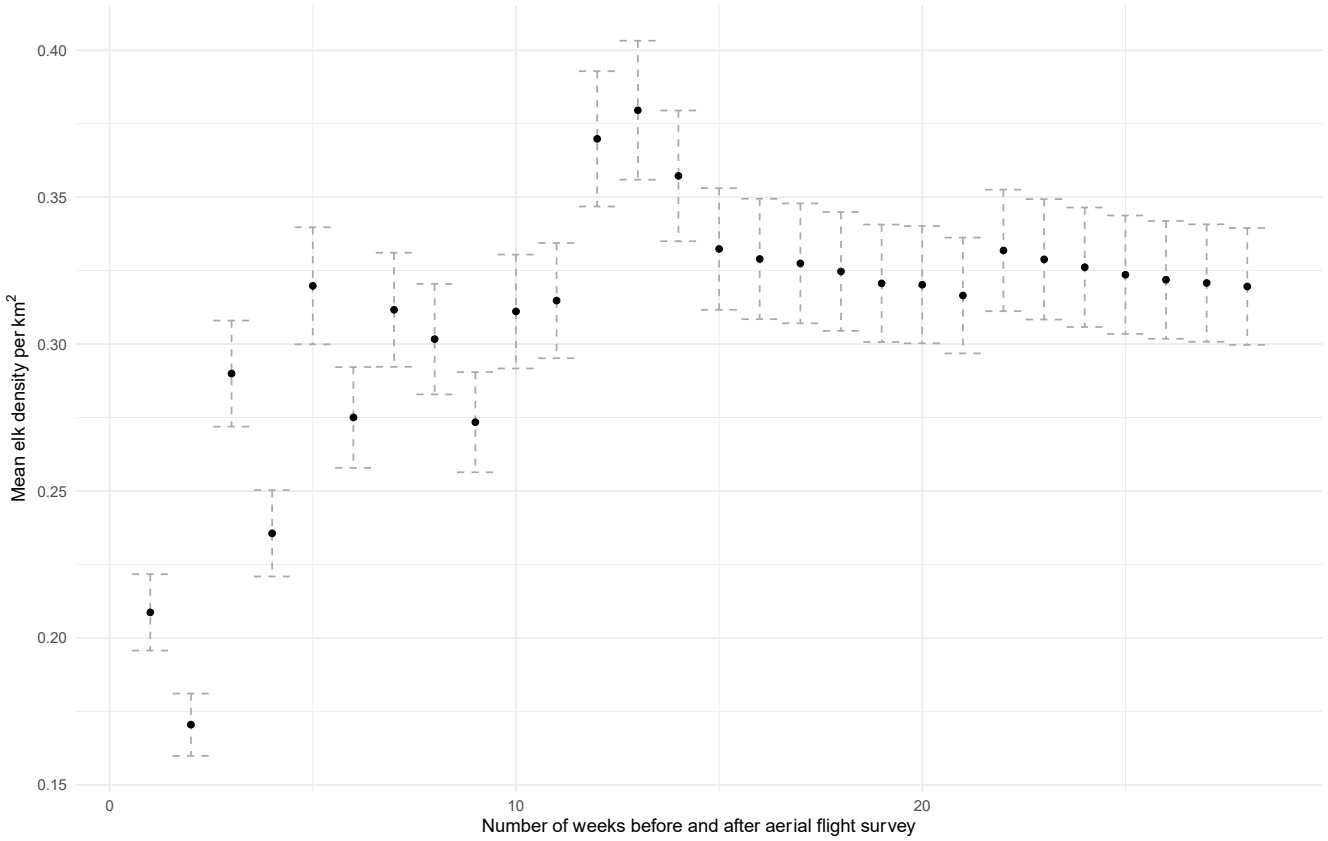

Figure S.3.5.3 Mean and theoretical 95% confidence intervals of elk density, per km^2, estimated from the Hogg-Random Encounter Staying Time Model, from all camera traps (n = 81) in Riding Mountain National Park at increasing biweekly time intervals surrounding aerial flight surveys in February 2022.

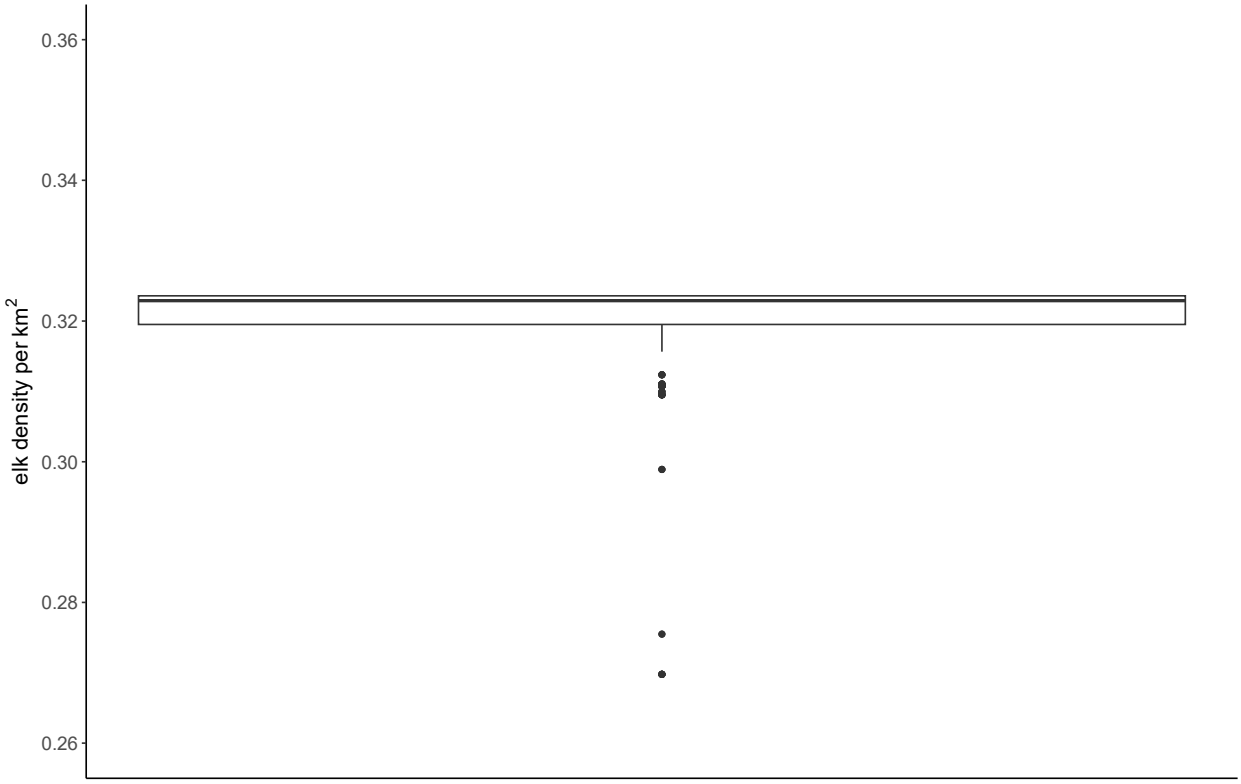

Figure S.3.5.4 Boxplot of observed spatial variability of park-level elk density estimates, per km^2, compared to the theoretical mean and 95% confidence intervals from the Hogg-REST mean and variance equation from all camera traps (n = 81) in the 2022 study year.

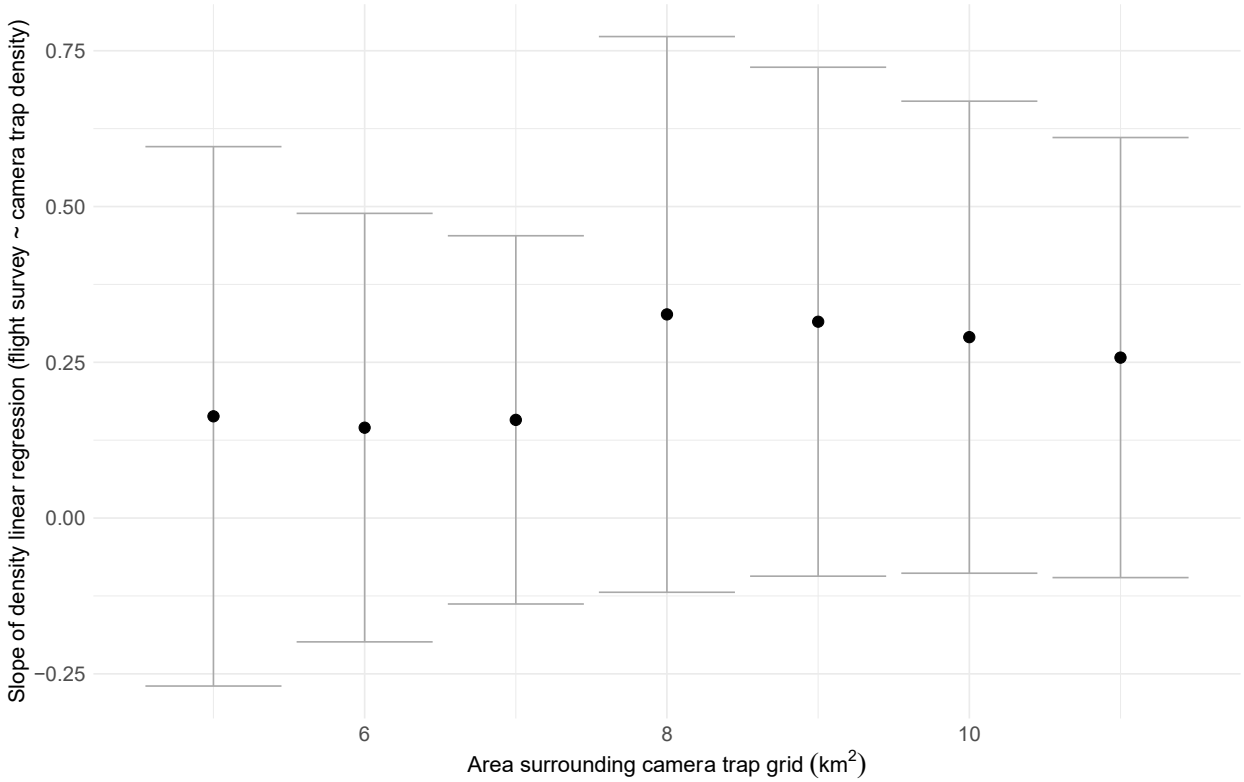

Figure S.3.5.5 Slope (±95% confidence intervals) of the linear regressions that predicted fine-scale elk density estimates, at various spatial scales (5–11km^2), from aerial flight surveys conducted in Riding Mountain National Park in February 2022. Fine-scale flight densities were predicted by mean Random Encounter Staying Time density estimates at camera trap grids (n = 9) for the 2022 study year.

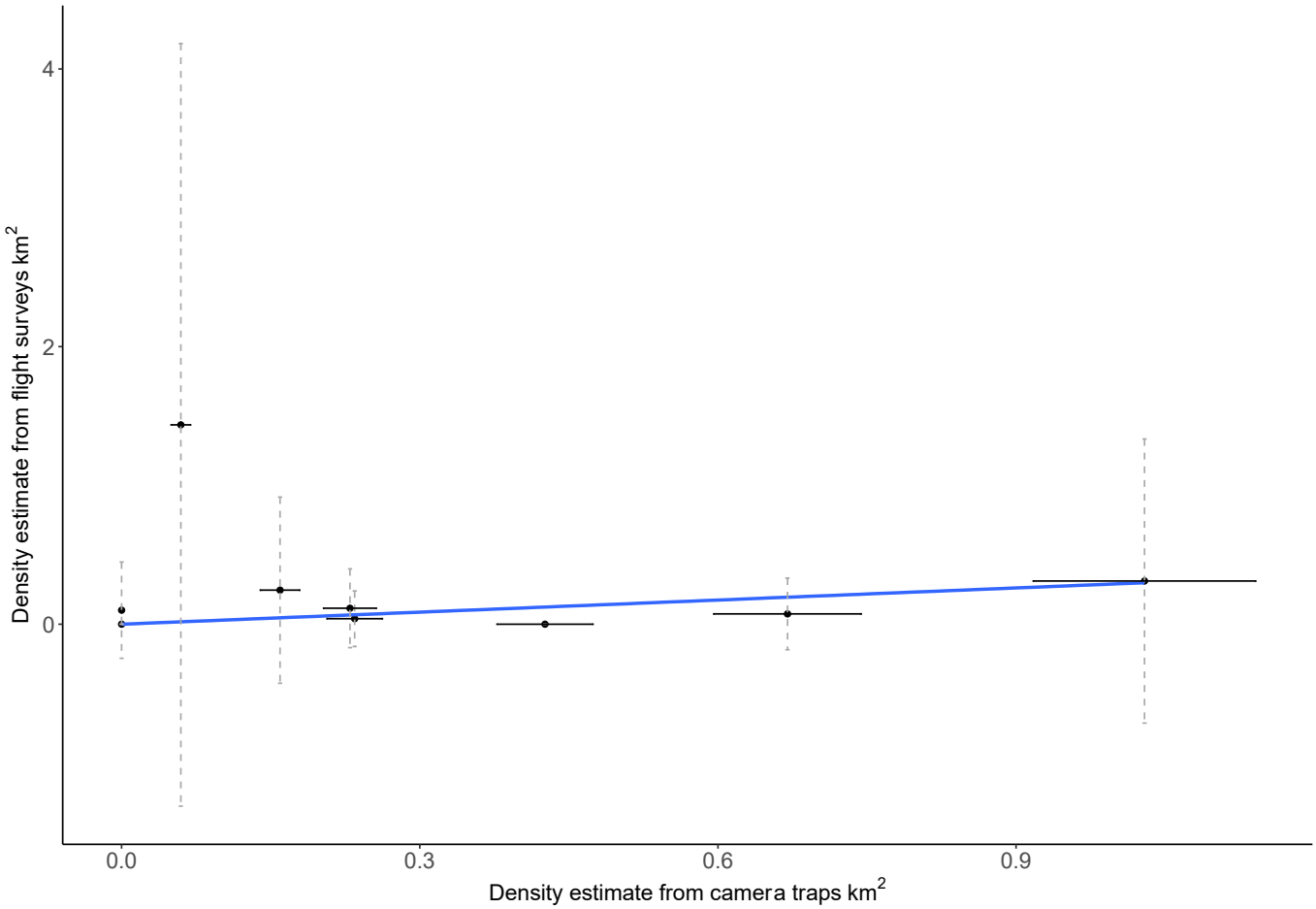

Figure S.3.5.6 The linear regression model predicting fine-scale elk density estimates from the 2022 aerial flight survey and 2022 study year with 10km^2 polygons surrounding each camera trap grip (n = 9). Horizontal error bars represent the 95% confidence intervals generated from the theoretical REST variance equation, whereas vertical error bars represent the 95% confidence intervals from aerial flight surveys.

Supplement S.3.6 — Partial aerial flight survey lines in Riding Mountain National Park in 2021

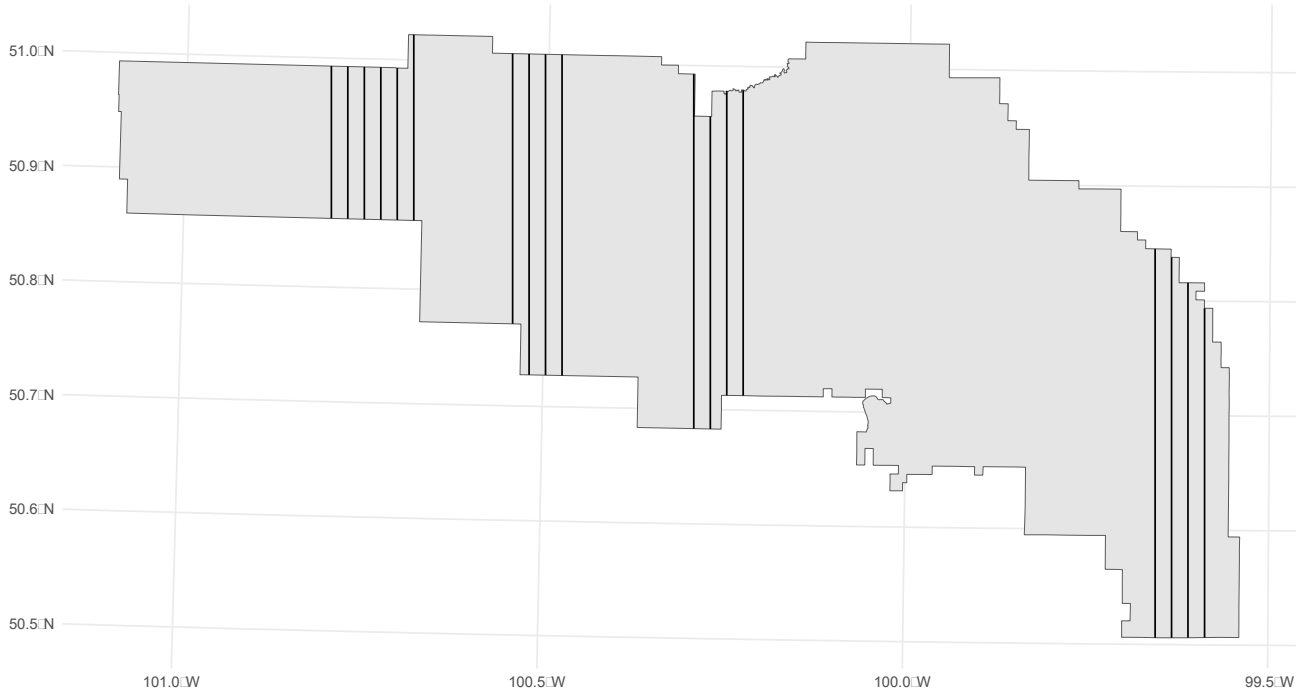

Figure S.3.6.1 The partial aerial flight survey lines (n = 18) that occurred in Riding Mountain National Park in 2021 due to the COVID-19 pandemic.

Chapter 4: Summary and Conclusions

4.1 — Summary

In my thesis, I developed and tested a novel field and analytical framework to produce standardized estimates of the spatial footprint camera traps monitor with perfect, 100%, capture probability, the Effective Capture Area (ECA; Chapter 2). The ECA is a reproducible, precise, and predictable metric of a camera traps spatial footprint and will contribute to camera trap research, particularly with occupancy modeling and viewshed density estimators. I used the ECA method to estimate the spatial footprint of camera traps in a long-term monitoring program distributed across Riding Mountain National Park (RMNP; Chapter 3). I showed that, when using the ECA with the Random Encounter Staying Time (REST) viewshed density estimator (Hogg 2021), camera trap-based density estimates can correlate well with a traditional density estimator at multiple spatial scales.

In Chapter 2, I showed that a camera traps spatial footprint, though ECA estimation, is a sensitive and unique parameter that varies by individual camera trap. The ECA was influenced by external biotic and abiotic characteristics where camera traps were placed, i.e., shrub and horizontal cover, temperature, the movement speed of focal individual, and the time of day. In addition, ECAs were highly influenced by camera traps internal settings and functioning, i.e., camera trap model, camera refractory period, sensitivity settings, and number of photos taken per PIR motion trigger. In the RMNP monitoring program, ECAs varied by nearly 40 m^2, from ~5 m^2 to 39 m^2 at different camera traps.

When using ECAs to parameterize the REST model for estimating moose and elk density and abundance across RMNP, fine- and coarse-scale estimates compared well given an adequate temporal interval for camera data and a broad enough spatial scale for aerial flight surveys. I

demonstrated that camera traps, and the REST viewshed density estimator, can be used as a supplement to traditional aerial surveys for ungulates to validate population level abundance, population trends, and fine-scale density dependent processes.

4.2 — Management considerations

Understanding species densities and distributions are the pinnacle for all rightsholders interested in wildlife conservation and management. Despite the long-standing history of traditional survey types, i.e., aerial flight surveys for ungulates, uncertainty in species density estimation underpins all wildlife management in Canada (Buckland 2004; Morellet et al. 2007; Rönnegård et al. 2008; Liberg et al. 2011; Burton et al. 2015; Moll et al. 2022). In addition, in Canada, traditional survey methods such as aerial flights for ungulates, are incredibly difficult and costly to implement, resulting in long gaps between surveys and exclusion of non-colonial governments from participating in population monitoring (Nature United 2018). Wildlife management in Canada needs new, accurate, reliable, and inclusive methods to monitor wildlife species.

Camera traps are a relatively affordable, accessible, and an ever-increasing method of wildlife management and monitoring (Burton et al. 2015; Fisher 2023). Their utility has contributed to a growing field of decolonizing science in Canada by allowing many Indigenous nations to participate in wildlife population monitoring (Nature United 2018; Fisher et al. 2021). The utility of my ECA modeling and application of the REST model can stretch far beyond academic exercise and comparison to traditional estimators. Considering the increasing interest of Indigenous nations to participate in wildlife management (e.g., Menzies et al. 2022; Lamb et al. 2023), the REST model and framework set out in this thesis provides an opportunity for diverse shareholders to participate in wildlife management. For example, in Manitoba, Canada,

where much of my research took place, the Provincial government flies aerial surveys for ungulates in small management units inconsistently, i.e., once every 5–10 years (Manitoba Fish and Wildlife Division 2020; Manitoba Fish and Wildlife Division 2022). Yet, numerous Indigenous communities in Manitoba have initiated their own camera trap-based wildlife monitoring programs in addition to collaborations with institutionalized researchers. Having camera trap-based abundance data for wildlife will help supplement infrequent and unreliable abundance data throughout Canada. I hope to see, and will continue to work towards, making the contents of my thesis accessible to Indigenous-lead wildlife management in Canada.

4.3 — Future directions

Unfortunately, numerous years of data from Chapter 3 of my thesis were limited due to external circumstances. For example, the 2020 and 2021 years of camera trap data and aerial flight survey were incomparable due to safety concerns from the COVID-19 pandemic. If multiple year of reliable camera trap and aerial flight survey were available, I would have liked to integrate the two density estimate methods more meaningfully. For example, both camera and flight survey methods have fine- and coarse-scale mean and variance estimates. Neither method produces the true or exact number of moose or elk in RMNP, however, both methods provide an estimate that we have varying levels of confidence in. To describe population levels trends with more evidence towards the true population size, I would have liked to integrate both aerial flight survey and camera trap-based methods. For example, using a Bayesian modeling approach, one could model population abundancies for a given year from the mean and uncertainty values from camera trap and flight surveys (Ellison 2004; McElreath 2018). In theory, we would have more confidence in an integrated value, as opposed to either flight survey or camera methods separately.

Viewshed density estimators can provide an entirely novel perspective on density estimation in wildlife—how density changes in fixed locations throughout time. The temporal fluctuations in density estimation are an outcome of camera traps Eulerian, i.e., place-based, perspective. Given an adequate spatial distribution of grouped camera traps, that are continually operational, species density could be estimated at fine temporal intervals such as at weekly, biweekly, or monthly scales. Currently, most traditional density estimate methods represent a single point, or a short period in time, resulting a loss of temporal precision. Using camera traps to estimate density at a fine temporal scale could provide researchers with novel perspectives on how species distributions (Wevers et al. 2021), habitat occupancy (Carswell et al. 2021), spatiotemporal patterns (Carswell et al. 2023), sociality (Wong et al. 2019), and behaviour Caravaggi et al. 2017) change throughout different times of the year.

Using viewshed density estimators to generate density estimates at fine temporal scales, however, come with added layers of complexity in parameterization. In my research, I generated density estimates during the winter season, i.e., after leaf senescence in the fall and before green up in the spring. This decision was largely to align with the timing of aerial flight surveys in winter, however, the ECAs of camera traps are consistent during the winter. ECA values of camera traps will be different in the summer, due to complex interactions of vegetation cover (Moll et al. 2020; Moeller et al. 2023), ambient air temperature (Apps and McNutt 2018; Urbanek et al. 2019), and temperatures emitted by wildlife species (Welbourne et al. 2016; Reconyx 2022). In addition, during periods of time of rapid environmental change, e.g., leaf fall or green up within a very short window, ECA values at individual cameras could change within days. Before implementing viewshed density estimators at fine temporal intervals, studies need to first investigate how the ECA changes at camera traps within through various seasons and

environmental conditions. Failure to account for these changes in ECA could result in highly biased fine-scale density estimates.

4.4 — Literature cited

Apps P, McNutt JW. 2018. Are camera traps fit for purpose? A rigorous, reproducible and realistic test of camera trap performance. African Journal of Ecology. 56(4):710–720. doi:10.1111/aje.12573.

Buckland ST. 2004. Advanced distance sampling: estimating abundance of biological populations. Anderson DR, Burnham KP, Laake JL, Borchers DL, Thomas L, editors. Oxford, UK: Oxford University Press.

Burton AC, Neilson E, Moreira D, Ladle A, Steenweg R, Fisher JT, Bayne E, Boutin S. 2015. Wildlife camera trapping: a review and recommendations for linking surveys to ecological processes. Stephens P, editor. Journal of Applied Ecology. 52(3):675–685. doi:10.1111/1365-2664.12432.

Caravaggi, A., Banks, P. B., Burton, A. C., Finlay, C. M. V., Haswell, P. M., Hayward, M. W., Rowcliffe, M. J., & Wood, M. D. (2017). A review of camera trapping for conservation behaviour research. Remote Sensing in Ecology and Conservation, 3(3), 109–122. https://doi.org/10.1002/rse2.48

Carswell BM, Boyle SP, Brook RK, Van Beest FM, Vander Wal E. 2023. Variation in spatiotemporal activity may reduce competitive interactions between invasive wild pigs (*Sus scrofa*) and native mammal species. Canadian Journal of Zoology. doi:10.1139/cjz-2022-0145.

Carswell BM, Rea RV, Rusch D, Johnson CJ. 2021. The influence of the root diseases *Armillaria solidipes* and *Inonotus sulphurascens* on the distribution of mule deer during winter. Forestry: An International Journal of Forest Research. 94(4):492–501. doi:10.1093/forestry/cpab002.

Considerations and recommendations for initiating Indigenous-led moose monitoring and research. 2018. Canada: Nature United.

Ellison AM. 2004. Bayesian inference in ecology. Ecology Letters. 7(6):509–520. doi:10.1111/j.1461-0248.2004.00603.

Fisher JT. 2023. Camera trapping in ecology: A new section for wildlife research. Ecology and Evolution. 13(3):e9925. doi:10.1002/ece3.9925.

Fisher JT, Grey F, Anderson Nelson, Sawan J, Anderson Nicholas, Chai S-L, Nolan L, Underwood A, Amerongen Maddison J, Fuller HW, et al. 2021. Indigenous-led camera-trap research on traditional territories informs conservation decisions for resource extraction. Facets. 6:1266–1284. doi:10.1139/facets-2020-0087.

Hogg J. 2021. The precision and accuracy of the Random Encounter Staying Time model's estimation of species population density [MSc. thesis]. Memorial University of Newfoundland and Labrador.

Lamb CT, Willson R, Menzies AK, Owens-Beek N, Price M, McNay S, Otto SP, Hessami M, Popp JN, Hebblewhite M, et al. 2023. Braiding Indigenous rights and endangered species law. Science. 380(6646):694–696. doi:10.1126/science.adg9830.

Liberg O, Aronson Å, Sand H, Wabakken P, Maartmann E, Svensson L, Åkesson M. 2011. Monitoring of wolves in Scandinavia. Hystrix, the Italian Journal of Mammalogy. 23(1). doi:10.4404/hystrix-23.1-4670. https://doi.org/10.4404/hystrix-23.1-4670.

Manitoba Fish and Wildlife division. 2020 big game surveys. 2020. Winnipeg, MB: Manitoba Fish and Wildlife division

Manitoba Fish and Wildlife division. 2022 big game surveys. 2022. Winnipeg, MB: Manitoba Fish and Wildlife division

McElreath R. 2018. Statistical rethinking: A Bayesian course with examples in R and Stan. USA: Chapman and Hall/CRC.

Menzies AK, Bowles E, Gallant M, Patterson H, Kozmik C, Chiblow S, McGregor D, Ford A, Popp JN. 2022. "I see my culture starting to disappear": Anishinaabe perspectives on the socioecological impacts of climate change and future research needs. Facets. 7:509–527. doi:10.1139/facets-2021-0066.

Moeller AK, Waller SJ, DeCesare NJ, Chitwood MC, Lukacs PM. 2023. Best practices to account for capture probability and viewable area in camera-based abundance estimation. Remote Sensing in Ecology and Evolution. 9(1):152–164. doi:10.1002/rse2.300.

Moll RJ, Ortiz-Calo W, Cepek JD, Lorch PD, Dennis PM, Robison T, Montgomery RA. 2020. The effect of camera-trap viewshed obstruction on wildlife detection: implications for inference. Wildlife Research. 47(2):158. doi:10.1071/WR19004.

Moll RJ, Poisson MKP, Heit DR, Jones H, Kantar L. 2022. A review of methods to estimate and monitor moose density and abundance. Alces. 58:31–49.

Morellet N, Gaillard J, Hewison AJM, Ballon P, Boscardin Y, Duncan P, Klein F, Maillard D. 2007. Indicators of ecological change: new tools for managing populations of large herbivores. Journal of Applied Ecology. 44(3):634–643. doi:10.1111/j.1365-2664.2007.01307

Reconyx. 2022. Reconyx Hyperfire 2 high performance camera instruction manual. https://www.reconyx.com/img/file/HyperFire_2_User_Guide_2018_07_05_v5.pdf.

Rönnegård L, Sand H, Andrén H, Månsson J, Pehrson Å. 2008. Evaluation of four methods used to estimate population density of moose Alces alces. Wildlife Biology. 14(3):358–371. doi:10.2981/0909-6396

Urbanek RE, Ferreira HJ, Olfenbuttel C, Dukes CG, Albers G. 2019. See what you've been missing: An assessment of Reconyx® PC900 Hyperfire cameras. Wildlife Society Bulletin. 43(4):630–638. doi:10.1002/wsb.1015.

Welbourne DJ, Claridge AW, Paull DJ, Lambert A. 2016. How do passive infrared triggered camera traps operate and why does it matter? Breaking down common misconceptions. Rowcliffe M, Disney M, editors. Remote Sensing in Ecology and Evolution. 2(2):77–83. doi:10.1002/rse2.20.

Wevers J, Beenaerts N, Casaer J, Zimmermann F, Artois T, Fattebert J. 2021. Modeling species distribution from camera trap by-catch using a scale-optimized occupancy approach. Rowcliffe M, Sollmann R, editors. Remote Sensing in Ecology and Evolution. 7(3):534–549. doi:10.1002/rse2.207.

Wong ST, Belant JL, Sollmann R, Mohamed A, Niedballa J, Mathai J, Street GM, Wilting A. 2019. Influence of body mass, sociality, and movement behavior on improved detection probabilities when using a second camera trap. Global Ecology and Conservation. 20:e00791. doi:10.1016/j.gecco.2019.e00791.